Multilayer graphene modified metal film electrodes for the determination of trace metals by anodic stripping voltammetry

UNIVERSITY *of the*
WESTERN CAPE

By

Salma Gumaa Amar Zbeda

UNIVERSITY *of the*
WESTERN CAPE

A thesis submitted in fulfilment of the requirements for the degree of Magister Scientiae in the Department of Chemistry, University of the Western Cape

Supervisor: Dr. Nazeem Jahed

Co-supervisors: Dr: Salam Titinchi and Prof: Emmanuel I. Iwuoha

May 2013

KEYWORDS

Graphene oxide

Graphene

High resolution transmission electron microscopy

Thin metal film

Raman spectroscopy

Square-wave anodic stripping voltammetry

Glassy carbon electrode

Trace metal analysis

Graphene modified glassy carbon thin film mercury electrode

Graphene modified glassy carbon thin film bismuth electrode

Graphene modified glassy carbon thin film antimony electrode

UNIVERSITY of the
WESTERN CAPE

ABSTRACT

In this study multilayer graphene nanosheets was synthesize by oxidizing graphite to graphene oxide using H_2SO_4 and $KMnO_4$ followed by reduction of graphene oxide to graphene using $NaBH_4$. The graphene nanosheets were characterized by Fourier Transform Infrared (FTIR) and Raman spectroscopy, high resolution transmission electron microscopy (HRTEM), Scanning electron microscopy (SEM) and X-ray diffraction (XRD). HRTEM images showed that the multilayer graphene were obtained.

The graphene was immobilized directly onto a glassy carbon electrode using the drop coating technique followed by the *in situ* deposition of mercury, bismuth or antimony thin films to afford graphene modified glassy carbon metal film electrodes (Gr-GC-MEs). The experimental parameters (deposition potential, deposition time, rotation speed, frequency and amplitude) were optimized, and the applicability of the modified electrode was investigated towards the individual and simultaneous determination of Zn^{2+}, Cd^{2+} and Pb^{2+} at the low concentration levels (µg L^{-1}) in 0.1 M acetate buffer (pH 4.6) using square wave anodic stripping voltammetry (SWASV). The detection limits values for the Gr-GC-HgE was 0.08, 0.05 and 0.14 µg L^{-1} for Zn^{2+}, Cd^{2+} and Pb^{2+}, respectively. The Gr-GC-BiE the detection limits for was 0.12, 0.22 and 0.28 µg L^{-1} for Zn^{2+}, Cd^{2+} and Pb^{2+} while the detection limits for the Gr-GC-SbE was 0.1, 0.3 and 0.3 µg L^{-1} for Zn^{2+}, Cd^{2+} and Pb^{2+}, respectively. A Gr-GCE prepared without any binding agents or metal film had detection limits for Zn^{2+}, Cd^{2+} and Pb^{2+} of 3.9, 0.8 and 0.2 µg L^{-1} for Zn^{2+}, Cd^{2+} and Pb^{2+}.

Real sample analysis of which was laboratory tap water was performed using the Gr-GC-MEs. Only Gr-GC-HgE was sensitive enough to detect metal ions in the tap water samples at the 3ppb level whereas, the GC-BiE and GC-SbE detected the metal ions at the 10 µg L^{-1} to 30 µg L^{-1} level.

UNIVERSITY of the
WESTERN CAPE

DECLARATION

I declare that "**Multilayer graphene modified metal film electrodes for the determination of trace metals by anodic stripping voltammetry"** is a dissertation generated from my own work, that has not been submitted for any degree or examination in any other university, and that all the sources I have used or quoted have been properly indicated and acknowledged by complete references.

Salma Zbeda May 2013

UNIVERSITY of the WESTERN CAPE

Signature _____

DEDICATION

I dedicate this thesis to my parents, my husband, my son and all my family in Libya.

ACKNOWLEDGEMENT

In the name of Allah, the Most Gracious and Most Merciful all Praises to Allah the Almighty, for thee (alone) we worship and thee (alone) we ask for help. Praises and Salutations upon Muhammad S.A.W. who guided and led us to the right path.

I would like to thank my husband who stood with me through all the rough times, and my son whose presence gladdened my life.

I would like to thank my parents, Thank you very much for your love, care, education and upbringing. You are just the best gift from God. I am also indebted to my brothers, sisters and my husband's family for your prayers, supports and love.

I am grateful to my supervisor Dr. Nazeem Jahed and my co-supervisors Dr. Salam Titinchi and Prof. Emmanuel Iwuoha for their academic guidance and kindness.

UNIVERSITY of the
WESTERN CAPE

To the members of the department of Chemistry, University of the Western Cape, South Africa, I say thank you for the good and the cordial working relationship I enjoyed during my studies.

Many thanks go to Dr. Abd Almonam Baleg, Dr. Hanna Abbo and all SensorLab colleagues and all other colleagues for their support and motivation.

LIST OF ABBREVIATION

AAS	Atomic absorption spectrometry
AdSV	Adsorptive stripping voltammetry
ASV	Anodic stripping voltammetry
BiFE	Bismuth film electrode
CNS	Central nervous system
CSV	Cathodic stripping voltammetry
CVD	Chemical vapor deposition
DPSV	Differential pulse stripping voltammetry
EDS	Electronic data system
FT-IR	Transformed infrared spectroscopy
FTO	Fluorine tin oxide
GCE	Glassy carbon electrode
Gr-GC-BiE	Graphene modified glassy carbon thin film bismuth electrode
Gr-CGE	Graphene glassy carbon electrode
Gr-GC-HgE	Graphene modified glassy carbon thin film mercury electrode
GO	Graphene oxide
Gr-GC-SbE	Graphene modified glassy carbon thin film antimon electrode
GC-Gr-TFE	Graphene modified glassy carbon thin film electrode

UNIVERSITY of the
WESTERN CAPE

HMDE	Hanging mercury drop electrode
HRTEM	High resolution transmission electron microscopy
ICP-OES	Coupled plasma optical emission spectrometry
ITO	Indium tin oxide
LSSV	Linear sweep stripping voltammetry
MCL	Maximum contamination level
MFE	Mercury film electrode
N.D	Not determined
NPSV	Normal pulse stripping voltammetry
ppb	parts per billion
RDE	Rotating disk electrodes
RGO	Reduced graphene oxide
RSD	Relative standard deviation
SbFE	Antimony film electrode
SCE	Saturated calomel electrode
SEM	Scanning electron microscopy
SiC	Silicon carbide
SV	Stripping voltammetry
SWSV	Square wave stripping voltammetry

UNIVERSITY of the
WESTERN CAPE

TEM	Transmission electron microscopy
TMFE	Thin mercury film electrode
WDS	Windows deployment services
XRD	X-ray diffraction
XRF	X-ray fluorescence

TABLE OF CONTENTS

UNIVERSITY of the
WESTERN CAPE

UNIVERSITY of the
WESTERN CAPE

UNIVERSITY of the
WESTERN CAPE

UNIVERSITY of the
WESTERN CAPE

UNIVERSITY of the
WESTERN CAPE

UNIVERSITY of the
WESTERN CAPE

UNIVERSITY of the
WESTERN CAPE

LIST OF FIGURES

UNIVERSITY of the WESTERN CAPE

UNIVERSITY of the
WESTERN CAPE

UNIVERSITY of the
WESTERN CAPE

UNIVERSITY of the
WESTERN CAPE

UNIVERSITY of the WESTERN CAPE

UNIVERSITY of the
WESTERN CAPE

UNIVERSITY of the WESTERN CAPE

UNIVERSITY of the
WESTERN CAPE

LIST OF TABLES

UNIVERSITY of the WESTERN CAPE

UNIVERSITY of the
WESTERN CAPE

CHAPTER 1

Introduction

1.1 Heavy metals and their effect on the human health

A heavy metal is any metal which has a high density and is toxic at low concentrations [1]; they are natural components of earth's crust. Their amounts in soil varies from very low (femtograms) to high (milligrams) [2]. In addition they are normally found in raw or treated drinking water as they enter the water distribution system. These metals also become available in the consumer's tap water as a result of decaying pipes and fixtures of water distribution systems. Heavy metals are noted as being one of the main sources of pollution in the environment [3-4]. At present heavy metal pollution of aquatic environments is a worldwide problem that has grown at a startling rate [5] and presents a concern for human health and for life in general [6]. Heavy metal toxicity causes grave health effects such as; cancer, nervous system damage, organ damage, retarded growth, and in extreme cases, death. Furthermore, heavy metals are toxic to the sensitive, rapidly developing systems of fetuses, infants, and young children. For example, the heavy metals mercury and lead easily cross the placenta into the blood and cause childhood memory impairment, learning difficulties, damage to the nervous system and behavioural problems such as, aggressiveness and hyperactivity [7]. As a consequence of the aforementioned health concerns the United States Environmental Protective Agency (EPA) has set a maximum contamination level (MCL), for cadmium, lead, copper and zinc at 5 ppb, 15 ppb, 1.3 ppm and 5 ppm, respectively [8].

UNIVERSITY of the
WESTERN CAPE

The copper present in the body is obtained from the daily intake of food which contains copper in various forms. After absorption from the intestinal track the copper passes to the organs where some is retained, while much is excreted in the urine and the faces. The normal copper requirement of the body as determined by balance studies has been found to be about

2 mg a day, of which an average of 0.25 mg per day is excreted and the total body content apart from that in the brain is approximately 100 mg to 150 mg [9].

Cadmium is a natural element in the earth's crust, and does not break down in the environment, but can change forms. Some forms of cadmium dissolve in water while others bind strongly to soil particles. Eating food, drinking water or breathing air with very high levels of cadmium annoys the stomach, leading to vomiting, diarrhea and damages the lungs [10].

Mercury (Hg) is toxic and does not occur naturally in living organisms. It causes damage to the central nervous system (CNS) which displays itself as despair, muscle tremors, quarrelsome behavior and headaches. Mercury is active at about 50 µg/100 mL of blood [11].

Lead is released into the environment from both natural and anthropogenic sources. Exposure can occur through drinking water, food, air and soil which cause brain and / or kidney damage, disruption of the nervous system, miscarriages and subtle abortions. The average daily lead ingestion for adults in the UK is valued at 1.6 µg from air, 20 µg from drinking water and 28 µg from food [1]. Pollution by heavy metals in the environment is a mounting problem worldwide and is now a cause for concern. As a consequence many techniques are now being used to detect trace heavy metals, including atomic absorption spectrometry (AAS), inductively coupled plasma optical emission spectrometry (ICP-OES), X-ray fluorescence (XRF) and stripping techniques [12].

UNIVERSITY of the
WESTERN CAPE

1.1.1 Stripping voltammetry techniques

Stripping voltammetry is an important electroanalytical technique used for the determination of trace heavy metals [13-14]. Stripping techniques offer a significant increase in sensitivity and low detection limits due to their unique ability to pre-concentrate the target analyte [15] at a thin film metal (mercury, bismuth or antimony) working electrode. The pre-concentration

is carried out at a specific reduction potential for a pre-determined time followed by the stripping out of the analyte from the metal film through oxidation back into solution. [13-14]. Electrochemical techniques are economical, portable and have easy process procedures [12]. In addition, the anodic stripping voltammetric technique is capable of measuring four to six analytes in a sample simultaneously in the sub-parts per billion (sub-ppb) range [16-17].

The mercury film electrode (MFE) and the hanging mercury drop electrode (HMDE) have been extensively used over the past decades to detect trace heavy metals by anodic stripping voltammetry (ASV) due to their capability of working in a wide negative potential range [18]. However, the use of mercury in some countries is harshly limited because of its toxicity and the increased health risks [19]. Recently, other types of metal film electrodes have been used as an alternative to mercury; amongst them is the bismuth-film electrode (BiFE) which compares well with mercury electrode. Moreover, it is environmentally friendlier owing to the lower toxicity of bismuth (and its salts) and thus has been used widely for trace heavy metal analysis by ASV [20-23].

UNIVERSITY of the
WESTERN CAPE

More recently, the performance of an antimony-film electrode (SbFE), has been suggested to be similar to MFEs and BiFEs in ASV [24]. At present there is not much toxicological data regarding the health effects of antimony and its compounds, but their toxicity is highly dependent on the speciation. The related data published by various governing bodies show that SbFEs are environmentally friendlier than MFEs and also much less toxic [24].

1.1.2 Graphene

Graphene, a two-dimensional (2D) honey-comb lattice of carbon atoms [25] has recently appeared as an exciting material for electronics due to awesome electron transporter movement in bulk graphene [26], low density and large specific surface area [27]. Graphene acts like massless relativistic Dirac fermions with vanishing density of states due to unusual

energy dispersion relations, the low-lying electrons in single layer [25]. However, it is a very important material not only for fundamental research but also for device applications [28] and, since its production in 2004 it has shown to improve the sensitivity in various applications [28].

Much research regarding the growth and exfoliation of graphene has been reported [29-33] The most efficient and consistent method to produce high-quality graphene sheets is by micromechanical cleavage [33]. The disadvantage of this method is its low yield, which makes it unfit for large-scale applications and as a consequence, working with chemically modified forms of graphene was proposed as an alternative. Exfoliation of graphite oxide (GO) whether by fast thermal extension or ultrasonic dispersion has been one of the best approaches to obtain graphene in bulk [34-35]. Graphite oxide is easy to disperse in water or organic solvents with sonication forming single layers of graphene oxide (GO) in solution. The GO can be treated further by reacting it with various reducing agents (e.g. hydrazine or $NaBH_4$), thermal expansion and electrochemical reduction to yield the reduced graphene oxide (RGO). The reduced graphene oxide (RGO) has excellent electronic properties and is often referred to as graphene, since it has a wider layer distance and better conductivity than graphitic nano-sheets [36]. In comparison to other production techniques, this method is best because of its reliability, amenability to large-scale production and exceptionally low material costs [37].

UNIVERSITY of the
WESTERN CAPE

1.2 Rationale and motivation

Amongst all the classes of contaminants introduced into the environment by human activities the trace metals continuously increase in the environment. It is well-known that heavy metal ions are deleterious to human health for example excessive Pb^{2+} can lead to a wide range of health problems, such as nausea, convulsions, coma, renal failure, cancer, and negative effects on metabolism and intelligence [38-40]. The stripping voltammetric techniques are

suitable for the determination of ultra-low levels of trace metals include anodic stripping voltammetry (ASV) and adsorptive cathodic stripping voltammetry (AdCSV). The first available electrode used in anodic stripping voltammetry was the mercury electrodes which include the dropping mercury electrode and mercury thin film electrode. They have advantages in the determination of trace metals due to the wide cathodic potential range and really good reproducibility [41]. However, mercury is a highly toxic metal and hence several new types of metal film electrodes have come into use to replace it. The bismuth film electrode (BiFE) and antimony film electrode have been drawing increasing attention in the field of stripping analysis due to their low toxicity and many other advantages they have, which has proved to be equal to or even more superior to that of the mercury film electrodes [20, 42]. Recently graphene has been used improve the sensitivity of metal detection due to its unusual electronic, thermal and mechanical properties [43-48]. Wang's group [49-50] have confirmed the usefulness of the graphene nano-sheets in developing a high-sensitivity sensor for the determination of lead and cadmium ions. Khomyakov *et al.* [51] evidenced the interaction and charge transfer between graphene and metal ions and concluded that the interaction and the charge transfer between graphene and metal ions made the modified electrode very sensitive.

UNIVERSITY of the
WESTERN CAPE

Previous researchers have shown that graphene mixed with binding agents such as nafion and then drop coating it onto GCEs surfaces have successfully been used to detect trace heavy metals in water samples [50,52]. Hong An Wong *et al.* has shown that a glassy carbon electrode (GCE) modified only with graphene without any binding agents can be used for the determination of cadmium [53].

In this project the idea of avoiding a binding agent is expanded by modifying the GCE with graphene alone followed by *in situ* coating with a various thin metal films namely, Hg, Bi and Sb. The modified GCEs will be investigated for their applicability in trace metals analysis.

Improved detection limits may be expected when a "binder free" graphene modified glassy carbon-thin film electrode (GC-Gr-MFE) is used.

1.3 Objectives

The focus of this study is to synthesize and characterize graphene and investigate its applicability towards the detection of selected heavy metals at various metal thin film electrodes. To achieve this, the following must be met:

(i) Synthesis of graphene by subjecting graphite to a harsh oxidation process using H_2SO_4 and $KMnO_4$, to produce graphite oxide, which is then in turn is reduced with $NaBH_4$ to graphene.

(ii) To characterize graphene using FT-IR, XRD, TEM, SEM and Raman spectroscopy.

(iii) Modify the GCE with the graphene and electrochemically deposit a metal thin film (Hg, Bi or Sb) onto the graphene surface and investigate the modified electrode's applicability towards the detection of trace metals.

UNIVERSITY of the
WESTERN CAPE

(iv) To conduct a comparative study of the different graphene metal film electrodes.

(v) Conduct recovery studies to establish the accuracy of the analysis in test solutions, followed by real sample analysis.

1.4 Thesis structure

This thesis is comprises of five chapters and is structured as follows:

Chapter 1 - Introduction

Chapter 1 gives an introduction to stripping analysis and graphene. The rationale and motivation of this project are also given as well as, the objectives that need to be met.

Chapter 2 - Literature review

Chapter 2 presents a review of the literature, which covers relevant aspects of graphene, trace metals and stripping voltammetry; as well as the characterization techniques used to characterize graphene.

Chapter 3 - Materials and method

Chapter 3 gives an account on the specific equipment used in the analysis, before explaining in detail the protocols involved in the synthesis, characterization, electrode preparation and electrochemical analysis.

Chapter 4 - Results and discussion

Chapter 4 presents the results and discussion with relevant references to literature. The main trends of the results are discussed and connecting the results with the literature and any correlation that has emerged in the data are highlighted.

Chapter 5 - Conclusion and future work

Chapter 5 concludes this thesis by summarizing the main points highlights the novelty of the research and, provides conclusions and recommendations as well as future work.

UNIVERSITY of the
WESTERN CAPE

Chapter 6 - References

Chapter 6 lists the references that were consulted during this project.

CHAPTER 2

Literature Review

2.1 General basis for voltammetry

2.1.1 Voltammetry

Voltammetry is a section of electrochemistry developed from the discovery of polarography in 1922 by the Czech chemist Jaroslav Heyrovsky. In earlier times voltammetric methods experienced many of difficulties and limitations, making them less than ideal for routine analytical analysis. Some of the difficulties of the method were slowness, inconvenient apparatus and more importantly, low detection limits. However, in the 1960s and 1970s major improvements in theory, methodology and instrumentation of voltammetry were made which resulted in improved sensitivity [54]. Furthermore, voltammetric analysis methods nowadays make use various potential stepping and current sampling strategies which can differentiate between faradaic and non-faradaic processes and, thus lead to improved detection limits [55]. In all voltammetric methods a variable excitation signal is imposed on a working electrode in an electrochemical cell and in turn produces a current response which is then measured [56]. The electrochemical cell consists of a working electrode, reference electrode, auxiliary electrode and a non-reactive electrolyte or supporting electrolyte [57]. The working electrode which is usually made of platinum, gold, silver, glassy carbon, nickel, or palladium [58], offers the surface for electron transfer to occur for the system under investigation [59]. A reference electrode is used to measure the working electrode potential of an electrochemical cell of which, the saturated calomel electrode (SCE) and the silver/silver chloride (Ag/AgCl) electrodes are the most common [60]. The third electrode called the auxiliary electrode is used only to make an electrical connection to the electrolyte so that a current can be applied

UNIVERSITY of the
WESTERN CAPE

to the working electrode; these electrodes are commonly made of noble metals or carbon/graphite [61].

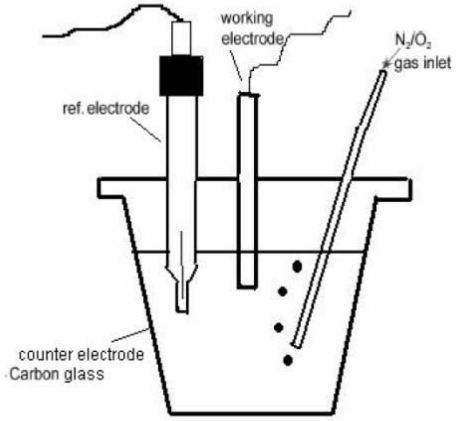

Figure 2.1: Three electrode system for voltammetry

2.1.2 Stripping voltammetry

Stripping voltammetry is a suitable electroanalytical technique for determining ultra-low levels of trace metals and there have been many new developments in stripping voltammetry over the past 25 years. Some of the advantages of stripping voltammetry are its very low detection limits (10^{-10} - 10^{-12} M), its multi-element and speciation capabilities and *in-situ* applications [62]. In general, the stripping voltammetry experiment consists of three steps these are; the deposition (or pre-concentration) step the equilibration step (or quiet time) and the stripping step [63].

Metal ions in solution are accumulated (deposited) onto or in a working electrode which is fixed at the reduction potential of the metal being analyzed. This potential is referred to as the "deposition potential" and the time in which deposition occurs is the "deposition time". The solution is stirred at a constant rate during deposition so that the maximum amount of metal is deposited onto the working electrode. In the second step, the stirring is stopped and the solution becomes quiet (quiet time) allowing for homogeneous dispersal of the analyte to

occur and to allow for the restoration of calm solution conditions to return. The final step (stripping step) involves the stripping out of the metals from the working electrode back into the solution at their characteristic half-wave potentials. The current observed during the stripping step can be related to the amount of metal ion present in the solution. There are various types of stripping analysis techniques namely, anodic stripping voltammetry, cathodic stripping voltammetry and adsorptive stripping voltammetry [64].

2.2. The various types of stripping analysis techniques

2.2.1 Anodic stripping voltammetry (ASV)

Anodic stripping voltammetry (ASV) is one of the most sensitive well- established and widely used voltammetric techniques. In ASV the potential is held at a negative potential followed by scanning in a positive direction [65]. Due to its comparatively low cost, small size and portability the equipment has become widely used for the determination of heavy metals [66]. The enhanced sensitivity is attributed to the pre-concentration step in the measurement procedure. During ASV analysis, a deposition or pre-concentration step is carried out under conditions of forced convection, which may include solution stirring or flow. During this step the metal ions are collected usually in the Hg by reduction to a metallic state and amalgamation with the Hg [62]. This is followed by metals being stripped out anodically from the mercury amalgam back into solution. The mechanism can be described as follows:

UNIVERSITY of the
WESTERN CAPE

Deposition: $M^{n+} + ne \rightarrow M\ (Hg)$

Stripping step: $M\ (Hg) \rightarrow M^{n+} + ne$

2.2.2 Cathodic stripping voltammetry (CSV)

Cathodic stripping voltammetry (CSV) is a very sensitive technique for the analysis of a

variety of organic and inorganic compounds. It is similar to ASV, except that for the deposition step, the potential is detained at an oxidizing potential; the oxidized species are then stripped from the electrode surface by sweeping the potential positively. CSV can be used to determine those metals that form insoluble salts with mercurous ions. Application of a relatively positive potential to a mercury electrode in a solution containing such substances will result in the formation of an insoluble film on the mercury electrode surface. The potential scan in the negative direction will then strip (reduce) the deposited film form the electrode into the solution [65]. The mechanism can be described as follows:

Deposition: $M \rightarrow M^{n+}$ ne

$M^{n+} + A^{n-} \rightarrow MA$

Stripping step: $MA + ne \rightarrow M + A^{n}$

2.2.3 Adsorptive stripping voltammetry (AdSV)

UNIVERSITY of the
WESTERN CAPE

The AdSV method is characterized by the non-electrolytic nature of the accumulation process, where adsorption plays an important role. The adsorption of the analyte itself is however, not the only way of accumulation in AdSV. The reaction of a metal ion to be determined with a suitable reagent may lead to the formation of a complex which is adsorbed on the surface of the electrode. In AdSV determinations of reducible organic compounds the deposit is stripped off during a cathodic potential scan similarly as in CSV [67].

2.3 Why use stripping voltammetry (SV)

Stripping analysis is capable of measuring four to six trace metals simultaneously in the sub-parts per billion ranges. Its instrumentation is inexpensive and small in size. This technique also has a low power demand (small carbon footprint), requires no additional instrumentation or special installation [12]. No other technique for trace metal analysis can compete with

stripping analysis on the basis of sensitivity per money invested. Other advantages of stripping analysis include species characterization, its suitability for automatic on-line monitoring and for *in situ* measurements. Figure 2.2 indicates the different detection limits for different metal analysis techniques [68].

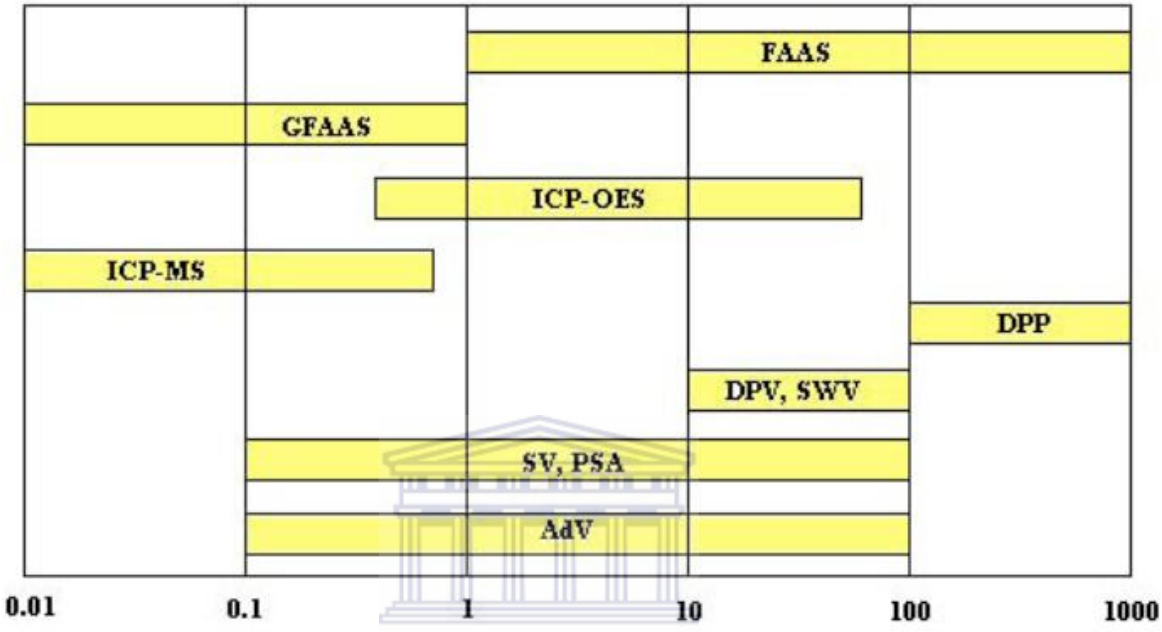

UNIVERSITY of the
WESTERN CAPE

Figure 2.2: Detection limits (μg L^{-1}) of the principal techniques for trace analysis. Refer to list of abbreviations.

2.4 Principle of stripping voltammetry

2.4.1 Deposition step

The technique of stripping voltammetry (SV) has been getting extensive attention because of low detection limits which mainly due to the pre-concentration of the analyte in accumulating metal (bismuth, antimony or mercury), under a specific reduction potential for a predetermined time [13-14]. During the deposition step the analyte of interest is electroplated onto/into the working electrode forming an amalgam with the metal film. In the anodic

variant of stripping analysis the analyte is accumulated by their reduction into or onto the working electrode and as for the cathodic variant of stripping analysis, it utilizes the deposition of various organic and inorganic species as sparingly soluble compounds on the surface of the electrode. Whichever method is employed, the deposition potential imposed on the working electrode depends on the metal ion species to be determined and is maintained for a predetermined deposition time depending on the metal ion concentration [69].

2.4.2 Quiet time

After the pre-concentration step, the stirring of the solution is stopped. The solution is allowed to become quiet and which causes the concentration of the metal in the amalgam to reach equilibrium. The rest (equilibrium) period ranges from about 10 to 30 seconds, during which the applied potential remains unchanged, so certifying that no re-oxidation of the metal by traces of oxygen takes place [69].

UNIVERSITY of the
WESTERN CAPE

2.4.3 Stripping step

During the stripping step, the trace metals oxidize back into solution by oxidation into the ionic form:

$$M\,(Hg) \rightarrow M^{n+} + ne$$

The voltammograms recorded in the stripping step, and the analytical information about the solution structure is obtained at the second stage of determination, where the deposited concentrate is oxidized or reduced. Depending on the rule of these processes, the analytical signal can be represented by different electrochemical techniques such as linear sweep, normal pulse, differential pulse, square wave, alternating current voltammetric and potentiometric techniques. In all of these techniques, the analytical signal can be measured as the quantity of electricity, equivalent to the amount of the metals that undergoes

electrochemical transformation [65].

2.4.4 Excitation signals or waveforms

In all voltammetric methods a variable excitation signal is imposed on a working electrode in an electrochemical cell and in turn produces a current response which is then measured [56]. The excitation signal is in a waveform; the type of waveform imposed on the working electrode gives the voltammetric technique its classification. Furthermore, by applying various waveforms better discrimination between faradaic and non-faradaic (capacitative) currents are achieved which result in better sensitivities and detection limits. In the following section some of the commonly used excitation signals (waveforms) are discussed.

2.4.4.1 Linear sweep stripping voltammetry (LSSV)

Linear sweep voltammetry is a common phrase used to describe a voltammetric method in which applied the potential to the working electrode changes linearly with time [70]. The scanning starts before the discharging potential and stops afterwards. The voltage (v) is calculated from the slope of the line. At higher scan rates the faradaic current is found to increase, owing to the amplified flux of electroactive material to the electrode at the higher scan rates [70]. It is important to note that factors such as; the rate of electron transfer reactions, the chemical reactivity of the electroactive species and the voltage scan rate affect the characteristic shape of the linear sweep voltammogram [71].

UNIVERSITY of the
WESTERN CAPE

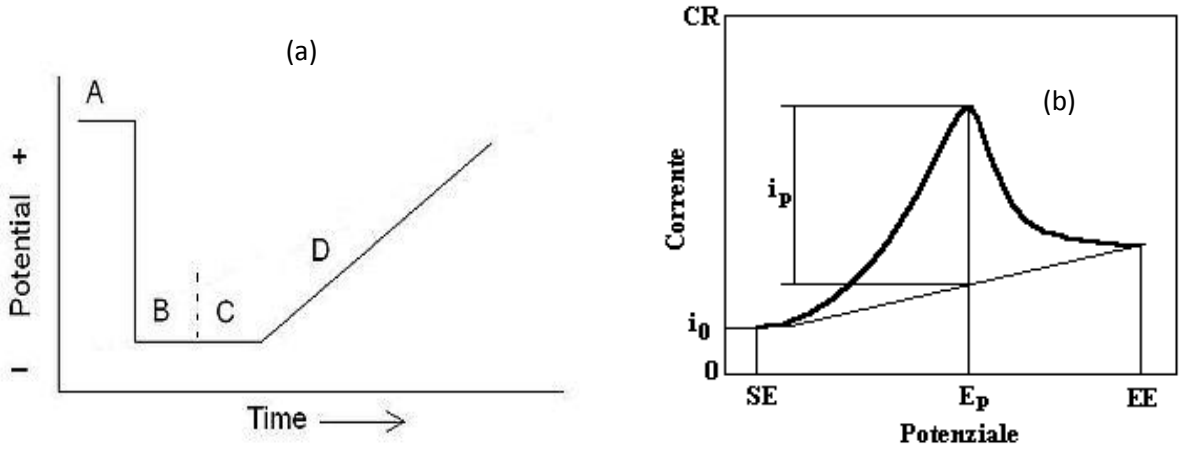

Figure 2.3: Excitation signal (a) and voltammogram (b) for Linear sweep stripping voltammetry (LSSV)

2.4.4.2 Normal pulse stripping voltammetry (NPSV)

Normal pulse stripping voltammetry is the classic pulse voltammetric measurement mode with direct recording of the current. For NP voltammetry, square-wave pulses with increasing amplitude are superimposed on a constant base voltage. The current *i* is measured as a function of the voltage *E* at the end of the pulse. This normally provides wave-shaped curves which can be evaluated using the tangent method [72].

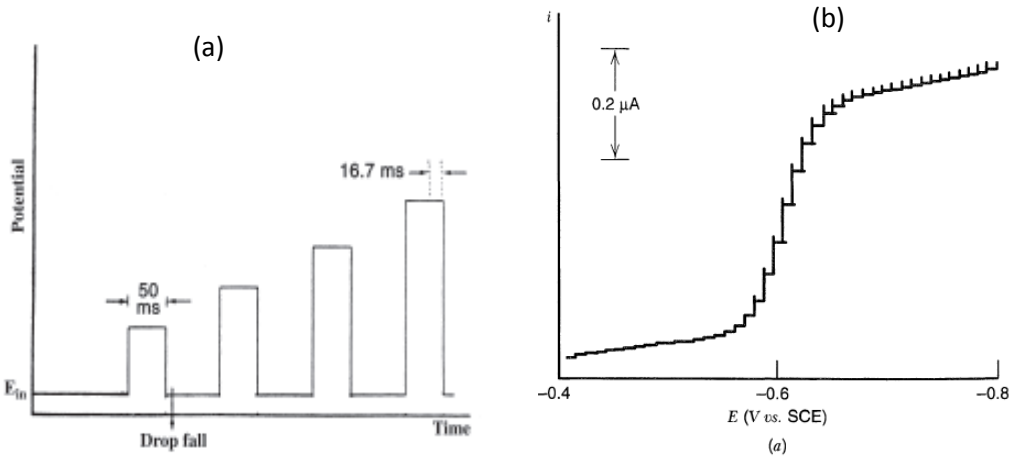

Figure 2.1: Excitation signal (a) and voltammogram (b) for normal pulse stripping voltammetry

2.4.4.3 Differential pulse stripping voltammetry (DPSV)

Differential pulse voltammetry is the most universal and frequently used for irreversible and reversible systems and offers a high sensitivity. For DP voltammetry, rectangular pulses with constant amplitude are superimposed on a stepwise rising direct voltage ramp. The current *i* is measured as a function of the voltage, *E* immediately before the pulse and at the end of the pulse. From the differences between the two current measurements, peak-shape curves are obtained which are evaluated using linear, polynomial, horizontal or exponential baselines [72].

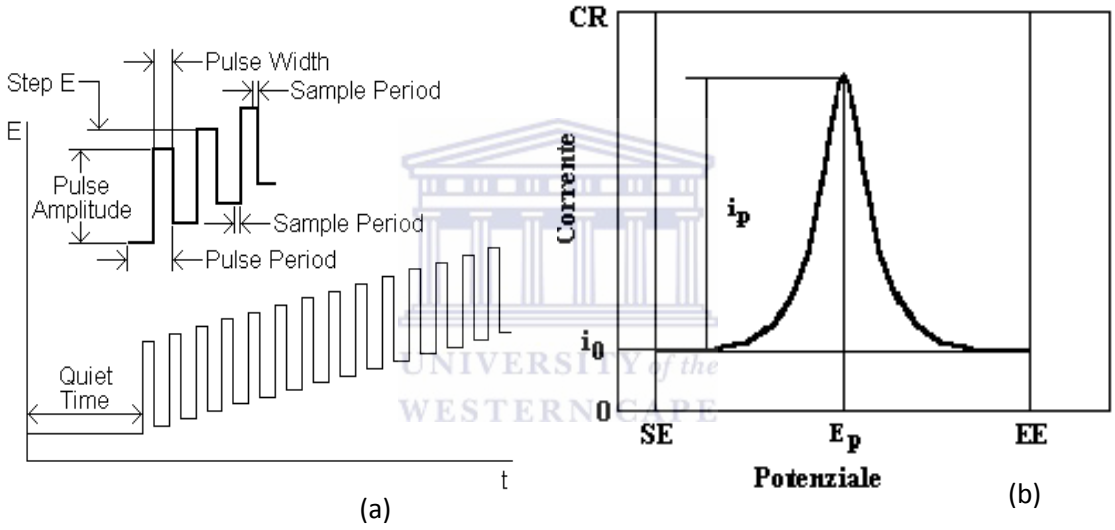

Figure 2.2: Excitation signal (a) and voltammogram (b) for differential pulse stripping voltammetry

2.4.4.4 Square wave stripping voltammetry (SWSV)

Square wave stripping voltammetry is primarily suitable for the reversible electrode processes. It is used particularly for sensitive stripping voltammetric determination at the HMDE or Rotating Disk Electrodes (RDE). For SWSV, a square wave alternating voltage with small, constant amplitude is superimposed on a stepwise rising direct voltage ramp. The current *i* is measured as a function of the voltage *E* at the maximum (*i*2) and minimum (*i*1) of

the square wave voltage [72].

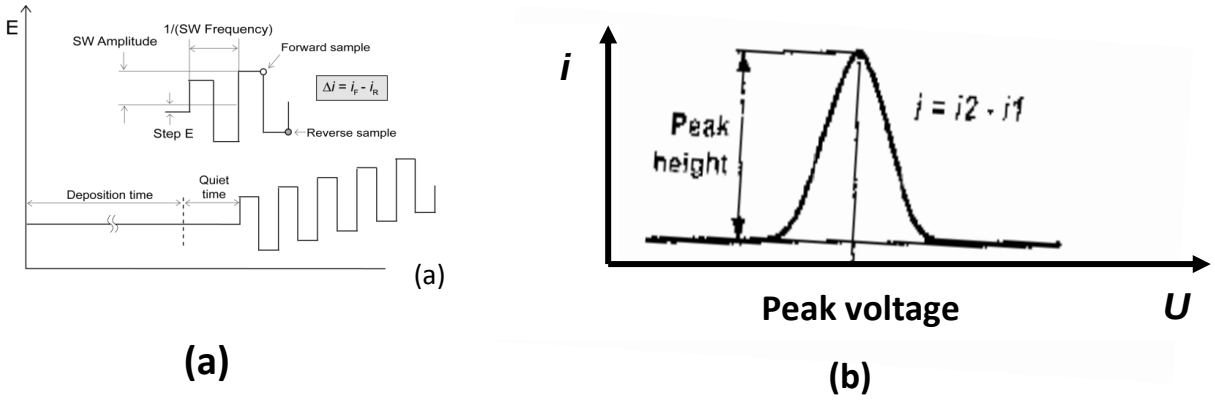

Figure 2.3: Excitation signal (a) and voltammogram (b) for Square wave stripping voltammetry

2.5 Working electrode types in stripping analysis

The working electrode is the electrode in an electrochemical system at which the reaction of interest takes place [73-74]. In addition to the HMDE, the thin metal-film electrodes have become widely used in electrochemical stripping analysis due to their relatively simple fabrication and surface regeneration [75].

2.5.1 The hanging mercury drop electrode (HMDE)

HMDEs have been extensively used for striping voltammetry. The automatic HMDE and the rotating Hg coated electrodes are particularly suitable for stripping voltammetry. The advantage of an HMDE is its reliability. With the formation of a new drop each time, a new electrode surface is produced, which is important for unattended trace metal monitoring activities. The drops generated by modern Hg drop electrodes are very small (e.g. VA Stand 663 from Metrohm (Switzerland) produces drops with an area of 0.52 mm^2, and safe storage and recycling of the used Hg ensures minimal environmental risks [76].

The HMDE finds wide applicability, in conjunction with stripping techniques for the

determination of metals such as lead [77-80], copper [81], cadmium [77-80], zinc [77-78], indium [80], cobalt, nickel[82], gallium, uranium [81, 83], platinum, selenium [84] and molybdenum. In conjunction with these, it has attracted a significant amount of attention for speciation studies of metals in natural waters [82,85-87].

2.5.2 Thin mercury film electrode (TMFE)

Mercury thin film electrodes (MTFEs) are widely used for anodic stripping voltammetric (ASV) determination of mercury soluble trace elements [88]. The film is deposited on an inert substrate, typically, a glassy carbon electrode (GCE). MTFEs may be prepared in a pure mercury(II) solution (*ex situ*), after which the electrode is transferred into the sample solution or, they may be formed *in situ* by simply adding mercury(II) ions into the medium to be analyzed. The rate of mercury deposition is a function of the pH of the electrolyte, deposition potential, stirring rate and mercury ion concentration. Optical examinations of the mercury film electrodes revealed the formation of fewer and larger drops instead of a homogeneous film [89].

UNIVERSITY of the
WESTERN CAPE

Glassy carbon has been the electrode of choice for the vast majority of work involving MTFEs, for the following reasons:

(i) Due to its non-metallic nature, its degree of interaction with the deposited mercury is extremely low.

(ii) Glassy carbon has a high over-potential for hydrogen reduction. This is an important consideration since, as noted by Yoshida [90], electrodes such as glassy carbon, when coated with mercury, have a hydrogen over-potential which is largely determined by the electrochemical properties of the substrate.

(iii) The glassy carbon surface is easily renewed by mechanical polishing with diamond laps or alumina unlike the softer metallic substrates [90].

Furthermore, metallic substrates such as silver [91-92], platinum [93], copper [94], gold, nickel, lead and stainless steel [90] have also been used as substrates for MTFEs, although they have not found wide applicability.

2.5.3 Bismuth film electrode (BiFE)

The bismuth film electrode (BiFE), as one of the possible alternatives to mercury film electrodes, was applied to stripping analysis in 2000. The number of the related publications has been increasing and the stripping voltammetric applications of the bismuth film electrodes has become one of the most concentrated research fields in electroanalytical chemistry. The behavior of bismuth electrodes has been shown to compare favorably to that of mercury electrodes, with brilliant properties such as high sensitivity, well-defined stripping signals, good resolution of neighbouring peaks, wide cathodic potential range and insensitivity to dissolved oxygen. The advantageous properties of bismuth are attributed to its remarkable low toxicity and its ability to form alloys with heavy metals [95-99] as a result, *in situ* as well as *ex situ* formed BiFE have been studied [100]. Many different types of materials have been used as substrates for BiFE, including glassy carbon [97], wax- impregnated graphite carbon paste [101], and carbon fibers [100].

UNIVERSITY of the
WESTERN CAPE

2.5.4 Antimony film electrode (SbFE)

The use of antimony as electrode material for pH measurements was first reported in 1923 [102], followed by other contributions using antimony microelectrodes. More recently, the antimony-film electrode (SbFE), has been claimed to perform on a par with MFEs and BiFEs in ASV [103]. The SbFE features some interesting characteristics such as, favorable negative over-voltage of hydrogen evolution, wide operational potential window and interestingly low stripping signal for antimony itself [104]. The available toxicological data regarding the health effects of antimony and its compounds are limited and inconclusive, but toxicity is

highly dependent on the speciation [105]. The relevant data published by different regulatory agencies indicate that antimony is much less toxic than mercury and therefore SbFEs are more environmentally friendly than MFEs [105]. In the past, antimony/antimony oxide electrodes were used as potentiometric sensors for measuring pH. Interestingly, there has very small number of works concerning successful application of the antimony-film electrode for electrochemical stripping analysis of trace heavy metals. Recently, Hocevar *et al.* and Svancara *et al*. [106], published a report on initial investigations of antimony-film electrode, revealing an attractive electroanalytical performance for measuring trace heavy metals in media with higher acidity (pH $\leq$ 2) in combination with ASV or stripping chronopotentiometry [103, 106].

2.6 Applications of stripping analysis

The remarkable sensitivity, broad scope, and low cost of stripping analysis have led to its application in a large number of analytical challenges The technique has proved useful for the determination of numerous trace metals in environmental, industrial and clinical samples, as well as for assays of foodstuffs, beverages, gunshot residues, and pharmaceutical formulations [107].

2.6.1 Environmental analysis

Reliable analytical measurements of environmental samples is a very important and an essential part of sound decision making involving various aspects for society safeguarding public health, facilitating advances in technology and improving the quality of the environment [12]. Unlike any other pollutants, heavy metals may be the most harmful due to the fact that they are not biodegradable and are retained in the ecosystem indefinitely. Heavy metals are present in water; air and soil are a consequence of both natural and anthropogenic sources.

2.6.1.1 Water analysis

The determination and the speciation of dissolved trace metals in environmental aquatic systems is essential because of their toxicity (through biomagnification) or to investigate their geochemistry [108-109]. Although there are a variety of analytical techniques available for trace metal analysis, anodic stripping voltammetry (ASV) with its range of scanning operating modes, is an alternative technique for determining dissolved trace metals in natural water systems. This is due to its low detection limit and specific sensitivity for different chemical forms of dissolved metals [12, 110], and it requires no chemical pre-concentration by the additional addition of other chemical reagents [110-112]. As a consequence of the many contributions by researchers and their ASV measurements, the technique has been widely used for measuring normal and pollution levels of more than 15 trace metals in different types of natural waters, such as oceans, rivers and lakes, of which some of these are toxic or important micronutrient elements [12].

UNIVERSITY of the
WESTERN CAPE

2.6.1.2 Other environmental applications

Several other environmental applications in addition to water applications have been reported with stripping voltammetry such as for heavy metals in, fly ash, airborne particulate matter, rocks, minerals and sediments. Khandekar *et al.*[113] used anodic stripping voltammetry for cadmium, zinc and lead in airborne particulates collected at various locations around Bombay. ASV was preferred over other techniques such as neutron activation and atomic absorption spectroscopy because of its ability to measure various metals simultaneously at the ultra-trace level.

2.6.1.3 Clinical analysis

In the case of the analysis of drugs it is important to monitor contamination by unsolicited

potentially toxic elements and to confirm that the tablets or formulations contain the correct amount of active ingredient [114-118]. For both purposes stripping voltammetry techniques have provoked particular interest because of its high sensitivity. However, since the ionic levels in the preparations are often high, the rotating mercury film electrode on glassy carbon, together with anodic stripping voltammetry, seem to provide the best results for studies on seawater or fly ash [119].

2.7. Graphene

2.7.1 Discovery of graphene

Graphene was first discovered by Novoselov and Geim in 2004 [120]. Graphene can be viewed as a monoatomic plane of carbon atoms arranged hexagonally in a 2D honeycomb lattice. The basic building block for all graphitic materials of other dimensionalities is graphene because the 2D material can be wrapped up into 0D fullerenes, rolled into 1D nanotubes or stacked into 3D graphite as shown in Figure 2.2 [121]. For example, graphite is a stack of graphene planes weakly held by van der Waals forces and hence graphene has been used historically to understand and predict the properties of graphite. Even though many people are unfamiliar with graphene, they are very familiar with graphite which is graphene's 3D counterpart which is commonly used as pencil lead. Graphene sheets are thermodynamically unstable with respect to other fullerene structures if its size less than about 20 nm (''graphene is the least stable structure until about 6000 atoms'') and becomes the most stable (as within graphite) only for sizes larger than 24,000 carbon atoms [122].

UNIVERSITY of the
WESTERN CAPE

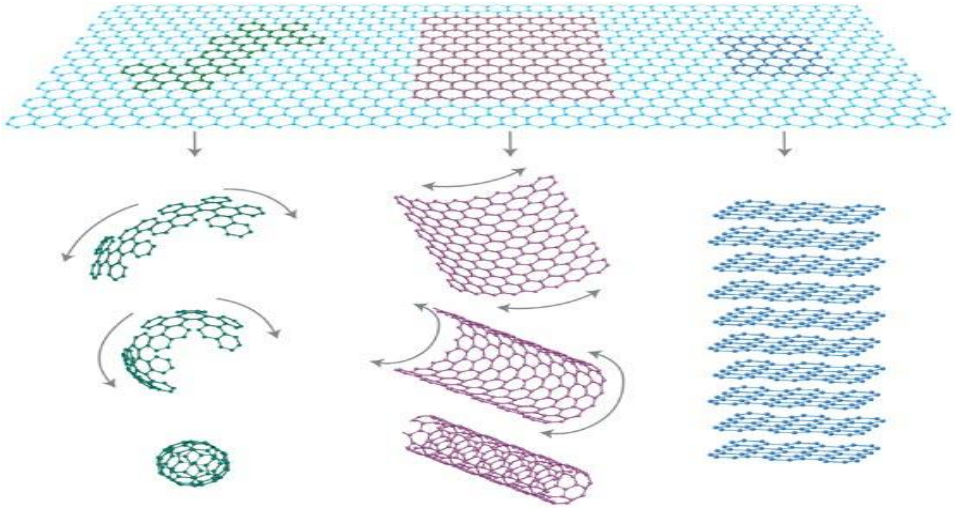

Figure 2.4: Formation of 0D, 1D and 3D materials from graphene

2.7.2 Structure and properties

UNIVERSITY of the
WESTERN CAPE

Graphene a one atom thick substance, made up of carbon atoms arranged in a honeycomb lattice (Figure 2.3) with the carbon-carbon bond length being approximately 0.142 nm. The carbon atoms have four valence electrons, bond together with three symmetric sp^3 orbitals. In graphene the 2s, $2p_x$ and $2p_y$ orbitals hybridize to form three new planar sp^2 orbitals each containing one electron. These orbitals are directed along lines with angles of 120° and form sigma bonds (σ-bonds) with other carbon atoms and, are responsible for the hexagonal lattice structure of graphene. Furthermore, the non-hybridized $2p_z$ orbital is oriented perpendicular to the plane overlap with the $2p_z$ orbitals of other carbon atoms forming π-bonds and electrons in them are responsible for electrical conduction in graphene and graphite [123] .

The band structure of graphene was first predicted in 1947 by Wallace [124] , shows a linear dispersive relationship between the energy of the π electrons and their wave vector in the crystal lattice. This gives rise to the unusual massless Dirac fermion behaviour of the electrons [125-126] . Graphene recently appeared as an exciting material for electronics due to its fast electron movement, current-carrying capacity [27], low density, large specific

surface area [28], thermal and mechanical properties[29-33].

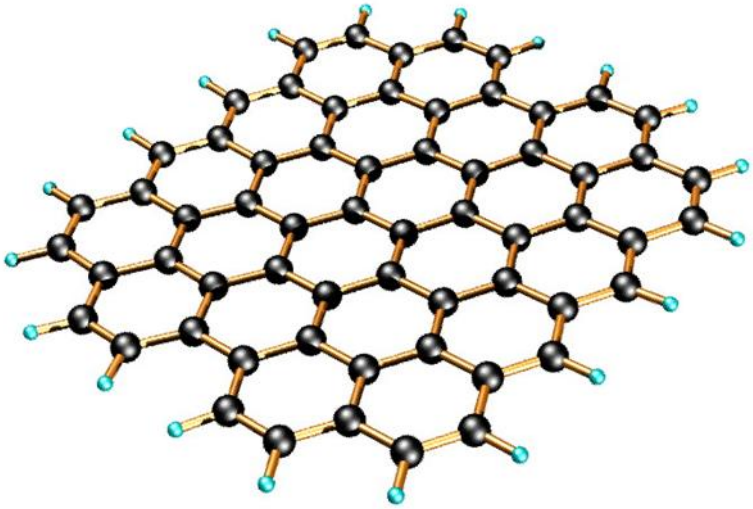

Figure 2.5: Structure of graphene

UNIVERSITY of the
WESTERN CAPE

2.7.2.1 Electronic properties

The electronic properties of graphene are determined by the bonding π and antibonding π^* orbitals that form the electronic valence conduction bands for graphene. In graphene the π and π^* bands touch at the corners of the 2D hexagonal [127-128], and are labeled by momentum vectors denoted by K and K′ as shown in Figure 2.4. The Femi surface of graphene is reduced to these six corner points where the cones of carrier touch are referred to as the "Dirac" points. Thus, the graphene is a semi-metal or zero band gap semiconductor [129]. Researchers at The University of Manchester have found that electrons move more easily in graphene than in all other materials, including gold, silicon, gallium arsenide and carbon nanotubes [130], and, have singled out graphene as the "best possible" material for electronic applications. Graphene has a high electronic quality, measured at around 200,000 cm^2/Vs, which is a 100 times higher than for silicon, these researchers believe graphene has the potential to improve upon the capabilities of current semiconductors and open up exciting

new possibilities [131].

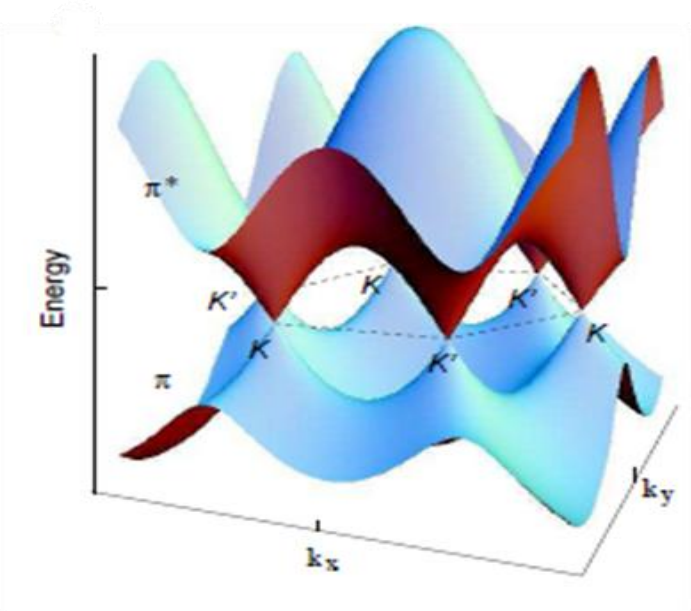

Figure 2.6: Energy dispersion as a function of the wave-vector components k_x and k_y. the valence (π) band is distinguished from the conduction (π^*) band. The Fermi level is situated at the points where the π band touches the π^* band [132].

UNIVERSITY of the
WESTERN CAPE

2.7.2.2 Mechanical properties

The strong C-C bond in graphene covalently locks carbon atoms in place giving them outstanding mechanical properties [123, 133]. The chemical bond strength plays a strong role in the physical and mechanical properties of a material such as; melting point, activation energy of phase transition, tensile and shear strength and, hardness [134]. As of 2009, graphene appears to be one of the strongest materials ever tested. Measurements have shown that graphene has a breaking strength 200 times greater than that of steel [123]. One of the more significant aspects in determining bond strength is the degree of overlap between atomic orbitals and a key advantage of hybridized systems is that, maximum overlapping occurs resulting in very strong bonds [134].

2.7.2.3 Optical properties

Many reports confirmed that single layer graphene absorbs 2.3% of incident light over a broad wavelength range in spite of being just a monolayer [135-136]. Graphene shows spectacular optical properties and absorbs considerable amounts of infrared radiation without bandwidth limitation [137]. Graphene is efficiently utilized as an absorber in mode-locked carbon laser [138] and its unique optical properties of renders it a promising candidate for optical fibers, telecommunication devices and photonic application [138-139].

2.7.2.4 Thermal properties

Another exciting property of graphene is its thermal properties. The thermal conductivity of graphene was recently measured to be between 4.84×10^{3} and 5.3×10^{3} Wm^{-1} K^{-1} which is higher than that of carbon nanotubes or diamond [46]. Graphene, though, unlike diamond is a two dimensional crystal and offers tantalizing opportunities for heat management in various areas, for example, it holds promise as a heat spreader in microelectronics system [134]. Graphite, the 3D version of graphene that has basal plane thermal conductivity is over a 1000 $Wm^{-1}K^{-1}$ (comparable to diamond). In graphite, the c-axis (out of plane) thermal conductivity is over a factor of ~100 smaller due to the weak binding forces between basal plane as well as the larger lattice spacing [140].

UNIVERSITY of the
WESTERN CAPE

2.7.3 Synthesis of graphene

Various attempts have been made to synthesize graphene to improve the quality of samples or to increase the cost-efficiency of the synthesis including; chemical vapor deposition on metal, the thermal decomposition of SiC the mechanical exfoliation of graphite and exfoliation of Graphite oxide.

2.7.3.1 Mechanical exfoliation of graphite

To exfoliate graphite using mechanical exfoliation a small piece of graphite flake is placed on Scotch tape and peeled several times [120]. Each time the flake splits into thinner flakes. The removed layers are then pressed onto a silicon wafer with an oxide layer. A silicon wafer with 300 nm of silicon dioxide is a preferred substrate to get the maximum contrast and thus make the visual detection of graphene easier. After several presses, a few single layers of graphene eventually adhere to the wafer. Most of these areas are in the order of microns in size or less. The disadvantage though is that it is very time consuming to find where the graphene is and, it is also labor intensive which is not good for industrial scale preparation.

2.7.3.2 Chemical vapour deposition (CVD) graphene

In 2009, Kim *et al.* [141] developed a procedure to grow graphene on a 300 nm- thick nickel film deposited on silicon wafer with an oxide layer by heating the substrate to 1000 $^{\circ}$C, then followed by passing methane, argon and hydrogen gases over the sample. They were successful in creating few- layer graphene and demonstrated the ability to transfer the graphene to other substrates. Li *et al.* [142] addressed this issue by growing graphene on a metal catalyst, 25 μm copper foil, at the same temperature of 1000 $^{\circ}$C but under pressure (~ 40 m Torr). No further treatment of graphene films were necessary and it exhibited outstanding properties in terms of optical transparency and electrical conductivity. The method is great for making large amounts of film and it requires very little labor. However, it often makes unpredictably arranged multilayers, with defects that are linked to the substrate being used. Another disadvantage is the metal surfaces on which this method works best are not what graphene devices should be built on.

UNIVERSITY of the
WESTERN CAPE

2.7.3.3 Exfoliation of graphite oxide

One possible route is towards the synthesis graphene is by the oxidation of graphite to suspensions of graphene oxide followed by reduction of these suspensions. The oxidation of graphite typically occurs in strong acids and oxidants such as sulfuric acid (H_2SO_4), sodium nitrate ($NaNO_3$) and potassium permanganate ($KMnO_4$) [143]. Sonication following the chemical modification releases the adhesive force between flakes resulting in a suspension of hydrophilic graphene oxide nano-platelets. These graphene oxide platelets can then be reduced to graphene *via* thermal, UV, or chemical methods [125]. The structure of GO contains epoxide functional groups along the basal plane of the sheets as well as carbonyl and hydroxyl moieties along the edges (Figure 2.4). The chemically converted graphene oxide is reduced by either hydrazine or sodium borohydride. The properties of chemically converted graphene can never truly be the same as those of graphene because, the oxidation to GO introduces defects and also chemical reduction does not fully restore the graphitic structure [144]. This method is more versatile than the epitaxial method, less time consuming and easier to scale up than mechanical exfoliation methods. The disadvantage though is the difficulty to keep the graphene solution free from re-aggregating into graphite, after reduction. Furthermore the graphene layers are partially oxidized, which could potentially result in changes in the electronic, optical and mechanical properties.

UNIVERSITY of the
WESTERN CAPE

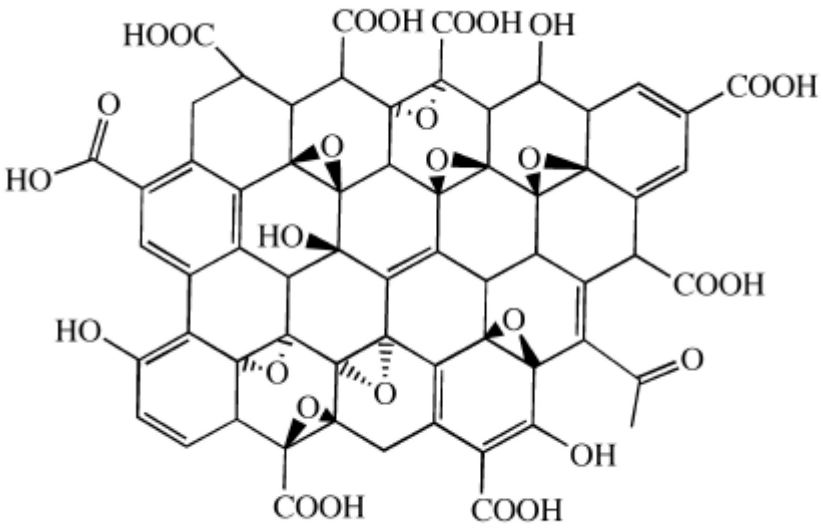

Figure 2.7: Idealized structure proposed for graphene oxide (GO). Adapted from C. E. Hamilton, PhD Thesis, Rice University (2009).

UNIVERSITY of the

2.7.3.4 Epitaxial graphene

Single and few-layer graphene can be grown over entire single- crystal wafers of SiC. This method is one such method by which to do this and is compatible with existing industrial wafer technologies. Producing graphene through ultra-high vacuum (UHV) annealing of the SiC surface has been an attractive approach especially, for semiconductor industries because the products are obtained on SiC substrates and requires no transfer before processing devices [145-148]. SiC has several polytypes which refer to the type of z-axis stacking of bilayers consisting of Si and C atoms [149]. In epitaxial graphene growth, a SiC wafer is heated in ultra-high vacuum to 1200-1700 ºC. Sublimation of the silicon at this temperature results in a formation of graphene on the surface of the wafer. The thickness of graphene layers depends on the annealing time and temperature. The formation of ‘‘few-layer graphene’’ (FLG) typically requires a few minutes of annealing of the SiC surface at temperature of approximately 1200 ºC [150].

2.7.4 Characterization techniques for graphene and graphene oxide

A variety of characterization techniques can be used to characterize graphene, each provide complementary information. Hereunder, are the methods that have been used for this project *i.e.* Fourier transformed infrared spectroscopy (FT-IR), x-ray diffraction (XRD), Raman spectroscopy, Transmission electron microscopy (TEM) and scanning electron microscopy (SEM).

2.7.4.1 Fourier transformed infrared spectroscopy (FT-IR)

Fourier transformed infrared spectroscopy (FT-IR) is more generally applicable towards graphene and graphene oxide, since it does not require a UV chromophore, but rather requires infrared light which is absorbed by the molecular bonds to cause transitions between molecular vibrational states [151]. Simply put, it is the absorption measurement of different infrared frequencies by a sample positioned in the path of an infrared beam. The main goal of IR spectroscopic analysis is to determine the chemical functional groups in the sample. The IR spectrum refers to electromagnetic waves whose wavelengths ranges from 0.78 µm 1000 µm. However the more manageable, the wavenumber unit (cm^{-1}) is generally used instead of microns thus the total IR spectrum ranges from 14,286 cm^{-1} to 28.5 cm^{-1}. The advantages of FT-IR are its superior speed, sensitivity and have been applied to many areas that are very difficult or nearly impossible to analyze by IR-dispersive instruments. Instead of viewing each component frequency sequentially, as in a dispersive IR-spectrometer, all frequencies are examined simultaneously in Fourier transform infrared (FTIR) spectroscopy [152].

UNIVERSITY of the
WESTERN CAPE

2.7.4.2 Raman spectroscopy

The Raman Effect is one of several types of interaction between light and matter. When a photon interacts with a molecule it may either be absorbed, elastically scattered or

inelastically scattered. The inelastic scattering of light is Raman scattering. Scattered photons have an energy either higher or lower than incident photon and this difference is proportional to photon energies in the material [153]. When light is incident upon a sample, there is a small, but finite probability that some of the energy in the electromagnetic field will be transferred and raise the molecules from their ground state to an exited vibrational state. The strength of this coupling is proportional to the polarizability of the molecules, and the inelastically scattered light emerges with less energy than with which it entered. This energy difference is called the Raman shift and, is traditionally expressed in units of wavenumber (cm^{-1}) [154]. The spectral features of the Raman scattered light can be used to identify molecules with high specificity. Furthermore, the Raman spectrum of a heterogeneous sample composed of several chemicals is simply a linear combination of each component chemical's Raman spectrum, with relative weighting coefficients determined by concentration and Raman scattering cross section. Raman spectroscopy can be used to study liquid, solid and gaseous samples [155], and it has been successfully utilized as a convenient technique for identifying and counting graphene layers on the Si/SiO_2 substrate [156-157].

UNIVERSITY of the
WESTERN CAPE

2.7.4.3 X-ray diffraction (XRD)

X-ray diffraction is based on the assumption that x-ray radiation with wavelengths on the order of Angstroms can elastically scatter off the electronic structure of a crystal (Figure 2.5). The periodicity of the crystal will cause this scattering of the x-ray plane-wave to constructively interfere at certain scattering directions while destructively interfering at other scattering directions [158]. The diffraction of X-rays by matter results from combinations of different phenomena namely, the scattering by each atom and interference between the waves scattered by these atoms. This interference occurs because the wave scattered by the individual atoms are coherent with the incident wave, and therefore between themselves [159].

There are two different machines used for the X-ray diffraction analysis. The first machine used is a Bruker D8 Diffractometer with general area detector diffraction system that simultaneously collects data over a range of 30 degrees 2θ and 30 degrees χ (where χ is rotation about the x-axis, and is called the title axis). Subsequent analysis is done on a PANALYTICAL X-PERT PRO Multipurpose Diffractometer, to take more accurate, longer scans. Wobble scans are done on the three specimens so that the χ title of the specimen is effectively increased 1° between each analysis, thereby examining a 5° χ title range in five different scans.

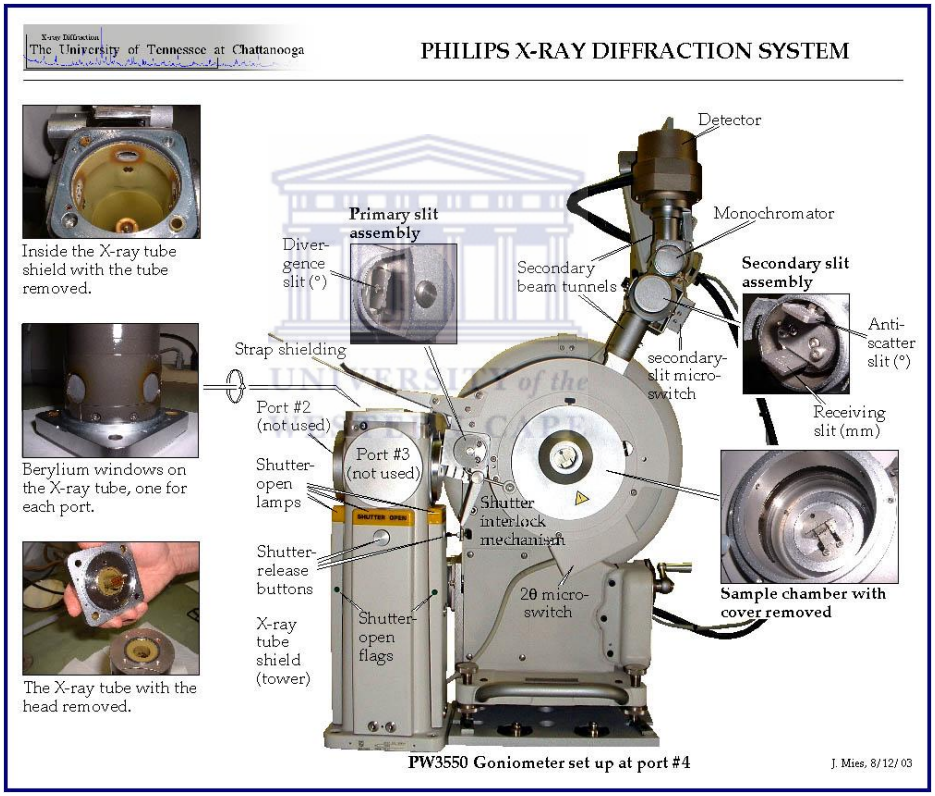

Figure 2.8: X-ray Diffraction system

2.7.4.4 Transmission electron microscopy (TEM)

Transmission electron microscopy (TEM) is a form of microscopy that uses a high energy electron beam rather than optical light (Figure 2.6). A beam of electrons are focused on a single spot or element on the sample being analyzed. The electrons interact with the sample

and those that go past unobstructed hit the phosphorous screen on the other side. The electrons are then converted to light and an image is formed. The TEM can be used for both imaging and electron diffraction analysis. The major components of a TEM are an electron source, the electromagnetic lenses for focusing the electron beam, a movable sample stage, a vacuum system and the electron detector. TEM was primary technique used to study face separation because it provides a direct view microstructure of a material. The contrast seen in a TEM image arises from strain fields or chemical modulations in the sample, depending on the 2-beam conditions selected [160]. A standard sample is thinned by mechanical or chemical means and mounted on a copper grid or ring of 3 mm diameter. TEM is used to determine the difference between the mono-layer and bi-layer graphene.

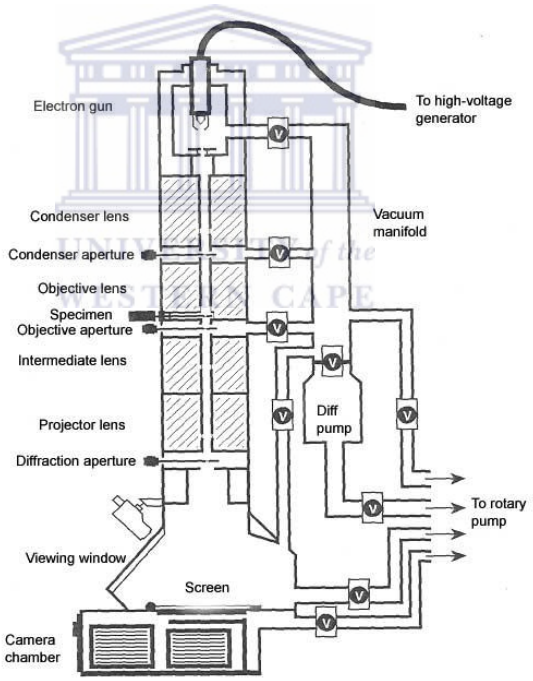

Figure 2.9: Transmission electron microscopy system

2.7.4.5 Scanning electron microscopy (SEM)

Over the past fifty years, the scanning electron microscope (SEM) has grown from a specialized research device to a universal industrial tool. SEM imaging was first

characterized to be used as a benchmark. SEM is known to have issues such as image drift and noise, which make stationary features on a specimen appear moving in the image frame. Thus, characterization of drift and noise in SEM imaging was conducted. SEM image noise refers to random variations of pixel values, arising from a few sources. Image drift refers to the movement of the entire image due to electron beam drift, charge drift on a specimen, and/or electromagnetic interferences from the environment [161]. The scanning electron microscope has two main parts (Figure 2.7). The electronics are used to control electron beam to specimen, identify and analyze signals, form image and do other functions to control the microscope. The electron column creates electrons including the group of lenses that focus the electron beam exactly to the specimen [162]. A focused electron beam is scanned over a specimen such that the interaction between the beam and the specimen excites various forms of radiation including backscattered electrons, secondary electrons, and x-rays. This radiation is then detected and analyzed to reveal information concerning the specimen's composition and topography. SEM has the advantages in detecting impurities, ruptures, folds, voids and discontinuities of synthesized or transferred graphene on a variety of substrates.

UNIVERSITY of the
WESTERN CAPE

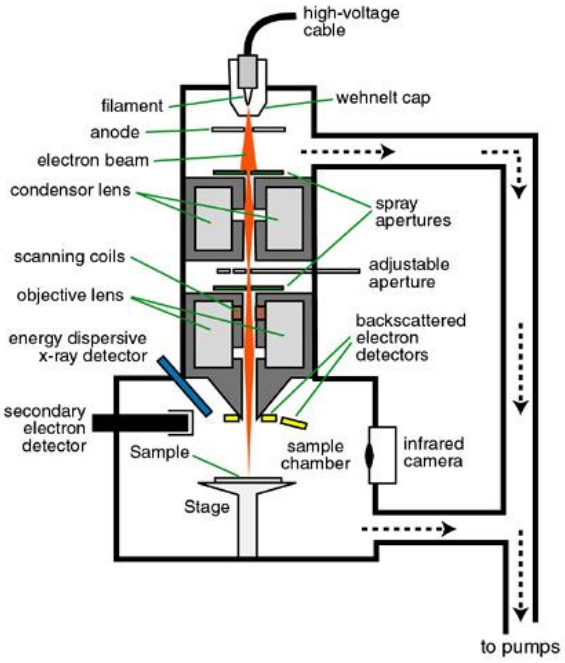

Figure 2.10: Scanning electron microscopy system

2.8 Applications of graphene

2.8.1 Electrochemical sensors

Graphene is the most recent member of the multi-dimensional carbon-nano-material family, starting with fullerenes as a 0D material, SWCNTs as 1D nanomaterials, and ending with graphite as a 3D material. Graphene fills the gap for 2D carbon nanomaterials. Graphene is considered as an ideal material for electrochemistry due to its large 2D electrical conductivity, large surface area and its availability at a cheaper cost. In comparison with carbon nanotubes, two advantages of graphene are apparent. Firstly, graphene does not contain metallic impurities, as in CNTs [163] and secondly, the production of graphene is cheaper since its synthesis requires only graphite as the starting material. Furthermore, the latest studies on the electrochemical behavior of graphene indicates that graphene exhibits a wide electrochemical potential window of approximately 2.5 V in 0.1 M phosphate buffer solution (pH 7.00) [164].

UNIVERSITY of the
WESTERN CAPE

2.8.1.1 Graphene electrochemical sensors for enzymes

The direct electrochemistry of an enzyme refers to the direct electron communication between the electrode and the active center of the enzyme without the precipitation of mediators or other reagents [165-167]; this is very significant in the development of biosensors, biofuel cells and biomedical devices. However, the realization of direct electrochemistry of redox enzymes on common electrodes is very difficult because the active centers of most redox enzymes are located deeply in a hydrophobic cavity of the molecule [168-169]. Carbon nanotubes and metal nanoparticles have exhibited excellent performance in enhancing the direct electron transfer between enzymes and electrodes, and are widely

used now [170-172]. Due to its extraordinary electron transport property, functionalized graphene is expected to promote the electron transfer between electrode substrates and enzymes [168]. According to Kang's report [173], glucose oxidase (GOx) can be adsorbed onto the graphene – chitosan nano-composite film modified glassy carbon electrode. This modified electrode was used for glucose sensing and exhibited great sensitivity in comparison with widely investigated carbon nanotubes–based ones. Compared to this, Wu *et al*. [174] assembled GOx directly onto the unmodified graphene surface and could obtain the same direct electron transfer characteristics of GOx, but with a simpler electrode fabrication procedure, a higher sensitivity and a lower detection limit.

2.8.1.2 Transparent conducting electrodes

It has been demonstrated that thin film (< 30 nm) of RGO is semi-transparent in visible and NIR regions while thick films are opaque. The transmittance and conductivity of the GO/RGO film can be tuned by tuning the thickness of the film and the degree of reduction [175]. Indium tin oxide (ITO) and fluorine tin oxide (FTO) have been widely used as window electrodes in optoelectronic devices [176]. These metal oxides, however, appear to be increasingly problematic due to:-

(1) the limited availability of the element indium on earth,

(2) their instability in the presence of acid or base,

(3) their susceptibility to ion diffusion into polymer layers,

(4) their limited transparency in the near-infrared region and

(5) the current leakage of FTO devices caused by FTO structure defects [177].

The RGO thin film is considered to be a promising electrode material for organic electronic

UNIVERSITY of the
WESTERN CAPE

and optoelectronic applications, due to their transparency, conducting and flexible nature.

2.8.1.3 Graphene electrochemical sensors for heavy metal ions detection

Wang's group [178-179] have demonstrated the use of the graphene nano-sheets to develop a high-sensitivity determination of lead and cadmium ions. Khomyakov *et al.* [180] evidenced the interaction and charge transfer between graphene and metal ions and concluded that the interaction and the charge transfer between graphene and metal ions made the modified electrode very sensitive. However, chemical binders (e.g. Nafion) are usually used to mix with graphene to form films, powders and graphene pastes with thicknesses in the order of nanometers (nm) or millimeters (mm). Furthermore, mixing binders with graphene helps to immobilize graphene onto the surfaces of electrodes in order to develop new chemical sensors for heavy metal determination [178-179]. Graphene pastes can reduce its electrical conductivity and surface activity due to the effect of the binder. Li *et al*. [181-182] demonstrated that Nafion-graphene composite film-based electrochemical sensor not only exhibited improved sensitivity for the detection of lead and cadmium, but also alleviates the interference due to synergistic effect of graphene nano-sheets and Nafion [181].

UNIVERSITY of the
WESTERN CAPE

The first available metal film used to enhance the sensitivity for graphene is mercury, due to the helpful analytical properties such as, in the negative potential range [18]. However, the use of mercury in some countries is harshly limited because of its dangerous toxicity and the increased health risks [183]. Recently, other types of metal film electrodes have been used as an alternative to mercury; amongst them is the bismuth-film electrode (BiFE) and antimony-film electrode (SbFE), which compare well with mercury electrode. Wong *et al*. [53], coated graphene prepared by different methods onto a GCE without any binder and demonstrated that cadmium could be detected.

In this project we intend to demonstrate that chemically synthesized graphene coated on a GCE without using a binding agent in combination with an *in-situ* deposited metal film is capable of detecting selected heavy metal ions and does yield admirable detection limits.

CHAPTER 3

Materials and Method

3.1 Chemicals and reagents

All chemicals used in this study were analytical reagent grade and used without further purification.

Chemicals	Source
Glacial Acetic Acid	Sigma – Aldrich
Sodium Acetate	Sigma – Aldrich
Zinc (1000 mgL-1)	Fluka
Cadmium (1000 mgL-1)	Fluka
Lead (1000 mgL-1)	Fluka
Bismuth (1000 mgL-1)	Fluka
Antimony (1000 mgL-1)	Fluka
Mercury (1000 mgL-1)	Fluka
55% Nitric Acid	Kimix
99% Ethanol	Sigma – Aldrich
Ultra Pure Water	Alfa - Aesar
Natural graphite	Milli-QTM system (Millipore)
Sodium borohydride	Sigma – Aldrich

UNIVERSITY of the
WESTERN CAPE

3.2 Standard solutions

3.2.1 Metal ion solutions

Target metal ion solutions were prepared by diluting 1,000 mg L^{-1}, atomic adsorption standard solutions with nitric acid (2%).

3.2.2 Nitric acid solution (6 M)

Nitric acid (6 M) was prepared by diluting nitric acid (55%) with ultra pure distilled water; this solution was used for cleaning and removing metal ions from glassware.

3.2.3 Supporting electrolyte

0.1 M Acetate buffer (pH 4.6) was used as supporting electrolyte and prepared by mixing glacial acetic acid and sodium acetate followed by diluting the solution with ultra pure distilled water. A pH meter (Metrohm 827 pH lab.) was calibrated using pH 4 and pH 7 calibration buffer solutions and, then used to verify the pH of the acetate buffer (supporting electrolyte).

UNIVERSITY of the
WESTERN CAPE

3.3 Equipment and apparatus

3.3.1 Electrochemical apparatus

Square-wave anodic stripping voltammetry (SWASV) measurements were carried out using a 797 VA COMPUTACE instrument connected to a personal computer. The graphene / metal nano-composite coated glassy carbon electrode served as the working electrode. An Ag/AgCl (saturated KCl) and platinum wire served as the reference and counter electrodes, respectively. All electrochemical measurements were carried out in a 20 mL cell.

Figure 3.1: 797 VA Computrace Metrohm 'Electrochemical Analyzer

Figure 3 2: Three electrodes system for voltammetry

3.4 Instrumental parameters for SWASV analysis

The instrumental parameters used for SWASV analysis are as follows;

Initial purge: t = 10 s

Cleaning step: E = +0.3 V at t = 60 s

Pre-concentration step (Deposition): E = -1.3 V at t = 120 s

Equilibrium time: t = 10 s

Potential scan range:	from -1.4 V to +0.6 V
Voltage step:	0.005951 V
Amplitude:	0.040 V
Frequency:	50 Hz
Stirring rate:	1000 rpm

3.5 Preparation of reduced graphene oxide (RGO)

Graphene oxide (GO) was synthesized from natural graphite using the modified Hummers method [184]. 50 mg of GO was added to 50 ml of distilled water and sonicated for 1 hour. A 0.15 g of sodium borohydride ($NaBH_4$) was added and the mixture stirred for 30 minutes. The mixture was then heated at 125 °C under reflux for 3 hours. The resulting black precipitate (RGO) was centrifuged, washed with water, ethanol and dried in vacuum oven. [185].

UNIVERSITY of the
WESTERN CAPE

3.6 Electrode cleaning

A glassy carbon electrode was polished with alumina powder in the order 1, 0.3 and 0.05 micron respectively, on a wet polishing cloth by pressing the electrode softly against the polishing surface. The electrode rinsed with ultra pure distilled water and polished again with ethanol on a clean polishing cloth. The electrode was then cycled (10 times) between -1.3 and -0.2 V in 6 M nitric acid to remove any other impurities. A SWASV run was then done in 0.1 M acetate buffer to check for any spurious peaks prior to modifying the glassy carbon electrode.

3.7 Coating the glassy carbon electrode

A 0.25 mg mL^{-1} of graphene solution in ethanol was sonicated for 30 min or until fully dispersed. Afterwards, 1 μL of the graphene suspension was drop coated onto the glassy

carbon electrode (GCE) and allowed to dry at room temperature to give the graphene modified electrode.

3.8 Procedure for SWASV analysis

Firstly, the cell, Teflon stirrer, counter electrode and reference electrode were cleaned with 6 M nitric acid and rinsed with distilled water. 20 ml of 0.1 M acetate buffer solution (pH 4.6) was pipeted into the voltammetric cell. Subsequently, Hg^{2+} (Bi^{3+} or Sb^{3+}) and target metal ions were added to the solution and purged with argon gas for 10 s to force out the dissolved oxygen while the solution was stirred. The stirring was stopped and the solution allowed to equilibrate for 10 s The voltammogram was then recorded by applying a potential from -1.4 V to 0.6 V using SWASV with rotation speed 1000 rpm, voltage step 0.005951 V and frequency 50 Hz. A cleaning step of 60 s at 0.3 V, with the solution stirring was used to remove the target metals and metal film.

UNIVERSITY of the
WESTERN CAPE

3.9 Characterization techniques

3.9.1 Scanning electron microscopy (SEM)

Scanning Electron Microscopy (SEM) measurements were performed using a LEO 1450 SEM 30 kV instrument equipped with Electronic Data System (EDS) and Windows Deployment Services (WDS); images were taken using the secondary electron detector. The samples were dried in a vacuum oven and deposited on the silicon grid surface before SEM observations.

3.9.2 High resolution transmission electron microscopy (HRTEM)

High Resolution Transmission Electron Microscopy (HRTEM) measurements were carried out with a Tecnai G2 F20X-Twin MAT Field Emission Transmission Electron Microscope

from FEI (Eindhoven, Netherlands) under an acceleration voltage of 200 kV. The samples were prepared by dropping a dilute suspension of graphene or graphene oxide in ethanol onto copper grids followed by air drying at room temperature.

3.9.3 Fourier transformed infrared (FT-IR) spectroscopy

A Fourier Transform Infrared (FT-IR) spectrum was recorded using a (Perkin Elmer Spectrum 100) coupled to an Attenuated Total Reflectance (ATR) sample holder. FT-IR was used to obtain information and confirmation on graphene or graphene oxide.

3.9.4 X-ray diffraction (XRD)

XRD measurements were carried out using a Bruker AXS D8 Advance diffractometer from BRUKER- AXS Germany with Cu-Kα radiation. The XRD operating parameters are given below;

UNIVERSITY of the
WESTERN CAPE

Radiation source	Cu-Kα
Radiation wavelength (λ)	1.506 Å
Tube Voltage	40 kV
Tube Current	40 mA
Variable Slits	0.28 mm

3.9.5 Raman spectroscopy

Raman spectroscopy was obtained using a Dilor XY Raman spectrometer with a Coherent Innova 300 Argon laser with a 514.5 nm laser excitation.

CHAPTER 4

Results and Discussion

4.1 Morphology and structural characterization of graphene oxide and graphene

4.1.1 Scanning electron microscopy (SEM)

The SEM images of GO and RGO are shown in Figure 4.1. A scanning electron microscope (SEM) image of feathery GO powder Figure 4.1a, shows an agglomeration of the exfoliated platelets, also it is noticed that the GO shows an uneven surface probably owing to the oxidation of sheets [186]. SEM images for RGO (Figure 4.1b) reveals that the RGO material consists of thin, haphazardly aggregated, wrinkly sheets closely linked with each other forming a shapeless solid [187].

UNIVERSITY of the
WESTERN CAPE

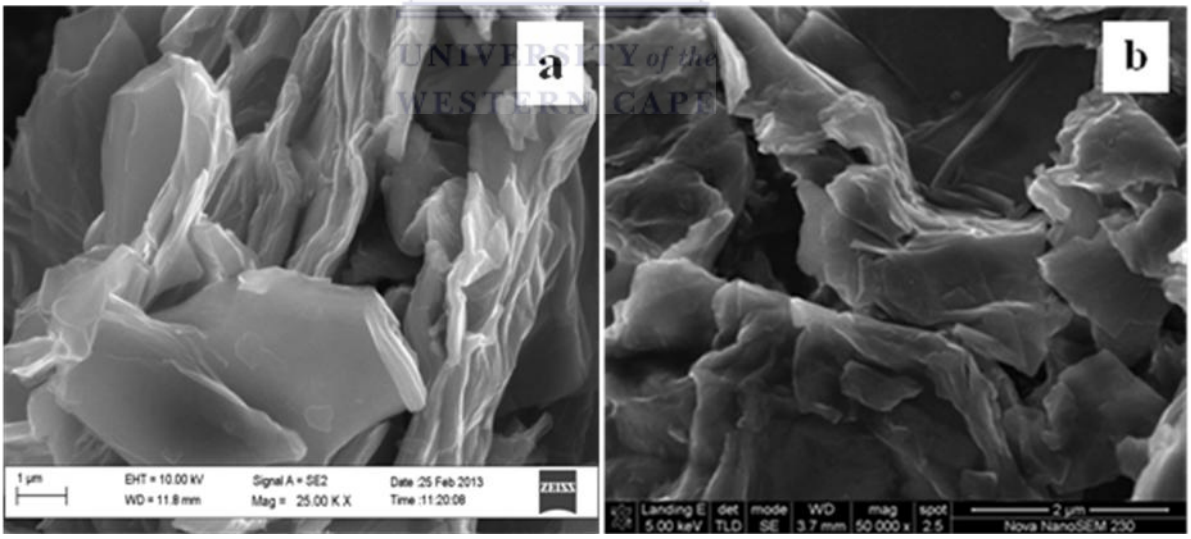

Figure 4.1: SEM images for (a) GO and (b) RGO.

4.1.2 High resolution transmission electron microscopy (HRTEM)

The HRTEM images of GO and RGO are shown in Figure 4.2. The GO images (Figure 4.2a), shows that the sample is a layered structure (indicated by arrow 1) consisting of stacked GO sheets in addition, the larger transparent sheets resemble wavy silk veils entangled with each another [188]. The HRTEM images for RGO (Figure 4.2b) show a crumpled and wrinkled transparent flake-like structure. The most transparent and featureless regions suggest (indicated by arrows) monolayer graphene sheets [189]. At higher magnification the HRTEM image (Figure 4.2c) show the monolayers of graphene.

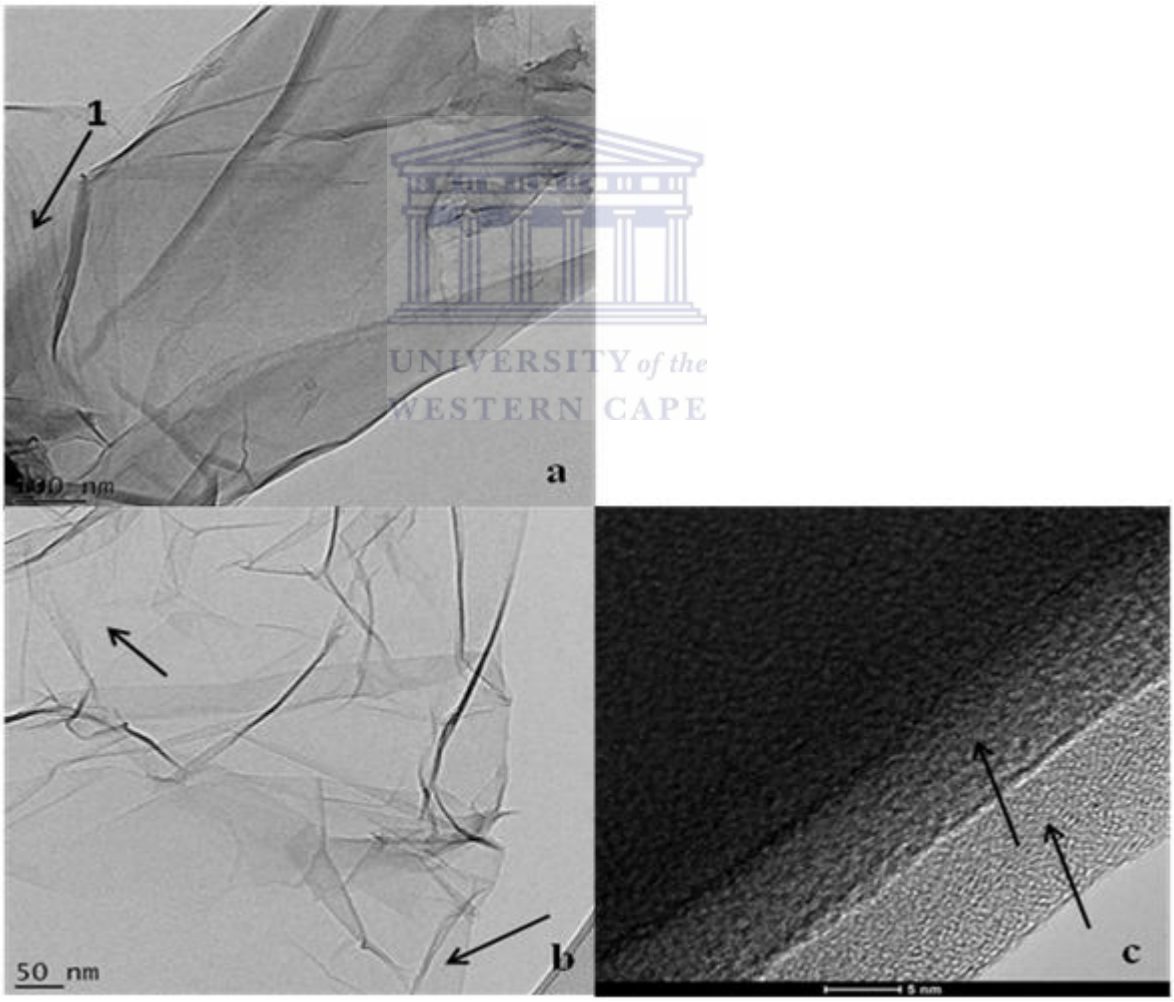

UNIVERSITY of the
WESTERN CAPE

Figure 4.2: TEM images of (a) GO, (b) RGO and (c) RGO layers

4.1.3 Fourier transformed infrared spectroscopy (FT-IR)

Previous researches have shown that the surfaces of graphene oxide are covered with a variety of oxygen functional groups namely, hydroxyl, ethers, epoxides, carbonyl and carboxylic groups.[190-191].

The FT-IR spectra of GO and RGO are shown in Figure 4.3. Graphene oxide showed a large compilation of diffused bands. The peak at 1406 cm^{-1} is due to C –OH stretching vibrations, whereas, the band at 1602 cm^{-1} is attributed to C=C configurable vibrations from the aromatic zones. A peak at 1023 cm^{-1} is attributed to C –O vibrations from alkoxy groups [192], while the deformation of the C–O was observed at 1159 cm^{-1} and the peak at 1279 cm^{-1} is attributed to the bending of the O–H group [193]. The peak at 2666 cm^{-1} corresponds to an asymmetric –C-H stretching vibration. [194]. After reduction with $NaBH_4$ greater part of the above mentioned bands was notably reduced or removed completely demonstrating that all or most of the oxygen was completely reduced.

UNIVERSITY of the
WESTERN CAPE

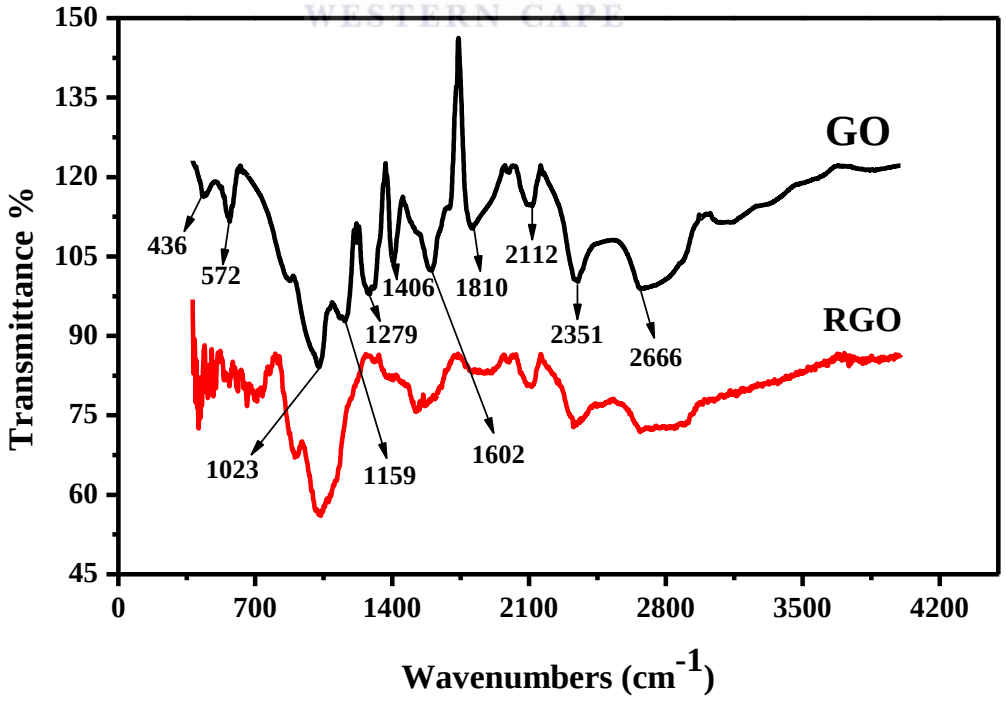

Figure 4.3: FT-IR spectra of graphene oxide (GO) and reduced graphene oxide (RGO)

4.1.4 X-ray diffraction (XRD)

The XRD analysis of GO and RGO are shown in Figure 4.4. GO showed a sharp, tall peak at 10° corresponding to the presence of oxygen containing functional groups formed during oxidation. These functional groups cause the GO sheets to stack more loosely [195] and, the broad peak at 25° may be due to appearance of exfoliated sheets in addition, the peak at 42° corresponds to the 100 crystal plane. After reduction (of graphene oxide) to graphene the peak at 10° completely disappeared and a broad peak centered at 25° was observed. The broadness of this 25° peak could be due to increased mass in the through-plane direction of the RGO sample and, also perhaps due to structural defects from sonication [196].

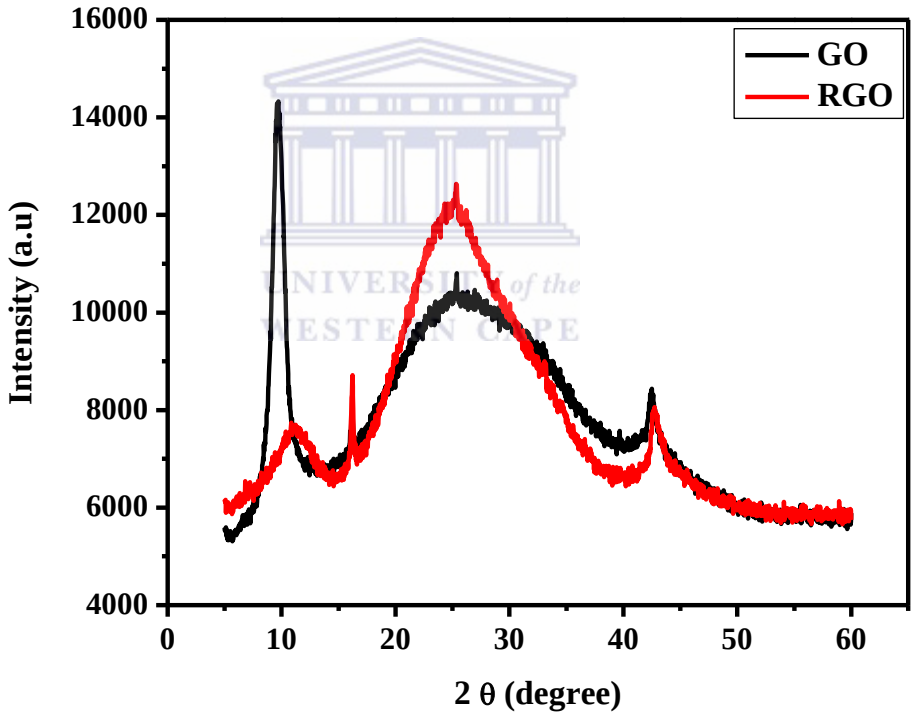

Figure 4.4: XRD analysis for graphene oxide (GO) and reduced graphene oxide (RGO).

4.1.5 Raman spectroscopy

The Raman spectra of graphene and graphene oxide are shown in Figure 4.5. The Raman spectrum of graphene includes the D peak located at 1348 cm^{-1}, G peak at 1591 cm^{-1} and 2D peak at 2866 cm^{-1}. The D peak is due to the presence of confusion in atomic arrangement or edge effect of graphene whilst, the G peak due to in-plane vibration of the sp^2 carbon atoms. The 2D band appears at almost double the frequency of the D band and originates from second order Raman scattering process [197-198]. For GO the G band is broadened and shifted to 1604 cm^{-1}, and the D peak at 1345cm^{-1} is absent. The ratio of the intensities (I_D/I_G) for GO is 0.98 while it increased for graphene to 1.08. This increase is attributed to the significant decrease in size of the in-plane sp^2 domains due to oxidation and ultrasonic exfoliation, and somewhat disordered graphite crystal structure of graphene nano-platelets [199].

UNIVERSITY of the WESTERN CAPE

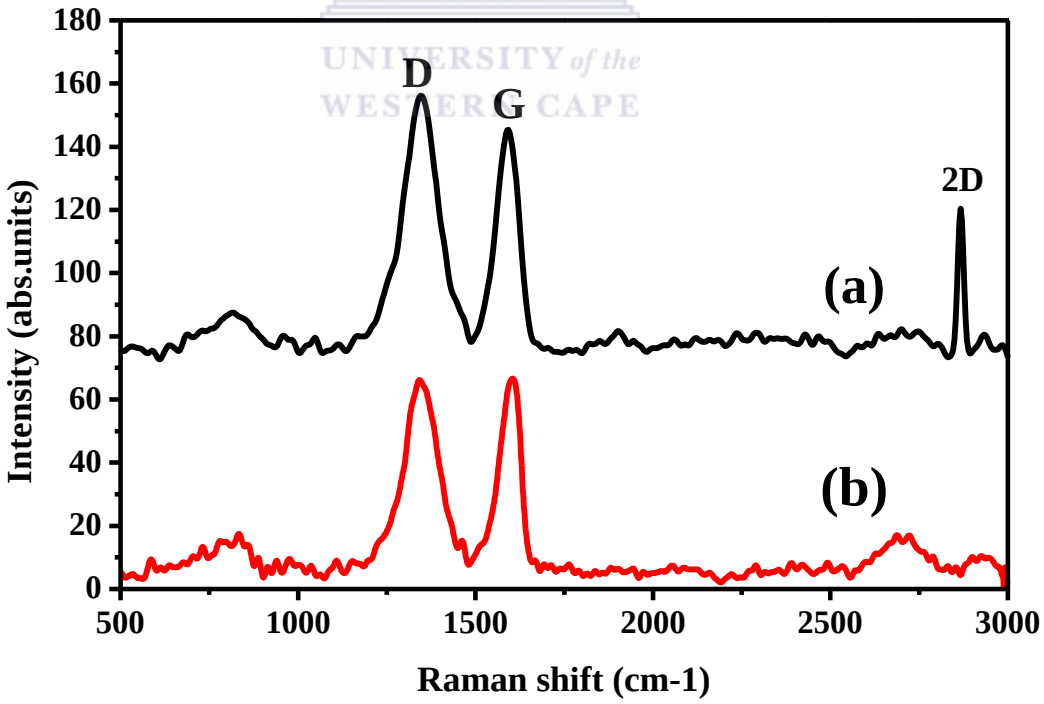

Figure 4.5: Raman spectra of graphene oxide (GO) (a) and reduced graphene oxide (RGO) (b).

4.2 Part A: The graphene modified glassy carbon thin film mercury electrode (Gr-GC-HgE)

In this section the stripping voltammetric responses of the target metal ions, were used to obtain the various optimized instrumental parameters and to determine the analytical parameters for the Gr-GC-HgE.

4.2.1 Current responses of graphene modified glassy carbon thin film mercury electrodes (Gr-GC-HgE)

Figure 4.6 shows the stripping voltammetric responses for 20 µg L^{-1} of each target metal ion (Zn^{2+}, Cd^{2+} and Pb^{2+}) in 20 ml of 0.1 M acetate buffer solution (pH 4.6) and 5 mg L^{-1} Hg^{2+} ions. The stripping voltammetric peaks appear at approximately −1.1 V, −0.7 V and −0.5 V for Zn^{2+}, Cd^{2+} and Pb^{2+} respectively. Furthermore, the peak responses (peak currents) of the Gr-GC-HgE prepared with varying concentrations of graphene solutions show a gradual decrease in peak response with the highest responses being observed with 0.25 mg mL^{-1}. This concentration (0.25 mg mL^{-1}) was used for all further modifications of the GCE. A plausible reason for this decrease in signal response can be attributed to the increase in the number of graphene sheets stacking on top of each other as shown in, Figure 4.2c to form multilayers (at higher concentrations). This stacking phenomenon restricts the passage of electron flow from the analyte solution to the surface of the GCE.

UNIVERSITY of the
WESTERN CAPE

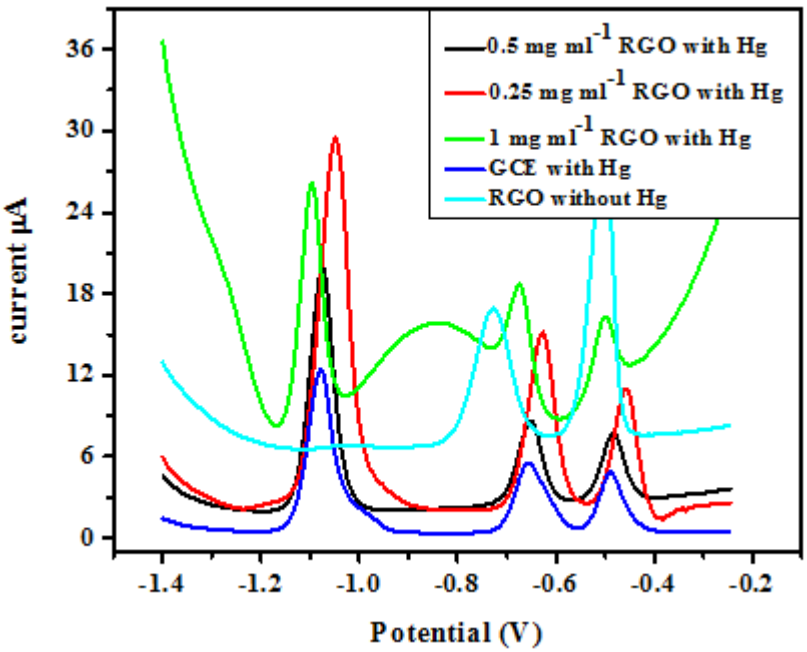

Figure 4.6: SWASV of 20 µg L^{-1} of Zn^{2+}, Cd^{2+} and Pb^{2+} at a glassy carbon electrode (GCE) modified with various concentrations of graphene with an *in situ* deposited Hg film at the optemized experimental parameters.

UNIVERSITY of the
WESTERN CAPE

4.2.1.1 The effect of mercury film

The absence of an *in situ* deposited Hg-film on the graphene modified GC electrode (Gr-GCE) is apparent and is demonstrated in Figure 4.7. The results show an increase in signal response for Cd^{2+} and Pb^{2+} but not for Zn^{2+} when using the Gr-GCE. The non-response for Zn^{2+} indicates that zinc is not sufficiently deposited onto the Gr-GCE hence, no stripping zinc peak is observed. In general, the voltammetric peaks for the graphene modified glassy carbon thin film mercury electrode (Gr-GC-HgE) shows taller, symmetrical peaks for Cd^{2+} and Pb^{2+} in comparison to either the bare glassy carbon mercury thin film electrode (GC-HgE) or the graphene modified GC electrode (Gr-GCE). It is evident from these results that enhanced sensitivity is achieved in the presence of an *in situ* deposited Hg-film.

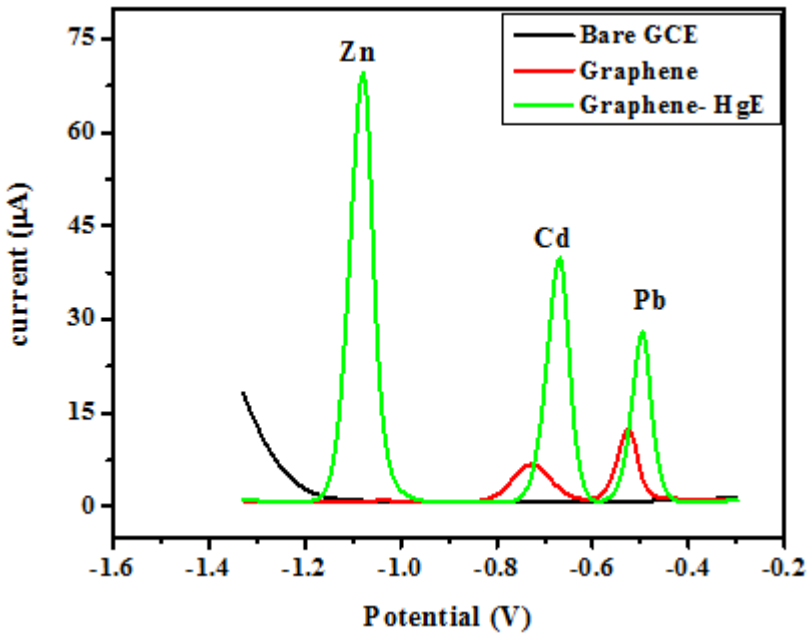

Figure 4.7: The effect of a mercury film on the peak current of 20 µg L^{-1} of Zn^{2+}, Cd^{2+} and Pb^{2+} at the Gr-GC-HgE. Supporting electrolyte (0.1 M acetate buffer pH 4.6), deposition time (120 s at -1.3 V), rotation speed (1000), frequency (50 Hz), amplitude (0.04 V) and sweep rate (0.2975 Vs^{-1}).

UNIVERSITY of the
WESTERN CAPE

4.2.2 Effect of instrumental parameters on the stripping peak currents of Zn^{2+}, Cd^{2+} and Pb^{2+} at the graphene modified glassy carbon mercury thin film electrode (Gr-GC-HgE)

4.2.2.1 Deposition potential

The influence of deposition potential on the peak currents of Zn^{2+}, Cd^{2+} and Pb^{2+} at the Gr-GC-HgE was studied in the potential range -0.4 V to – 1.4 V. The voltammograms in Figure 4.8 show that at potentials greater than their oxidation potentials of the target metal ions no response signals were observed since, no reduction of the metal ions from the analyte solution occurs. The reduction of Zn^{2+} occurred at potentials greater than -1.2 V. In general, the peak currents for all three metals increase as the deposition potential becomes more negative and is due to all three metals being positively charged ions, which are preferentially reduced at more negative potentials [200]. Thus, to effect simultaneous deposition of the target metal ions (Zn^{2+}, Cd^{2+} and Pb^{2+}) a potential of -1.3 V was selected for further analysis.

UNIVERSITY of the WESTERN CAPE

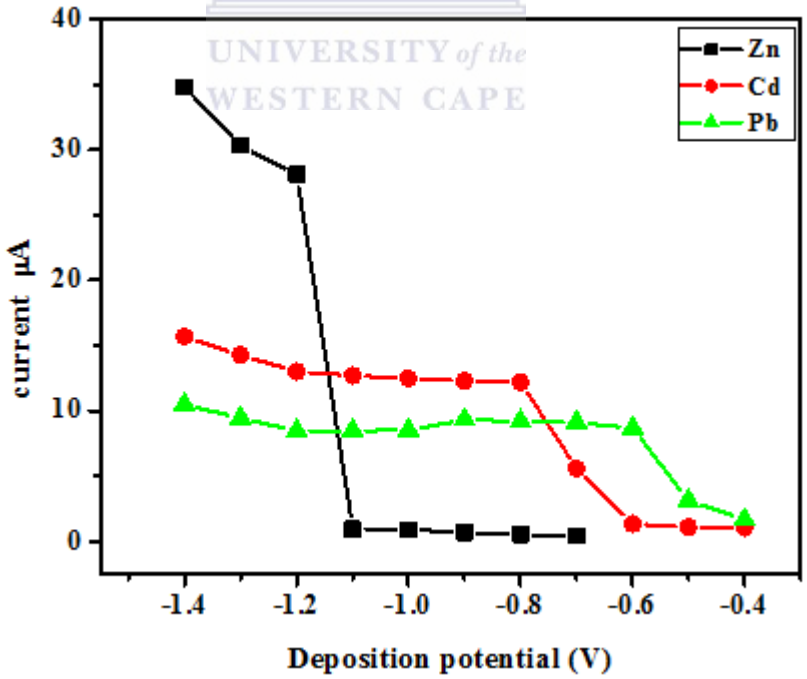

Figure 4.8: The effect of deposition potential on the peak current of 20 µg L^{-1} of Zn^{2+}, Cd^{2+} and Pb^{2+} at the Gr-GC-HgE. Supporting electrolyte (0.1 M acetate buffer pH 4.6), deposition time (120 s at varying deposition potentials), rotation speed (1000 rpm), frequency (50 Hz), amplitude (0.04 V) and sweep rate (0.2975 Vs^{-1}).

4.2.2.2.Deposition time

Figure 4.9 shows the effect of the deposition time on the peak currents of Zn^{2+}, Cd^{2+} and Pb^{2+} when using the Gr-GC-HgE. Here, the stripping responses of the metals increases rapidly with increasing deposition time from 30 to 200 s since more time is allowed for the analyte ions to undergo reduction and deposition at the Gr-GC-HgE surface. At deposition times greater than 200 s there is a gradual decrease in response due to surface saturation of the electrode [200]. A deposition time of 120 s was chosen for subsequent experiments to avoid possible surface saturation beyond 120 s.

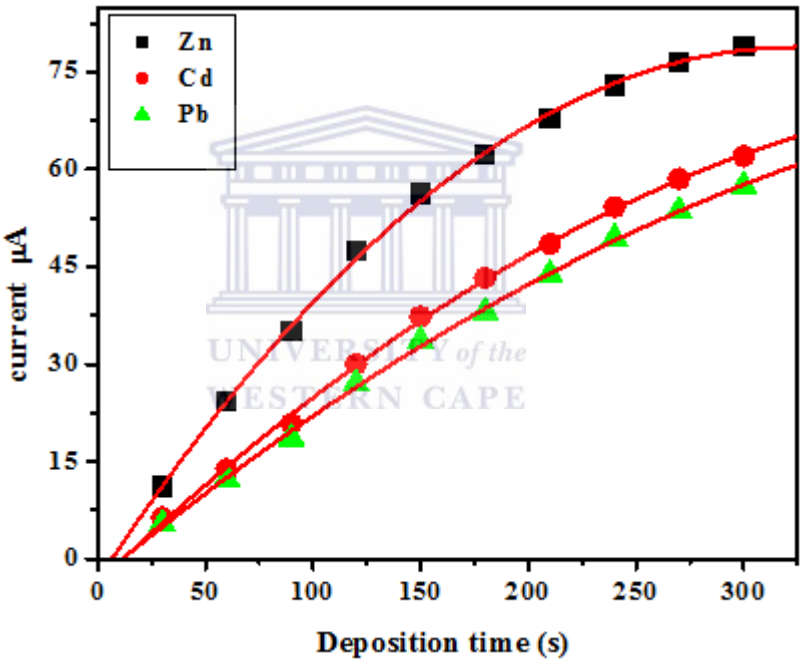

Figure 4.9: The effect of deposition time on the peak current of 20 µg L^{-1} of Zn^{2+}, Cd^{2+} and Pb^{2+} at the Gr-GC-HgE. Supporting electrolyte (0.1 M acetate buffer pH 4.6), varying deposition times at a -1.3 V), rotation speed (1000 rpm), frequency (50 Hz), amplitude (0.04 V) and sweep rate (0.2975 Vs^{-1}).

4.2.2.3 Rotation speed

The effect of rotation speed on the peak currents of Zn^{2+}, Cd^{2+} and Pb^{2+} applied to the Gr-HgFE was studied from 200-2000 rpm and is shown in Figure 4.10. As the square-root of

rotation speed increases so does the stripping peak currents of metal ions. The rotation speed enhances sensitivity of stripping analysis since it facilitates the migration of metal ions from the bulk analyte solution to the electrode surface where reduction of the ions takes place. A rotation speed of 1000 rpm was chosen for further study.

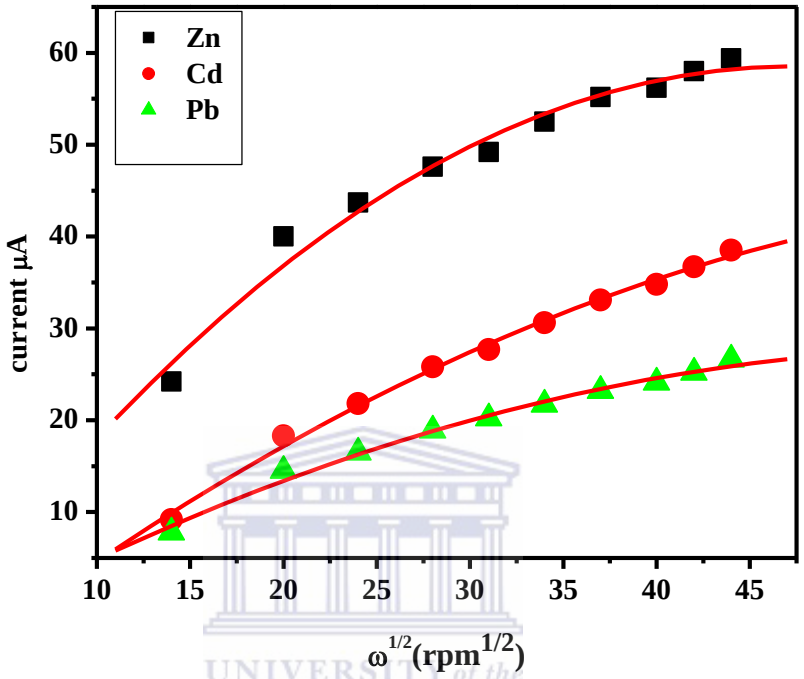

UNIVERSITY of the
WESTERN CAPE

Figure 4.10: The effect of rotation speed on the peak current of 20 µg L^{-1} of Zn^{2+}, Cd^{2+} and Pb^{2+} at the Gr-GC-HgE. Supporting electrolyte (0.1 M acetate buffer pH 4.6), deposition time (120 s at -1.3 V), at varying rotation speeds, frequency (50 Hz), amplitude (0.04 V) and sweep rate (0.2975 Vs^{-1}).

4.2.2.4 Frequency

Figure 4.11 shows the variation of frequency with the peak currents of Zn^{2+}, Cd^{2+} and Pb^{2+} applied over the frequency range from 10 to100 Hz. The peak current for all three metals increases as the frequency is increased. A frequency of 50 Hz was chosen as the optimum frequency.

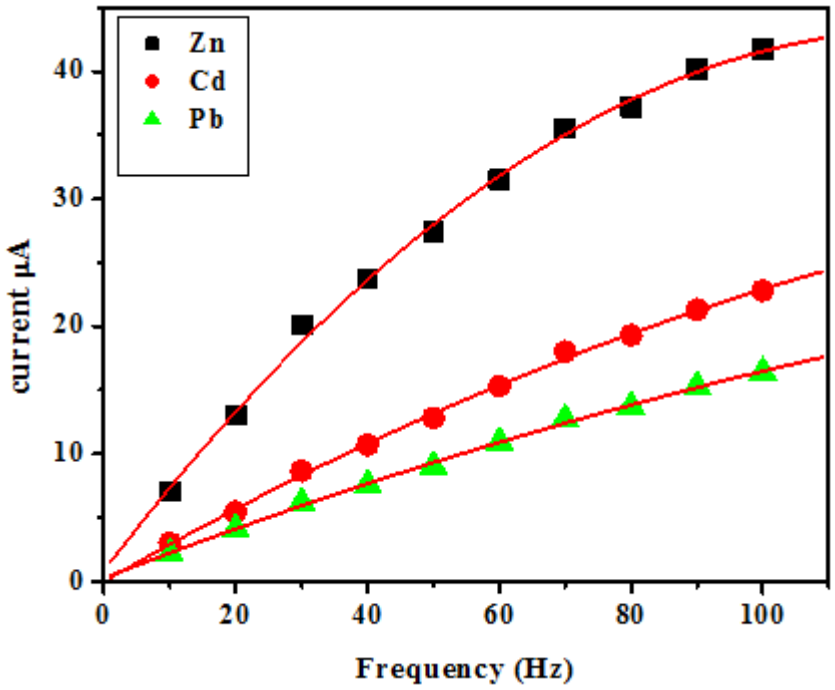

Figure 4.11: The effect of frequency on the peak current of 20 µg L^{-1} of Zn^{2+}, Cd^{2+} and Pb^{2+} at the Gr-GC-HgE. Supporting electrolyte (0.1 M acetate buffer pH 4.6), deposition time (120 s at -1.3 V), rotation speed (1000), at varying frequencies, amplitude (0.04 V) and sweep rate (0.2975 Vs^{-1}).

UNIVERSITY of the
WESTERN CAPE

4.2.2.5 Amplitude

Figure 4.12 shows the effect of the amplitude on the peak currents of Zn^{2+}, Cd^{2+} and Pb^{2+} which was investigated over the range 0.01 to 0.1 V. The peak heights of all three metals increased linearly up to 0.04 V, but levels off to 0.08 V and then increases after 0.1 V. An amplitude of 0.04 V was selected as the optimum amplitude.

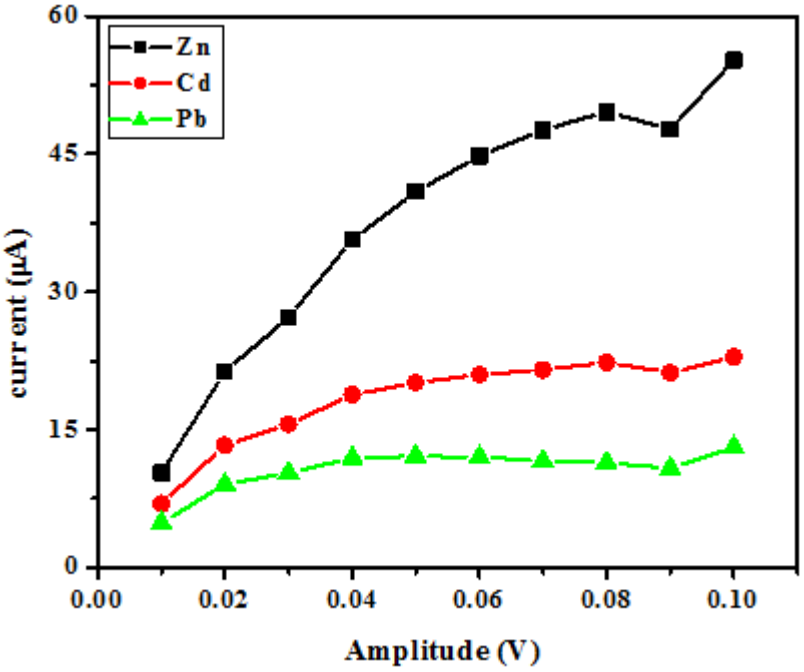

Figure 4.12: The effect of the amplitude on the peak current of 20 µg L^{-1} of Zn^{2+}, Cd^{2+} and Pb^{2+} at the Gr-GC-HgE. Supporting electrolyte (0.1 M acetate buffer pH 4.6), deposition time (120 s at -1.3 V), rotation speed (1000), frequency (50 Hz), at varying amplitudes and sweep rate (0.2975 Vs^{-1}).

UNIVERSITY of the
WESTERN CAPE

4.2.3 Film stability and reproducibility

The peak currents of Zn^{2+}, Cd^{2+} and Pb^{2+} remained almost the same each time a new Gr-GC-HgE was prepared and used to detect 20 µg L^{-1} of each metal ion in 20 ml of acetate buffer (pH 4.6), at the same conditions. The percentage relative standard deviation (RSD %) for the oxidation peaks was 1.13, 4.7 and 2 % for Zn^{2+}, Cd^{2+} and Pb^{2+} respectively, this indicates the excellent reproducibility in preparing the Gr-GC-HgE.

4.2.4 Analytical Performance of the graphene modified glassy carbon thin film mercury electrode (Gr-GC-HgE)

4.2.4.1 Simultaneous determination of Zn^{2+}, Cd^{2+} and Pb^{2+}

In simultaneous analysis all three metal ions are present or mixed together in the same solution and, the signal response (peak current) of each metal ion is obtained by measuring peak height of each. The calibration plots of concentration *versus* current were prepared by determining the peak currents of the metal ions from the voltammograms in Figures 4.13a and b for all three the metal ions in supporting electrolyte (0.1 M acetate buffer pH 4.6). Here, two calibration plots shown in Figures 4.14a(i) and b(ii) over two linear ranges namely, 1 – 10 µg L^{-1} and 5 - 60 µg L^{-1} were obtained with the Gr-GC-HgE.

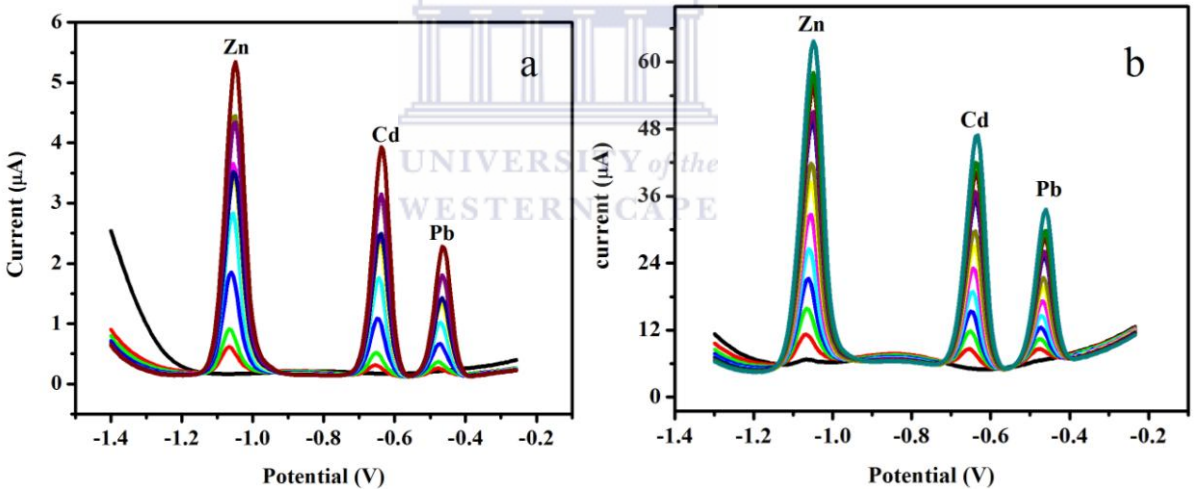

Figure 4.13: SWASV of Zn^{2+}, Cd^{2+} and Pb^{2+} at the Gr-GC-HgE with an *in situ* deposited Hg film. (a) 1 – 10 µg L^{-1} and (b) 5 - 60 µg L^{-1}. Supporting electrolyte (0.1 M acetate buffer pH 4.6), deposition time (120 s at -1.3 V), rotation speed (1000 rpm), frequency (50 Hz), amplitude (0.04 V) and sweep rate (0.2975 Vs^{-1}).

UNIVERSITY of the WESTERN CAPE

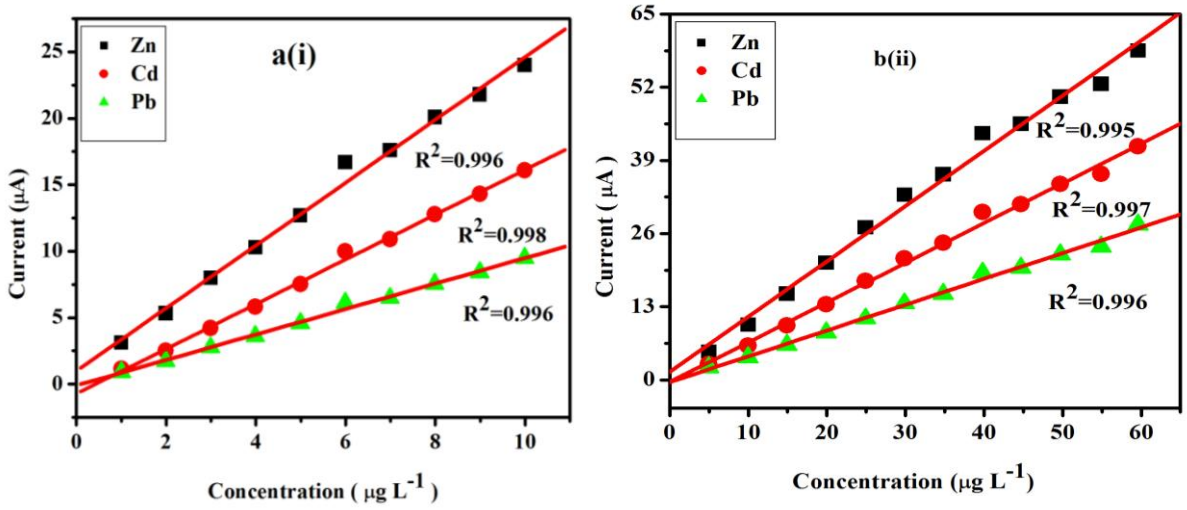

Figure 4.14: Calibration plots for Zn^{2+}, Cd^{2+} and Pb^{2+} at the Gr-GC-HgE with an *in situ* deposited Hg film. a(i) 1 – 10 µg L^{-1} and b(ii) 5 - 60 µg L^{-1}. Supporting electrolyte (0.1 M acetate buffer pH 4.6), deposition time (120 s at -1.3 V), rotation speed (1000 rpm), frequency (50 Hz), amplitude (0.04 V) and sweep rate (0.2975 Vs^{-1}).

Furthermore, from the calibration plots in Figure 4.14, the detection limits of the metal ions were determined based on three times the standard deviation ($3\sigma_{blank}$) of the blank divided by the slope of the calibration curve. The standard deviation of the blank was calculated from ten replications in the presence of Hg^{2+} ions. The excellent correlation coefficients and the detection limits for each metal ion are presented in the Table 4.1.

UNIVERSITY of the
WESTERN CAPE

Table 4.1: Correlation coefficient (r^2), and detection limits of Zn^{2+}, Cd^{2+} and Pb^{2+} determined simultaneously on Gr-GC-HgE.

	Range 1 -10 µg L^{-1}			**Range 5 -60 µg L^{-1}**		
	Zn^{2+}	**Cd^{2+}**	**Pb^{2+}**	**Zn^{2+}**	**Cd^{2+}**	**Pb^{2+}**
Slope	**2.65 ±0.42**	**1.99±0.43**	**0.96±0.01**	**0.84±0.12**	**0.66±0.05**	**0.41±0.04**
Standard Deviation (SD) of the blank	**0.07**	**0.035**	**0.046**	**0.05**	**0.038**	**0.057**
Correlation coefficient (r^2)	**0.996**	**0.998**	**0.996**	**0.995**	**0.997**	**0.996**
Detection limit (µg L^{-1})	**0.08**	**0.05**	**0.14**	**0.18**	**0.17**	**0.42**

*n = 3, where n is the number of replications.

4.2.4.2. Individual determination of Zn^{2+}, Cd^{2+} and Pb^{2+}

In individual analysis, each metal ion is present in a separate solution (0.1 M acetate buffer, pH 4.6) and the signal response (peak current) is obtained by measuring the peak height of each metal ion. The peak currents for Zn^{2+}, Cd^{2+} and Pb^{2+} were determined from well resolved, symmetrical voltammetric peaks in Figures 4.15(a), (b) and (c). Two linear concentration ranges 1 - 10 µg L^{-1} and 5 - 60 µg L^{-1} were observed for each metal ion as shown by the calibration plots presented in Figure 4.16.

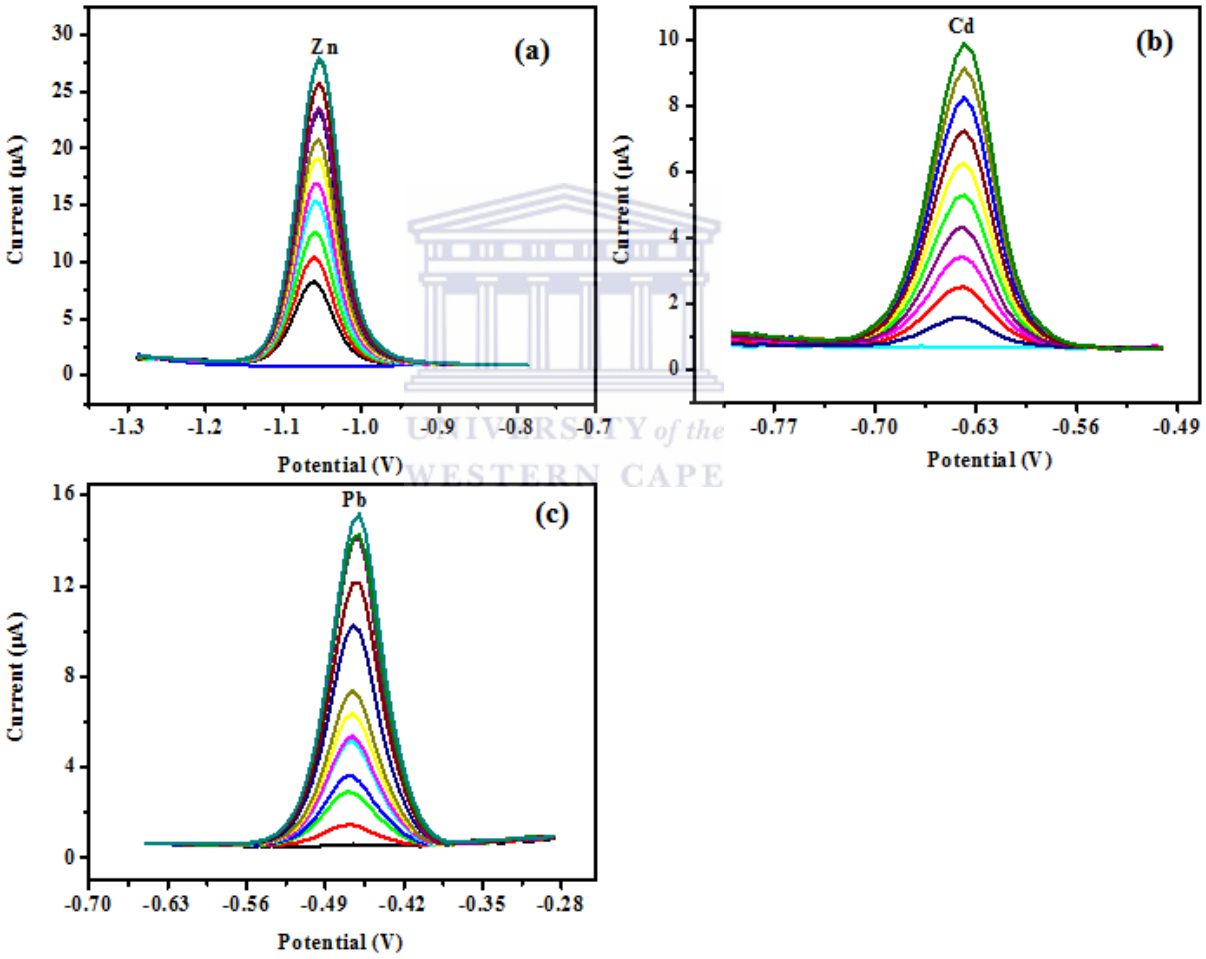

Figure 4.15: SWASV of (a) Zn^{2+}, (b) Cd^{2+} and (c) Pb^{2+} from 0 - 60 µg L^{-1} at the Gr-GC-HgE with an *in situ* deposited Hg film. Supporting electrolyte (0.1 M acetate buffer pH 4.6), deposition time (120 s at -1.3 V), rotation speed (1000 rpm), frequency (50 Hz), amplitude (0.04 V) and sweep rate (0.2975 Vs^{-1}).

UNIVERSITY of the WESTERN CAPE

The detection limit for each metal ion was determined from their respective calibration plots based on three times the standard deviation ($3\sigma_{blank}$) of the blank divided by the slope of the calibration curve for each metal ion. Table 4.2 shows the correlation coefficients and the detection limits for the metal ions obtained by individual analysis.

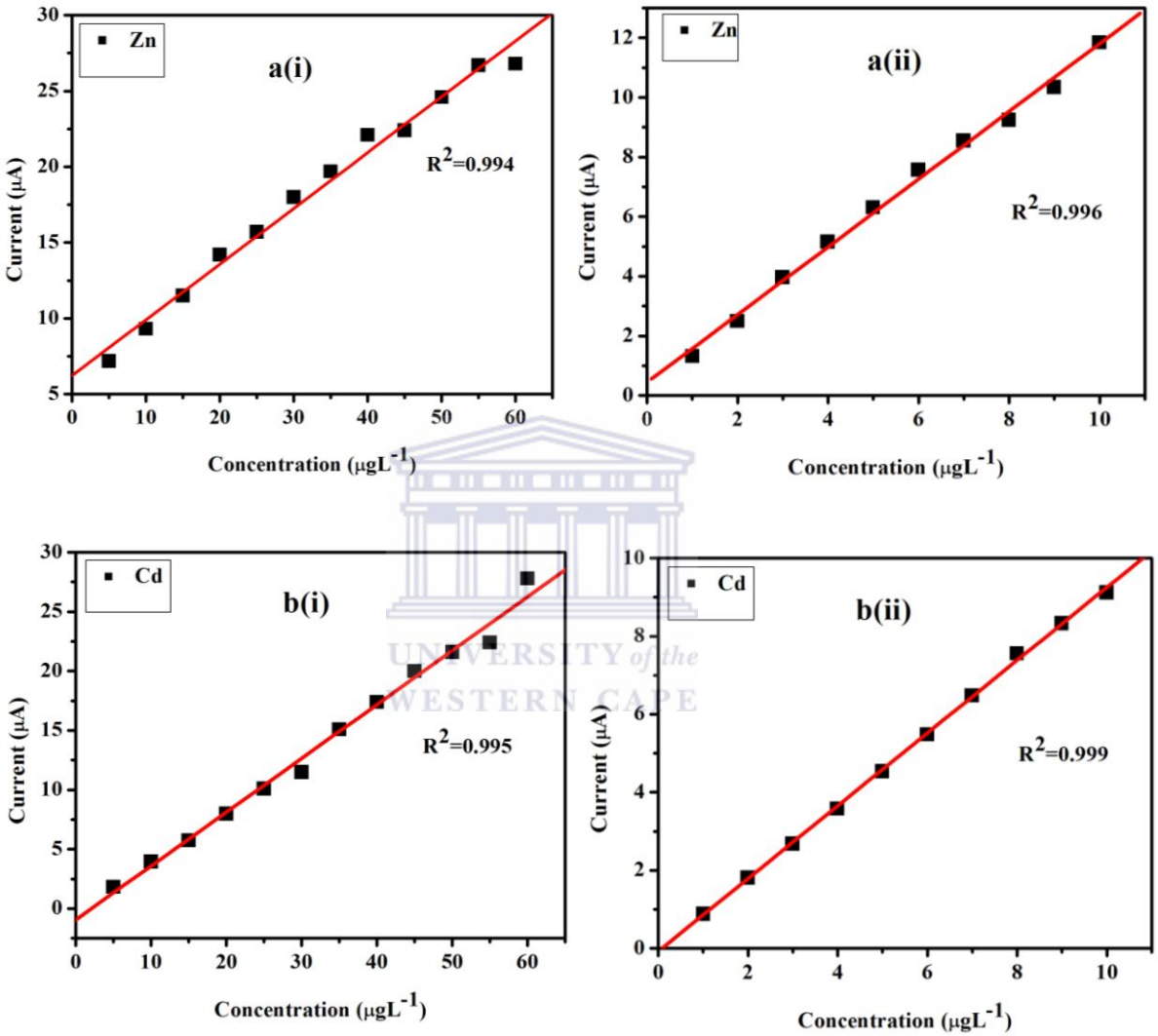

UNIVERSITY of the WESTERN CAPE

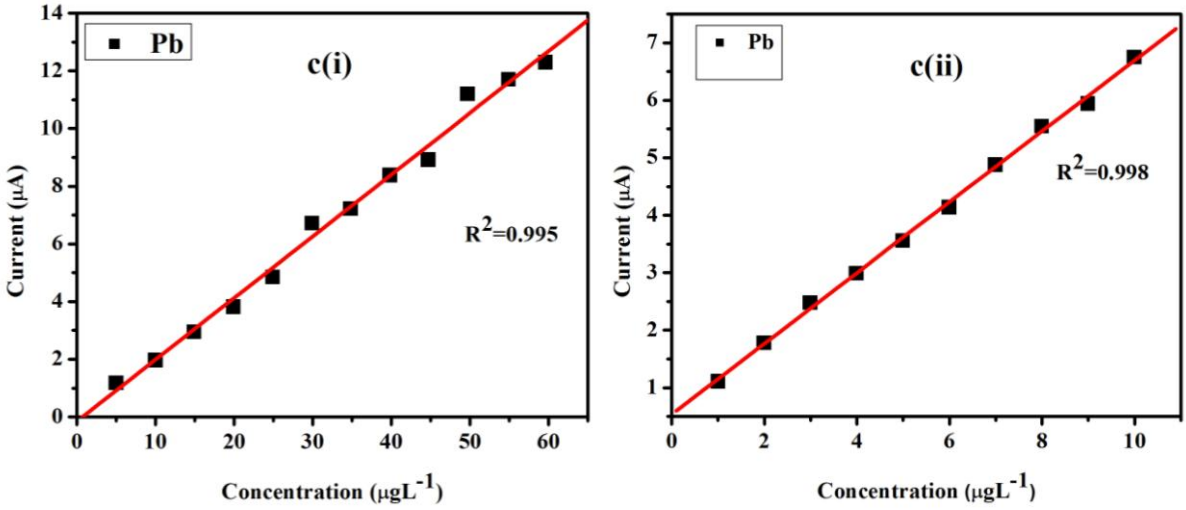

Figure 4.16: Calibration plots for (a) Zn^{2+}, (b) Cd^{2+} and (c) Pb^{2+} at the Gr-GC-HgE with an *in situ* deposited Hg film (i) 5-60 µg L^{-1} and (ii) 1-10 µg L^{-1}. Supporting electrolyte (0.1 M acetate buffer pH 4.6), deposition time (120 s at -1.3 V), rotation speed (1000 rpm), frequency (50 Hz), amplitude (0.04 V) and sweep rate (0.2975 Vs^{-1}).

Table 4.2: Correlation coefficient, (r^2) and detection limits of Zn^{2+}, Cd^{2+} and Pb^{2+} determined individually on Gr-GC-HgE.

UNIVERSITY of the
WESTERN CAPE

	Range 1 -10 µg L^{-1}			Range 5 -60 µg L^{-1}		
	Zn^{2+}	Cd^{2+}	Pb^{2+}	Zn^{2+}	Cd^{2+}	Pb^{2+}
Slope (µA/µg L^{-1})	**1.32±0.35**	**0.92±0.05**	**0.66±0.04**	**0.39±0.03**	**0.46±0.01**	**0.24±0.03**
Standard Deviation (SD) of the blank	**0.018**	**0.035**	**0.03**	**0.019**	**0.018**	**0.036**
Correlation coefficient (r^2)	**0.996**	**0.999**	**0.998**	**0.994**	**0.995**	**0.995**
Detection limits (µg L^{-1})	**0.04**	**0.11**	**0.14**	**0.15**	**0.12**	**0.45**

*n = 3, where n is the number of replications

The results in Table 4.1 and 4.2 show that the detection limits and analytical parameters for both the simultaneous and individual analysis makes the Gr-GC-HgE suitable for trace analysis of Zn^{2+} , Cd^{2+} and Pb^{2+}.

4.2.4.3 Comparison of individual and simultaneous determination

To compare individual and simultaneous analyses, the detection limit (3σ blank/slope) of each metal calibrated individually and in the mixture using the same deposition time of 120 s were compared; these detection limits are shown in Tables 4.1 and 4.2. Since the detection limit is determined from the slope (sensitivity) of the calibration curve a low detection limit implies high sensitivity and *vice versa*. The detection limits for individual analysis were higher while those for the simultaneous analysis were significantly lower. The lower sensitivities are due to mostly interferences from the other metal ions, which is fight for the limited active sites at the electrode surface.

UNIVERSITY of the
WESTERN CAPE

4.3 Part B: The graphene modified glassy carbon thin film bismuth electrode (Gr-GC-BiE)

In this section the behavior of a graphene modified glassy carbon thin film bismuth electrode (Gr-GC-BiE) towards Zn^{2+}, $Cd^{2+}$and Pb^{2+} was evaluated. The optimum instrumental conditions such as deposition potential, deposition time, rotation speed, frequency and amplitude were determined. Furthermore, the analytical parameters such as; the sensitivity, correlation coefficient and detection limits for the Gr-GC-BiF are also presented.

4.3.1 Current responses of graphene modified glassy carbon thin film bismuth electrodes (Gr-GC-BiE)

The SWASV peak responses of a Gr-GC-BiE prepared with varying concentrations of graphene coating solutions (0.25 mg mL^{-1}, 0.5 mg mL^{-1}, 1 mg mL^{-1}) followed by an *in situ* plated Bi-film were compared in 0.1 M acetate buffer (pH 4.6) containing 2 mg L^{-1} Bi^{3+} and 20 µg L^{-1} target metal ions. Figure 4.17 shows that the highest peak currents are obtained when using a concentration of 0.25 mg mL^{-1} graphene solution in preparing the Gr-GC-BiE followed by 0.5 mg mL^{-1} and 1 mg mL^{-1} graphene solutions. This decrease in peak currents can be attributed to an increase in the number of graphene sheets stacking on top of each other which restricts the passage of electron flow from the analyte solution to the surface of the GCE. It is obvious from this data that there is a strong dependency on the amount of graphene that gets coated onto the electrode and its SWASV peak responses towards the metal ions. The behavior of the Gr-GC-BiE is similar to that which was observed with the Gr-GC-HgE in Part A.

UNIVERSITY of the WESTERN CAPE

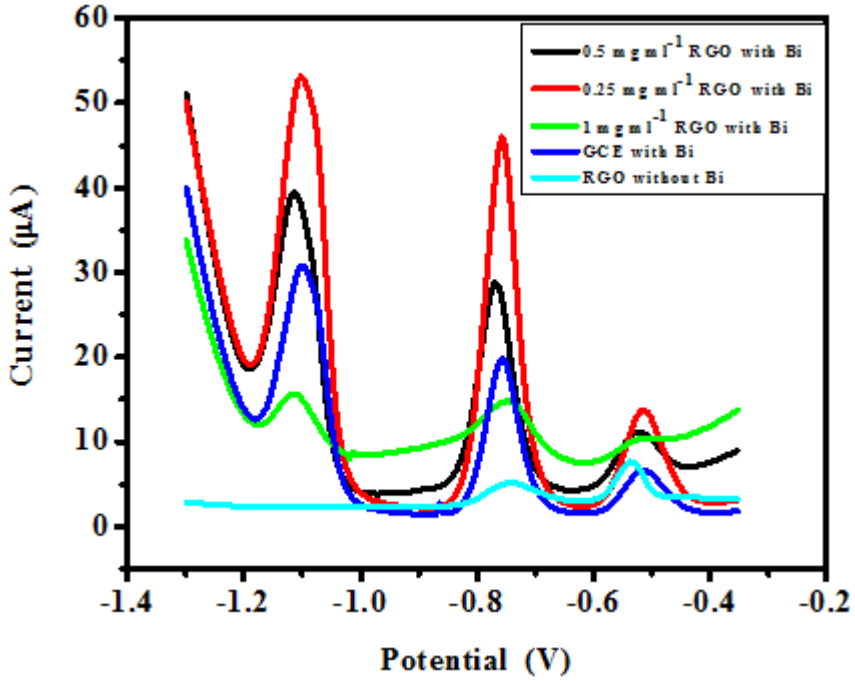

Figure 4.17: SWASV of 20 µg L^{-1} of Zn^{2+}, Cd^{2+} and Pb^{2+} at a glassy carbon electrode (GCE) modified with various concentrations of graphene with *in situ* deposited Bi film. Supporting electrolyte (0.1 M acetate buffer pH 4.6), after (120 s) deposition time at (-1.3 V) deposition potential, (1000 rpm) rotation speed, (50 Hz) frequency and (0.2975 Vs^{-1}) sweep rate.

UNIVERSITY of the
WESTERN CAPE

4.3.1.1 The effect of bismuth film

Figure 4.18 shows peak currents for Cd^{2+} and Pb^{2+} but not for Zn^{2+} when comparing the graphene modified GC electrode (Gr-GCE) to the *in situ* deposited bismuth film on graphene modified glassy carbon electrode (Gr-GC-BiE). The low response signal for Zn^{2+} at the Gr-GCE indicates that zinc does not or is, insufficiently deposited onto the electrode and hence, no stripping Zn^{2+} peak is observed. However, the *in situ* deposited Bi-film on graphene modified glassy carbon electrode (Gr-GC-BiE) shows strong peak currents for Zn^{2+}, Cd^{2+} and Pb^{2+} due to the ability of bismuth to form alloys with these metal ions [201].

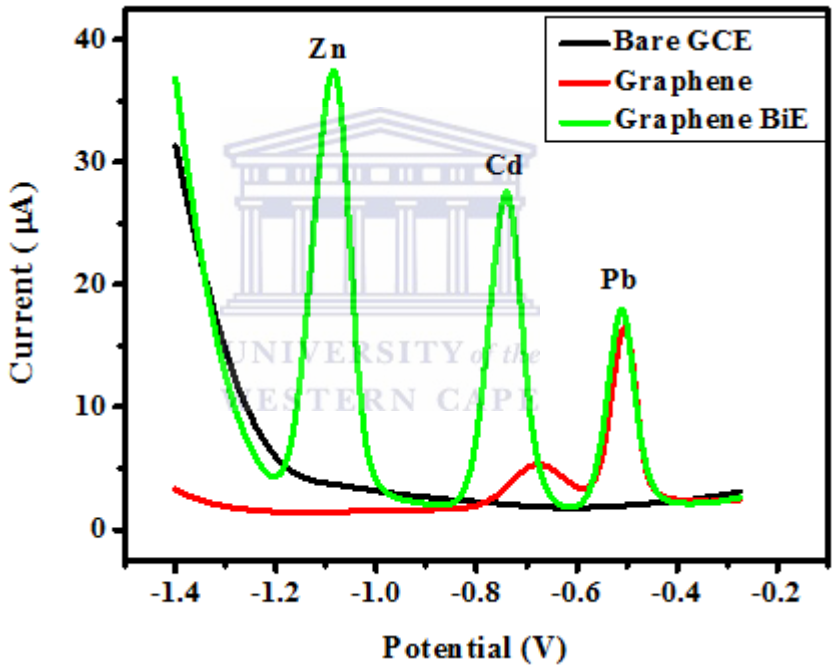

Figure 4.18: The effect of Bismuth film on the peak current of 20 µg L^{-1} of Zn^{2+}, Cd^{2+} and Pb^{2+} at the Gr-GC-BiE. Supporting electrolyte (0.1 M acetate buffer pH 4.6), deposition time (120 s at – 1.3 V), rotation speed (1000 rpm), frequency (50 Hz), amplitude (0.04 V) and sweep rate (0.2975 Vs^{-1}).

4.3.2 Effect of instrumental parameters on the stripping peak currents of Zn^{2+},Cd^{2+} and Pb^{2+} at the graphene modified glassy carbon bismuth thin film electrode (Gr-GC-BiE)

4.3.2.1 Deposition potential

The effect of the deposition potential on the peak currents of Zn^{2+}, Cd^{2+} and Pb^{2+} at the Gr-GC-BiE was studied in the potential range from -0.6V to -1.5V. Figure 4.19 shows the deposition potential had a significant influence on the current response of Zn^{2+}, Cd^{2+} and Pb^{2+} ions, thus the peak current for all the metals ions increased with increasing negative deposition potentials. On the other hand, at deposition potentials greater than the oxidation potentials of the target metal ions no response signals were observed since, no reduction and deposition of the metal ions from the analyte solution onto the electrode surface occurs [202]. As a consequence, the optimal value selected for the deposition and the determination of Zn^{2+}, Cd^{2+} and Pb^{2+} in further experiments was -1.3 V. This reduction potential (-1.3 V) is sufficient to effect the reduction and the deposition of all three metals ions onto the electrode surface.

UNIVERSITY of the
WESTERN CAPE

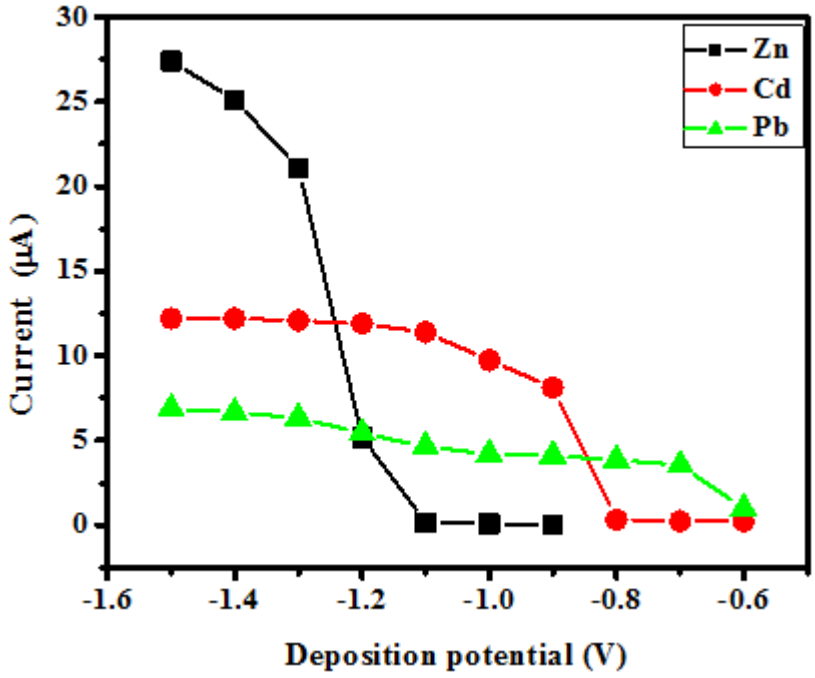

Figure 4.19: The effect of deposition potential on the peak current of 20 µg L^{-1} of Zn^{2+}, Cd^{2+} and Pb^{2+} at the Gr-GC-BiE. Supporting electrolyte (0.1 M acetate buffer pH 4.6), deposition time (120 s at varying deposition potentials), rotation speed (1000 rpm), frequency (50 Hz), amplitude (0.04 V) and sweep rate (0.2975 Vs^{-1}).

4.3.2.2 Deposition time

Figure 4.20 illustrates the behavior of deposition time on the peak currents of Zn^{2+}, Cd^{2+} and Pb^{2+} at the Gr-GC-BiE. The peak current of the metals increases linearly with increasing deposition time in the range from 30 to 300 s meaning that the longer the deposition time, the more the amount of metal that gets deposited [203]. A deposition time of 120 s was sufficient to avoid surface saturation of the electrode which may occur after 120 seconds and thus chosen for all subsequent experiments.

UNIVERSITY of the
WESTERN CAPE

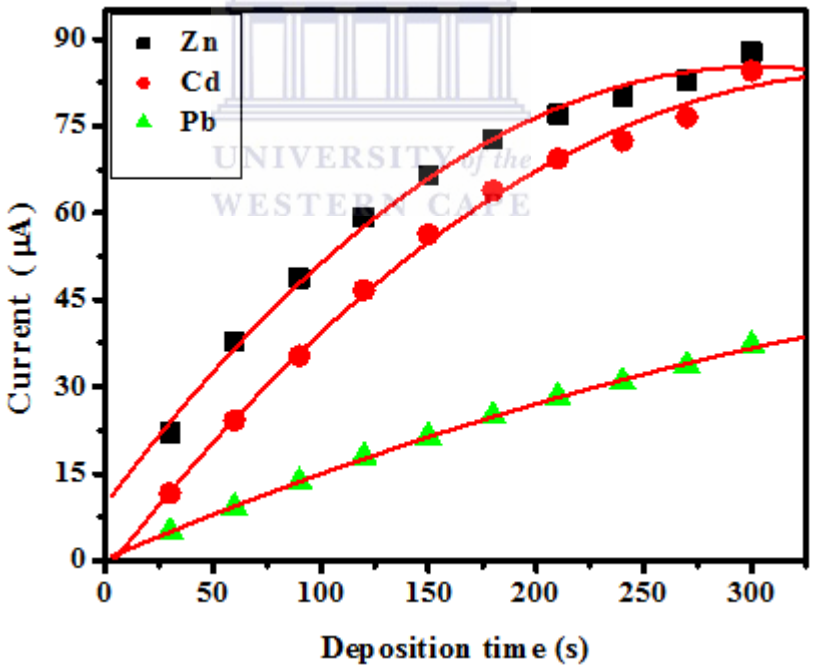

Figure 4.20: The effect of deposition time on the peak current of 20 µg L^{-1} of Zn^{2+}, Cd^{2+} and Pb^{2+} at the Gr-GC-BiE. Supporting electrolyte (0.1 M acetate buffer pH 4.6), varying deposition times at a -1.3 V), rotation speed (1000 rpm), frequency (50 Hz), amplitude (0.04 V) and sweep rate (0.2975 Vs^{-1}).

4.3.2.3 Rotation speed

The effect of rotation speed on the metal ion peak currents when applied to the Gr-GC-BiE was investigated in the range between 200 and 2000 rpm. As shown in Figure 4.21 the stripping peak currents of Zn^{2+}, Cd^{2+} and Pb^{2+} increased constantly with increasing square-root of rotation speed. The rotation speed enhances sensitivity of stripping analysis since it facilitates the transport of metal ions from the bulk solution to the electrode surface. However, in order to avoid electrode saturation a rotation speed of 1000 rpm was selected.

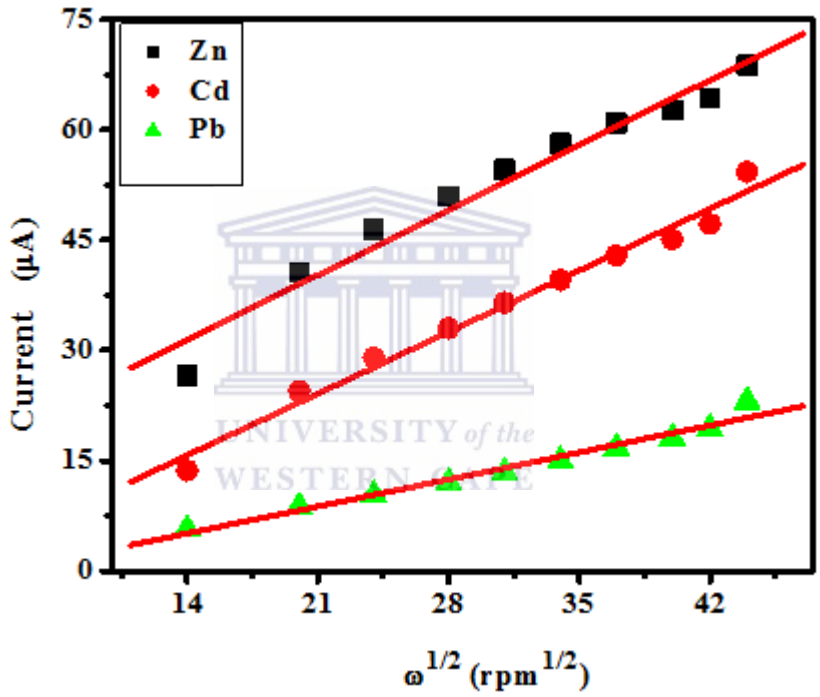

Figure 4.21: The effect of rotation speed on the peak current of 20 µg L^{-1} of Zn^{2+}, Cd^{2+} and Pb^{2+} at the Gr-GC-BiE. Supporting electrolyte (0.1 M acetate buffer pH 4.6), deposition time (120 s at -1.3 V), at varying rotation speeds, frequency (50 Hz), amplitude (0.04 V) and sweep rate (0.2975 Vs^{-1}).

4.3.2.4 Frequency

The effect of frequency on the peak currents of Zn^{2+}, Cd^{2+} and Pb^{2+} at the Gr-GC-BiE was studied in the range 10-100 Hz. As shown in Figure 4.22 the peak current for all three metals increases linearly with increasing frequency[202]. After a frequency of 50 Hz the zinc peak

current tends towards a plateau hence, a frequency of 50 Hz was chosen as the optimum frequency for all future experiments with the Gr-GC-BiE

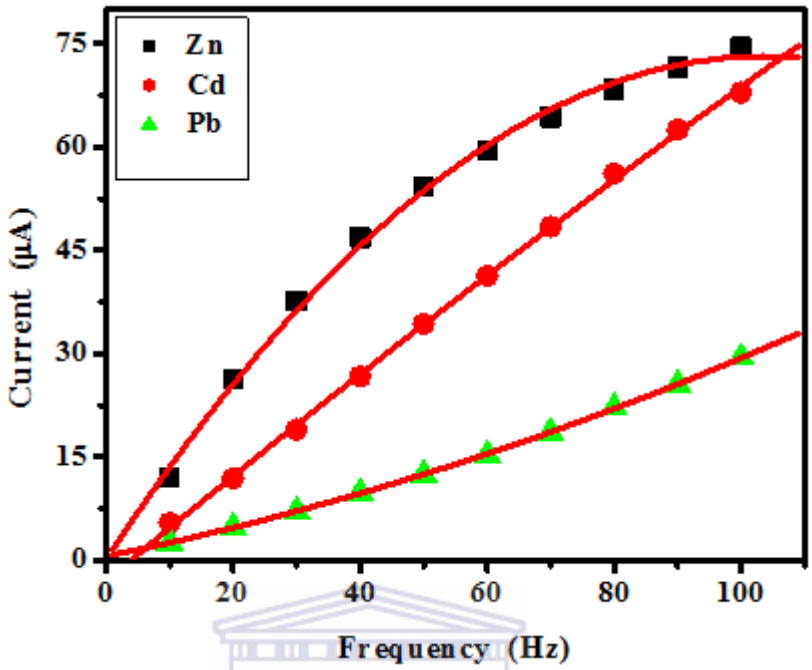

Figure 4.22: The effect of frequency on the peak current of 20 µg L^{-1} of Zn^{2+}, Cd^{2+} and Pb^{2+} at the Gr-GC-BiE. Supporting electrolyte (0.1 M acetate buffer pH 4.6), deposition time (120 s at -1.3 V), rotation speed (1000), at varying frequencies, amplitude (0.04 V) and sweep rate (0.2975 Vs^{-1}).

4.3.2.5 Amplitude

Figure 4.23 shows the effect of the amplitude on the peak currents of Zn^{2+}, Cd^{2+} and Pb^{2+} between 0.01 and 0.1 V. The peak height for all three metals increases continuously with increasing amplitude [204]. All three metal ions show that after an amplitude of 0.05 V, the current responses start to show non-linear behavior towards further increases in amplitude hence, an amplitude of 0.04 V was chosen as the optimum amplitude.

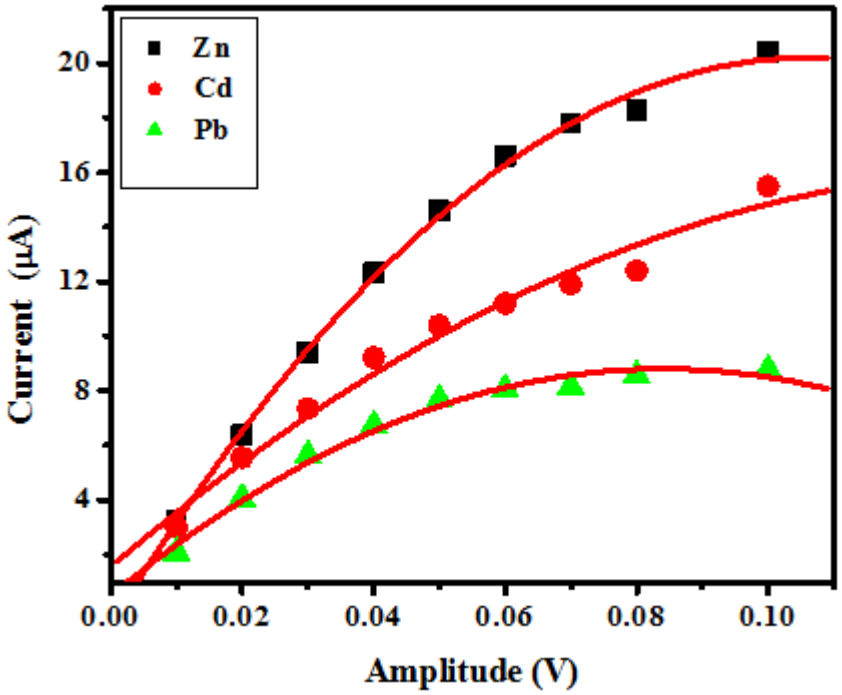

Figure 4.23: The effect of amplitude on the peak current of 20 µg L^{-1} of Zn^{2+}, Cd^{2+} and Pb^{2+} at the Gr-GC-BiE. Supporting electrolyte (0.1 M acetate buffer pH 4.6), deposition time (120 s at -1.3 V), rotation speed (1000), frequency (50 Hz), at varying amplitudes and sweep rate (0.2975 Vs^{-1}).

UNIVERSITY of the
WESTERN CAPE

4.3.3 Film stability and reproducibility

The Gr-GC-BiE showed very good reproducibility. The electrodes were stable and could do repetitive measurements yielding a relative standard deviation, RSD% of 7.2, 2.95 and 4.36% for Zn^{2+}, Cd^{2+} and Pb^{2+} respectively, in 0.1 M acetate buffer solution containing 20 µg L^{-1} of each metal ion and 2 mg L^{-1} Bi^{3+}.

4.3.4 Analytical performance of graphene modified glassy carbon thin film bismuth electrode (Gr-GC-BiE)

4.3.4.1 Simultaneous determination of Zn^{2+}, Cd^{2+} and Pb^{2+}

In simultaneous analysis the signal responses (peak currents) for Zn^{2+}, Cd^{2+} and Pb^{2+} ions mixed together in the same solution and measured under optimal conditions at the Gr-GC-

BiE are shown in Figures 4.24a and b. Calibration plots of current *versus* concentration for the metal ions extends over two concentration ranges 1 - 10 µg L^{-1} and 5 - 60 µg L^{-1}; these are shown in Figures 4.25a(i) and b(ii).

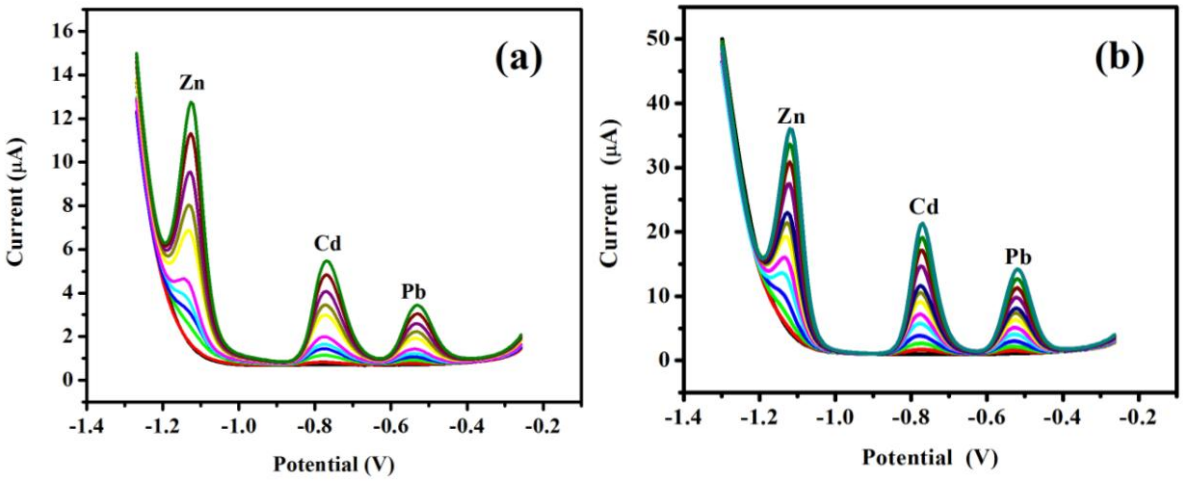

Figure 4.24: SWASV of Zn^{2+}, Cd^{2+} and Pb^{2+} at the Gr-GC-BiE with an *in situ* deposited Bi film. (a) 1 – 10 µg L^{-1} and (b) 5 - 60 µg L^{-1}. Supporting electrolyte (0.1 M acetate buffer pH 4.6), deposition time (120 s at -1.3 V), rotation speed (1000 rpm), frequency (50 Hz), amplitude (0.04 V) and sweep rate (0.2975 Vs^{-1}).

UNIVERSITY of the
WESTERN CAPE

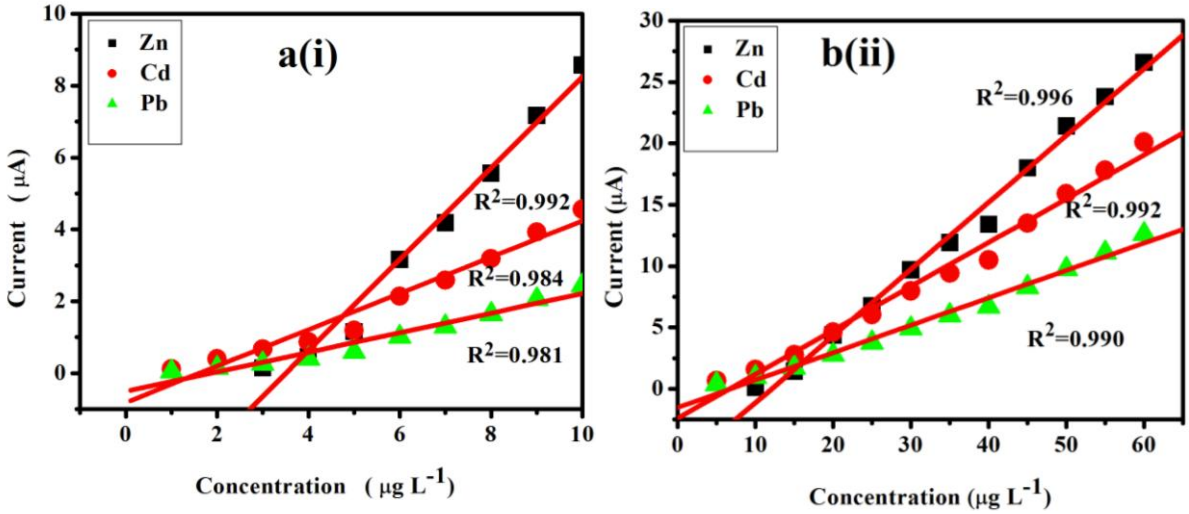

Figure 4.25: Calibration plots for Zn^{2+}, Cd^{2+} and Pb^{2+} at the Gr-GC-BiE with an *in situ* deposited Bi film. a(i) 1 – 10 µg L^{-1} and b(ii) 5 - 60 µg L^{-1}. Supporting electrolyte (0.1 M acetate buffer pH 4.6), deposition time (120 s at -1.3 V), rotation speed (1000 rpm), frequency (50 Hz), amplitude (0.04 V) and sweep rate (0.2975 Vs^{-1}).

In addition, the detection limits of the metal ions were determined in the same manner as that in Part A namely, by using the equation; detection limit = $3\sigma_{blank}$ / slope. The excellent correlation coefficients and the detection limits for the metal ions were obtained and these are presented in the Table 4.3.

Table 4.3: Correlation coefficient, (r^2) and detection limits of Zn^{2+}, Cd^{2+} and Pb^{2+} determined simultaneously on Gr-GC-BiE.

	Range 1-10 µg L^{-1}			**Range 5-60 µg L^{-1}**		
	Zn^{2+}	**Cd^{2+}**	**Pb^{2+}**	**Zn^{2+}**	**Cd^{2+}**	**Pb^{2+}**
Slope (µA/µg L^{-1})	**1.09±0.25**	**0.48±0.05**	**0.23±0.06**	**0.56±0.03**	**0.37±0.01**	**0.22±0.01**
Standard Deviation (SD) of the blank	**0.099**	**0.038**	**0.035**	**0.022**	**0.027**	**0.021**
Correlation coefficient (r^2)	**0.992**	**0.984**	**0.981**	**0.996**	**0.992**	**0.990**
Detection limit (µg L^{-1})	**0.27**	**0.24**	**0.46**	**0.12**	**0.22**	**0.28**

*n = 3, where n is the number of replications

UNIVERSITY of the
WESTERN CAPE

4.3.4.2 Individual analysis of Zn^{2+}, Cd^{2+} and Pb^{2+}

The stripping voltammograms obtained from the individual analysis of $Zn^{2+,}$ Cd^{2+} and Pb^{2+} in separate solutions of 0.1 M acetate buffer (pH 4.6) and 2 mg L^{-1} Bi^{3+} at a deposition time of 120 s are shown in Figures 4.26(a), (b) and (c). For the Zn^{2+} analysis it is difficult to identify a current peak at concentrations less than 5 µg L^{-1}. While for Cd^{2+} and Pb^{2+} the peak current increased linearly with increasing concentration in the 1 - 10 µg L^{-1} concentration range. The Zn^{2+} response signals in Figure 4.26a show broad peaks and are not as sharp as those obtained for the Zn^{2+} responses in Figure 4.24a this may be due to hydrogen evolution which distorts the peak shape.

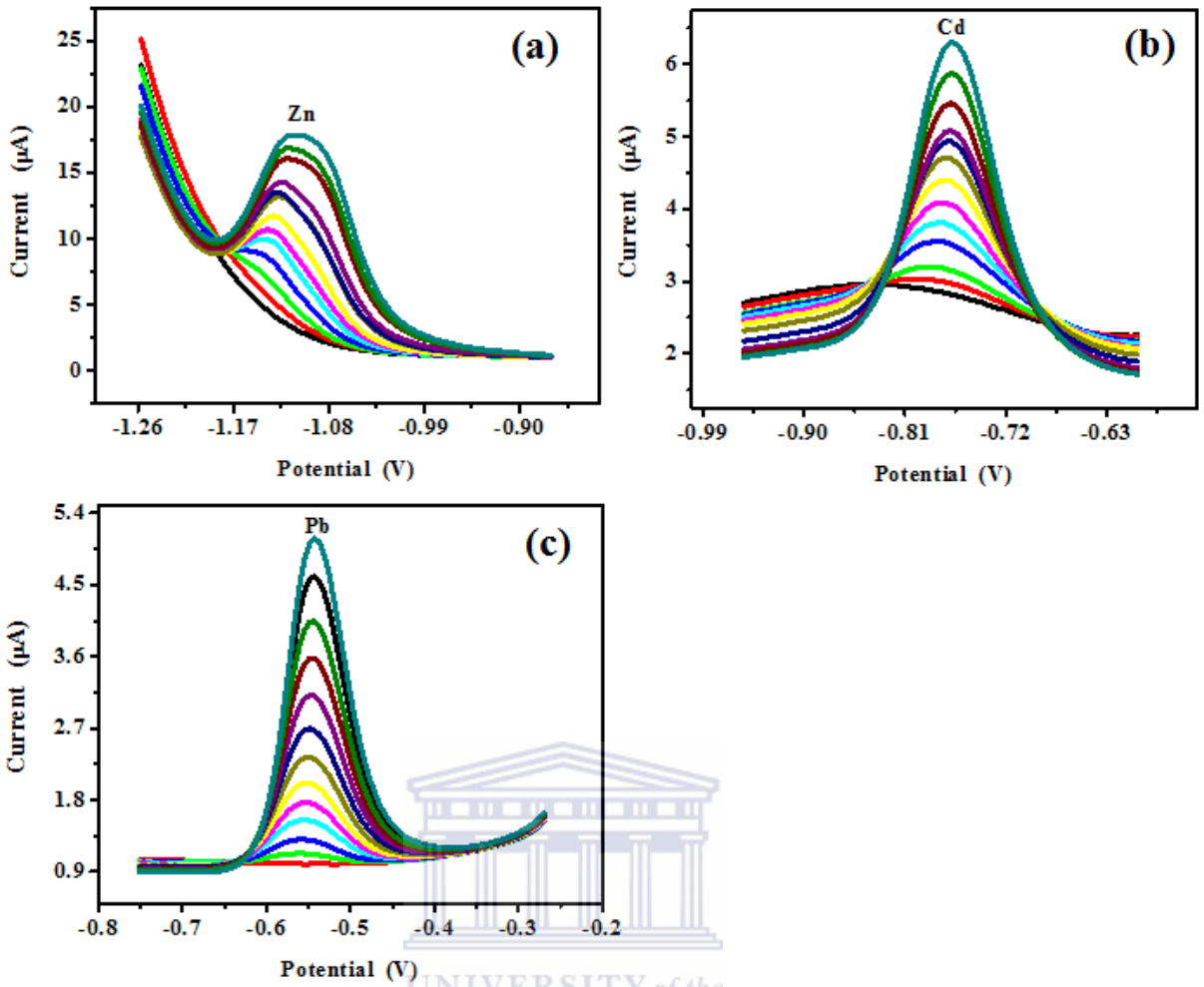

UNIVERSITY of the
WESTERN CAPE

Figure 4.26: SWASV of (a) Zn^{2+}, (b) Cd^{2+} and (c) Pb^{2+} from 1 - 60 µg L^{-1} at the Gr-GC-BiE with an *in situ* deposited Bi film. Supporting electrolyte (0.1 M acetate buffer pH 4.6), deposition time (120 s at -1.3 V), rotation speed (1000 rpm), frequency (50 Hz), amplitude (0.04 V) and sweep rate (0.2975 Vs^{-1}).

The calibration plots for Zn^{2+}, Cd^{2+} and Pb^{2+} at the two concentration ranges, 1 - 10 µg L^{-1} and 5 - 60 µg L^{-1} are presented in Figure 4.27 and were used in the determination of the detection limits. The detection limit for each metal was determined based on three times the standard deviation ($3\sigma_{blank}$) of the blank divided by the slope of the calibration curve for each metal ion. Table 4.4 shows the correlation coefficients and the detection limits for the metal ions.

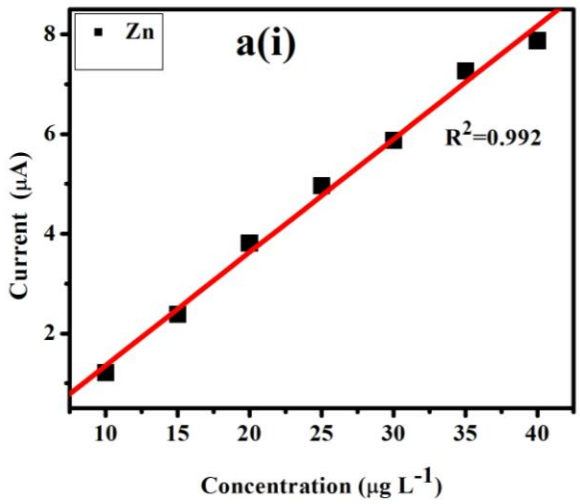

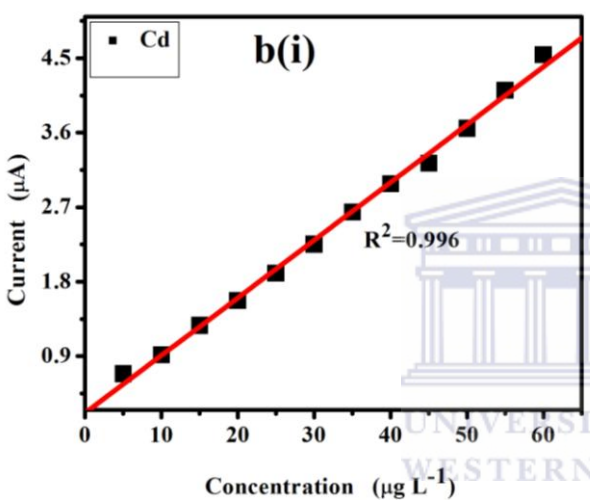

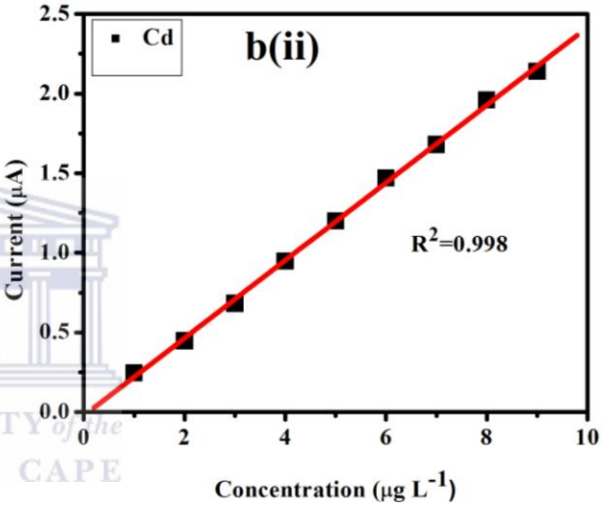

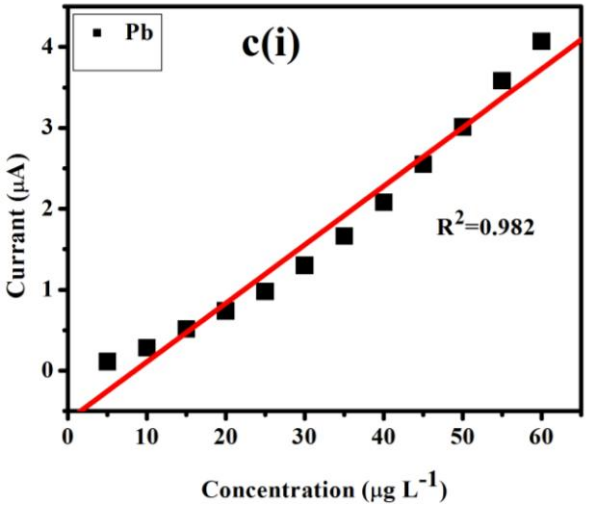

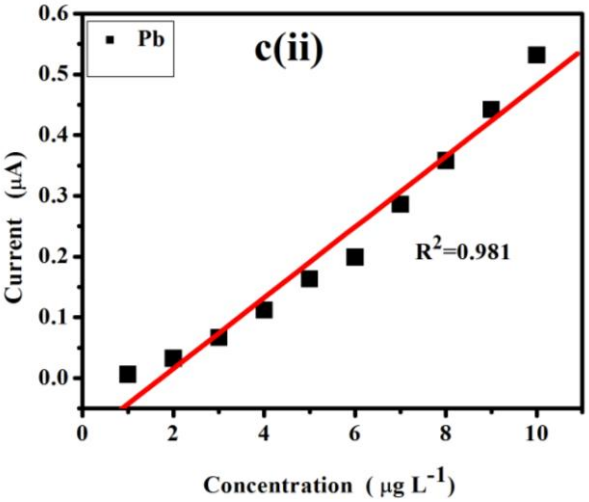

UNIVERSITY of the
WESTERN CAPE

Figure 4.27: Calibration plots for (a) Zn^{2+}, (b) Cd^{2+} and (c) Pb^{2+} at the Gr-GC-BiE with an *in situ* deposited Bi film (i) 5 - 60 µg L^{-1} and (ii) 1 - 10 µg L^{-1}. Supporting electrolyte (0.1 M acetate buffer pH 4.6), deposition time (120 s at -1.3 V), rotation speed (1000 rpm), frequency (50 Hz), amplitude (0.04 V) and sweep rate (0.2975 Vs^{-1}).

Table 4.4: Correlation coefficient, (r^2) and detection limits of Zn^{2+}, Cd^{2+} and Pb^{2+} determined individually on Gr-GC-BiE.

	Range 1 - 10 µg L^{-1}			**Range 5 - 60 µg L^{-1}**		
	Zn^{2+}	**Cd^{2+}**	**Pb^{2+}**	**Zn^{2+}**	**Cd^{2+}**	**Pb^{2+}**
Slope (µA/µg L^{-1})	**N.D**	**0.25±0.01**	**0.07±0.01**	**0.24±0.01**	**0.07±0.001**	**0.06±0.02**
Standard Deviation (SD) of the blank	**N.D**	**0.03**	**0.04**	**0.048**	**0.06**	**0.05**
Correlation coefficient (r^2)	**N.D**	**0.998**	**0.981**	**0.992**	**0.996**	**0.982**
Detection limits (µg L^{-1})	**N.D**	**0.36**	**1.7**	**0.6**	**2.6**	**2.5**

*n = 3, where n is the number of replications

*N.D = not determined

UNIVERSITY of the
WESTERN CAPE

4.3.4.3 Comparison of individual and simultaneous determination

The simultaneous and individual analysis were done in a acetate buffer 0.1M (pH 4.6), containing the same concentration of Bi^{3+} film and metal ions using 120 s deposition time and -1.3 V deposition potential. The detection limits obtained with both simultaneous and individual analyses for Cd^{2+} and Pb^{2+} but were for simultaneous lower than individual one. However, the detection limit of Zn^{2+} was much higher for the individual since no peak was detected at concentrations 5 µg L^{-1} and lower, while it can be seen in simultaneous analysis.

4.4 Part C: The graphene modified glassy carbon thin film antimony electrode (Gr-GC-SbE)

In the following section the instrumental parameters and the influence of graphene coating

solution concentrations were optimized in order to detect the target metal ions (Zn^{2+}, Cd^{2+} and Pb^{2+}) at the Gr-GC-SbE.

4.4.1 Current responses of graphene modified glassy carbon thin film antimony electrodes (Gr-GC-SbE)

Figure 4.28, shows the stripping voltammetric responses signals (peak currents) of 30 µg L^{-1} of each target metal ions (Zn^{2+}, Cd^{2+} and Pb^{2+}) in 20 ml of 0.1 M acetate buffer (supporting electrolyte) and 0.5 mg L^{-1} Sb^{3+} obtained at the Gr-GC-SbE. The signal responses were obtained with various concentrations of graphene solutions used in the preparation of the Gr-GC-SbE. A deposition potential of -1.3 V and deposition time 120 seconds was used showing oxidation potentials at -1.15 V, -0.76 V and -0.5 V for Zn^{2+}, Cd^{2+} and Pb^{2+}, respectively . The figure shows that the 0.25 mg L^{-1} graphene solution gives the highest, sharpest peak current and is the most sensitive in terms of electrode current response. These results further show that with increasing concentration graphene coating solutions the number of graphene layers due to stacking will increase and hinder the passage of electron flow to the electrode surface leading to lower current signal.

UNIVERSITY of the
WESTERN CAPE

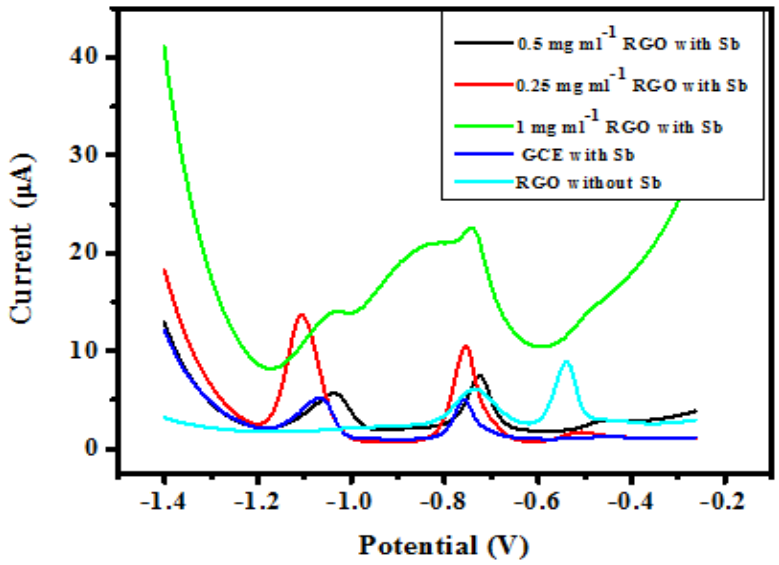

Figure 4.28: SWASV of 30 µg L^{-1} of Zn^{2+}, $Cd^{2+}$and Pb^{2+} at a glassy carbon electrode (GCE) modified with various concentrations of graphene with an *in situ* deposited Sb film.

Supporting electrolyte (0.1 M acetate buffer pH 4.6), deposition time (120 s at -1.3 V), rotation speed (1000 rpm), frequency (50 Hz), amplitude (0.04 V) and sweep rate (0.2975 Vs^{-1}).

4.4.1.1 The effect of antimony film

The influence of an antimony film on the stripping peak current of Zn^{2+}, $Cd^{2+}$and Pb^{2+} was investigated in acetate buffer (0.1 M, pH 4.6). As illustrated in Figure 4.29 the current responses of Zn^{2+} and Cd^{2+} increased significantly after adding the antimony film, while the signal of Pb^{2+} decreased. This decrease Pb^{2+} in the current is due to a pH effect and was similarly observed by *Eva Svobodová, et al*. [205] they reported that the maximum peak height for Pb^{2+} with SbFE was obtained at pH = 2, and that the Pb^{2+} peak decreases as the pH increases

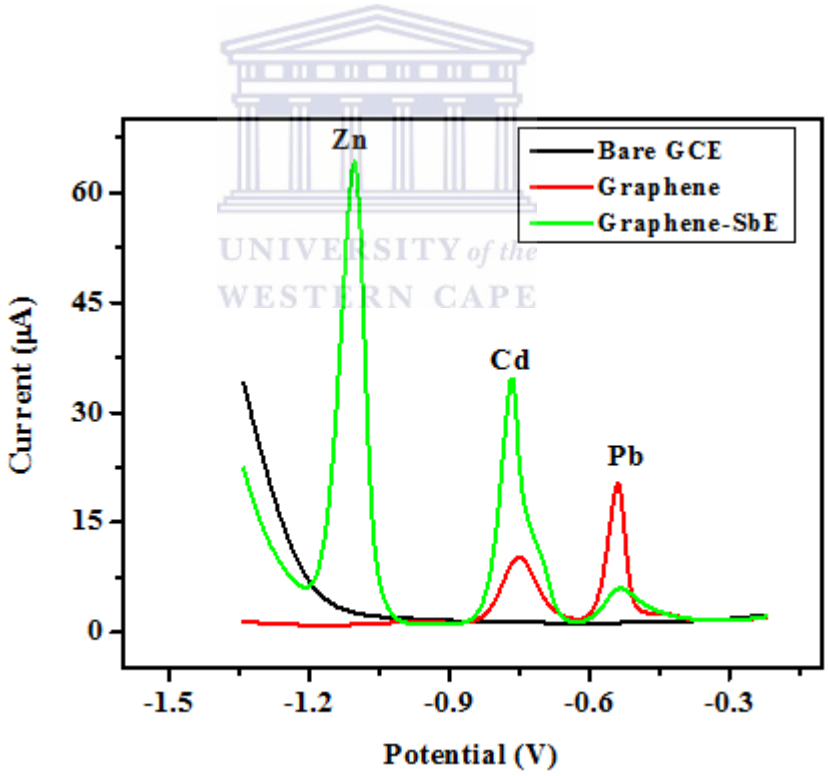

Figure 4.29: The effect of antimony film on the peak current of 30 µg L^{-1} of Zn^{2+}, Cd^{2+} and Pb^{2+} at the Gr-GC-SbE. Supporting electrolyte (0.1 M acetate buffer pH 4.6), deposition time (120 s at -1.3 V), rotation speed (1000), frequency (50 Hz), amplitude (0.04 V) and sweep rate (0.2975 Vs^{-1}).

4.4.2 Effect of instrumental parameters on the stripping peak currents of Zn^{2+}, Cd^{2+} and Pb^{2+} at the graphene modified glassy carbon antimony thin film electrode (Gr-GC-SbE)

4.4.2.1 Deposition potential

The influence of deposition potential on the peak currents of Zn^{2+}, Cd^{2+} and Pb^{2+} at the Gr-GC-SbE was investigated in the range of −0.6 to −1.4 V, in 0.1 M acetate buffer (pH 4.6). As can be seen in Figure 4.30, the peak currents of all three metals increases as the deposition potential becomes more negative and, is due to all three metals being positively charged ions which are preferentially reduced at more negative potentials [17]. A potential of -1.3 V was chosen as optimum deposition potential since at this potential Zn^{2+} and Cd^{2+} are sufficiently deposited to give adequate responses. The low current response for Pb^{2+} is due to the inappropriate pH of the acetate buffer namely, pH 4.6.

UNIVERSITY of the
WESTERN CAPE

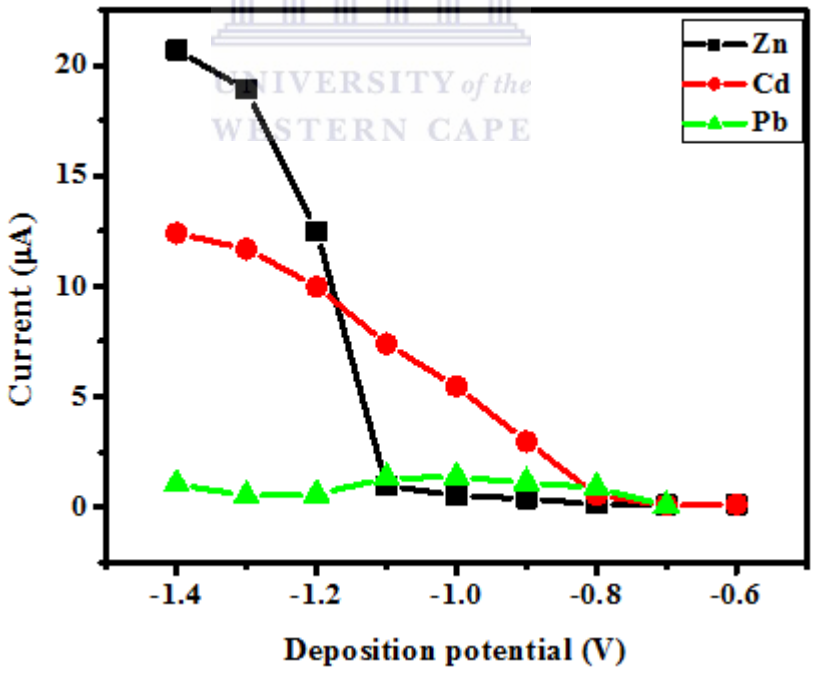

Figure 4.30: The effect of deposition potential on the peak current of 30 µg L^{-1} of Zn^{2+}, Cd^{2+} and Pb^{2+} at the Gr-GC-SbE. Supporting electrolyte (0.1 M acetate buffer pH 4.6), deposition time (120 s at varying deposition potentials), rotation speed (1000 rpm), frequency (50 Hz), amplitude (0.04 V) and sweep rate (0.2975 Vs^{-1}).

4.4.2.2 Deposition time

The sensitivity of the analysis was improved with deposition time. As Figure 4.31 shows, the peak current for target metal ions at the Gr-GC-SbE increased with increasing deposition time over range from 30 to 300 s. This is because of the increase in the amount of analyte that gets deposited onto the Gr-GC-SbE [20]. A deposition time of 120 s was chosen for all further experiments to avoid surface saturation of the electrode which may occur after 120 s and also to avoid long analysis times.

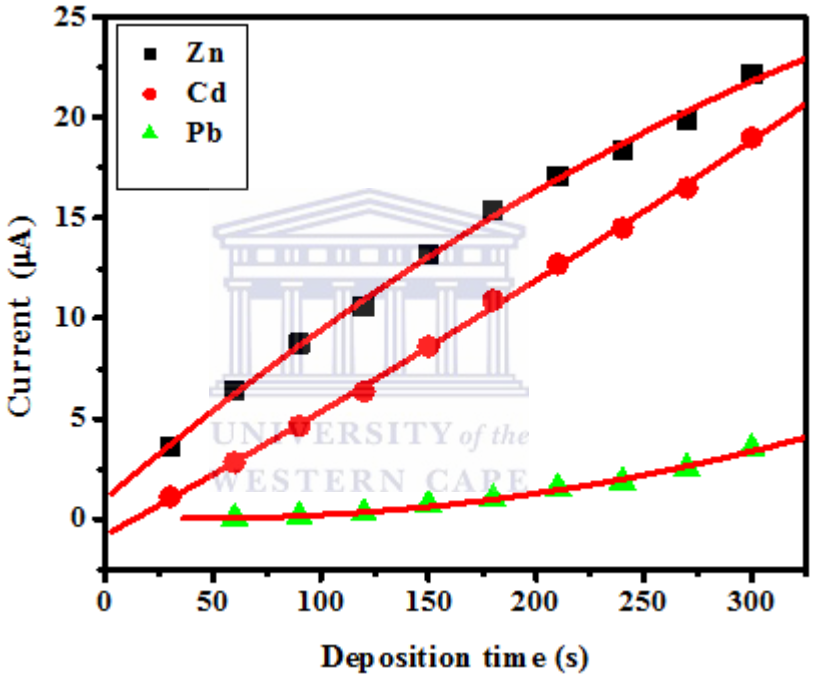

Figure 4.31: The effect of deposition time on the peak current of 30 µg L^{-1} of Zn^{2+}, Cd^{2+} and Pb^{2+} at the Gr-GC-SbE. Supporting electrolyte (0.1 M acetate buffer pH 4.6), varying deposition times at a -1.3 V), rotation speed (1000 rpm), frequency (50 Hz), amplitude (0.04 V) and sweep rate (0.2975 Vs^{-1}).

4.4.2.3 Rotation speed

The rotation speed influence on the peak current for Zn^{2+}, Cd^{2+} and Pb^{2+} at the Gr-GC-SbE was studied in the range from 200 to 2000 rpm. As shown in Figure 4.32 the stripping peak currents of the metal ions increased with increasing square-root of rotation speed. The

increased rotation speed leads to an increase the rate of migration of the target ions from the bulk solution to the electrode surface thus allowing more ions be deposited at the electrode surface within a shorter time. An adequate rotation speed of 1000 rpm was chosen as for all further stripping voltammetric analysis.

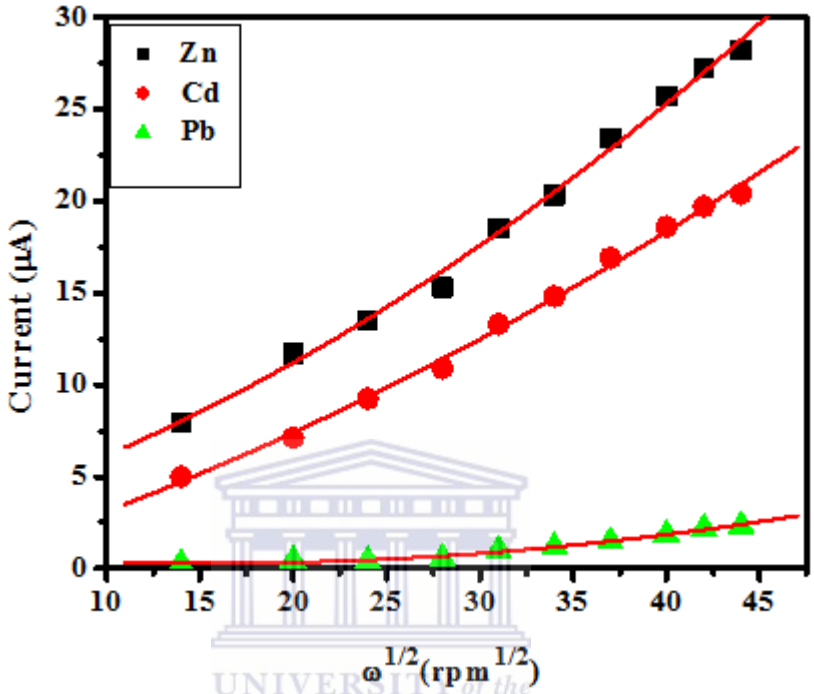

UNIVERSITY of the
WESTERN CAPE

Figure 4.32: The effect of rotation speed on the peak current of 30 µg L^{-1} of Zn^{2+}, Cd^{2+} and Pb^{2+} at the Gr-GC-Sb. Supporting electrolyte (0.1 M acetate buffer pH 4.6), deposition time (120 s at -1.3 V), at varying rotation speeds, frequency (50 Hz), amplitude (0.04 V) and sweep rate (0.2975 Vs^{-1}).

4.4.2.4 Frequency

Figure 4.33 shows the effect of frequency on the stripping peak currents of the target ions at the Gr-GC-SbE in the range 10 Hz to 100 Hz. As the frequency increased so did the peak current of all the metal ions, since the effective scan rate increases. [202]. A frequency of 50 Hz was chosen as the optimum frequency for all further experiments with the Gr-GC-SbE.

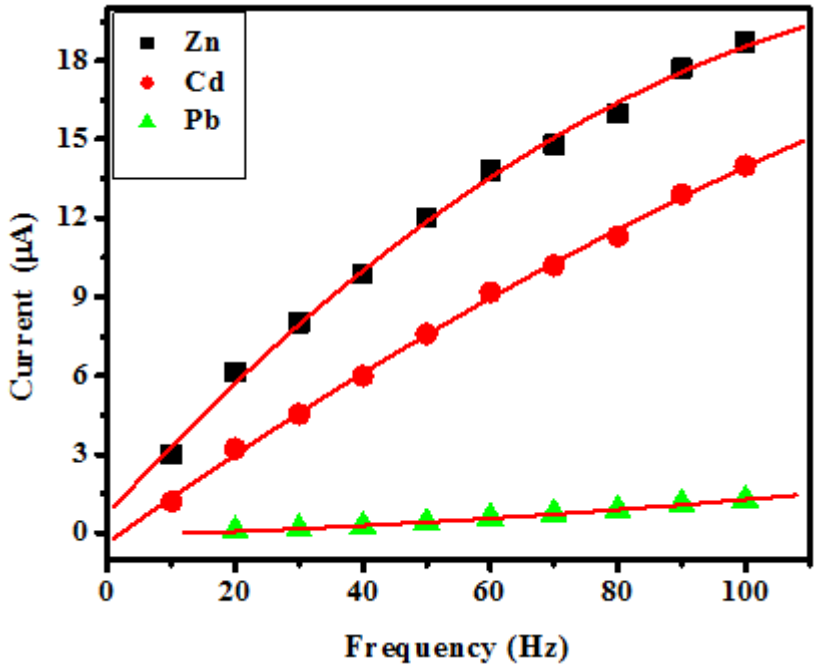

Figure 4.33: The effect of frequency on the peak current of 30 µg L^{-1} of Zn^{2+}, Cd^{2+} and Pb^{2+} at the Gr-GC-SbE. Supporting electrolyte (0.1 M acetate buffer pH 4.6), deposition time (120 s at -1.3 V), rotation speed (1000), at varying frequencies, amplitude (0.04 V) and sweep rate (0.2975 Vs^{-1}).

UNIVERSITY of the
WESTERN CAPE

4.4.2.5. Amplitude

The effect of increased amplitude on the stripping peak current of Zn^{2+}, Cd^{2+} and Pb^{2+} was investigated over the range 0.01 to 0.1 V and is shown in Figure 4.34. The peak current of Zn^{2+} increases up to 0.07 V then starts to trail off the same can be said for Cd^{2+}. However, the peak current of Pb^{2+} increases continuously all be it extremely slowly. The amplitude of 0.25 V was chosen as the optimum amplitude.

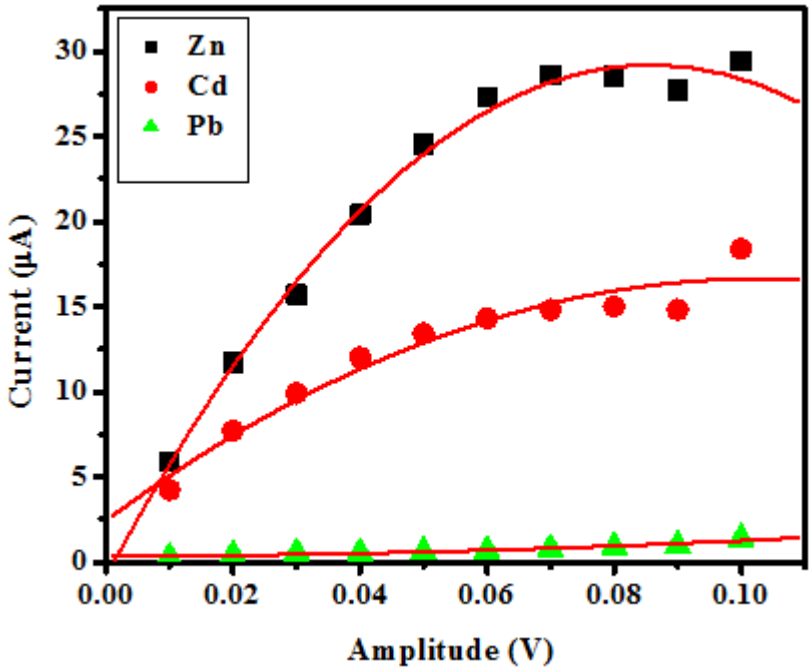

Figure 4.34: The effect of amplitude on the peak current of 30 µg L^{-1} of Zn^{2+}, Cd^{2+} and Pb^{2+} at the Gr-GC-SbE. Supporting electrolyte (0.1 M acetate buffer pH 4.6), deposition time (120 s at -1.3 V), rotation speed (1000), frequency (50 Hz), at varying amplitudes and sweep rate (0.2975 Vs^{-1}).

UNIVERSITY of the
WESTERN CAPE

4.4.3. Film stability and reproducibility

There was no problem with the Gr-GC-SbE stability, the electrochemical platform was stable after each preparation and its reproducibility which was based on its current response peaks towards of 30 µg L^{-1} of each metal ion (Zn^{2+}, Cd^{2+} and Pb^{2+}) in acetate buffer (pH 4.6) was measured. The percentage relative standard deviation (RSD%) of the oxidation peaks currents were 3.8, 2.7 and 9% for Zn^{2+}, Cd^{2+} and Pb^{2+} respectively. The larger percentage relative standard deviation for the Zn^{2+} oxidative peak can be attributed to hydrogen evolution which occurs close the Zn^{2+} half-wave potential.

4.4.4 Analytical Performance of the graphene modified glassy carbon thin film antimony electrode (Gr-GC-SbE)

4.4.4.1 Simultaneous determination of Zn^{2+}, Cd^{2+} and Pb^{2+}

The simultaneous analysis for Zn^{2+}, Cd^{2+} and Pb^{2+} using the Gr-GC-SbE was studied in 0.1 M acetate buffer and 0.5 mg L^{-1} Sb^{3+} at a deposition time of 120 s and deposition potential of -1.3 V. The peak current responses are shown in Figure 4.35(a), and the corresponding calibration plots in the concentration range 5 - 60 µg L^{-1} are presented in Figure 4.35a(i).

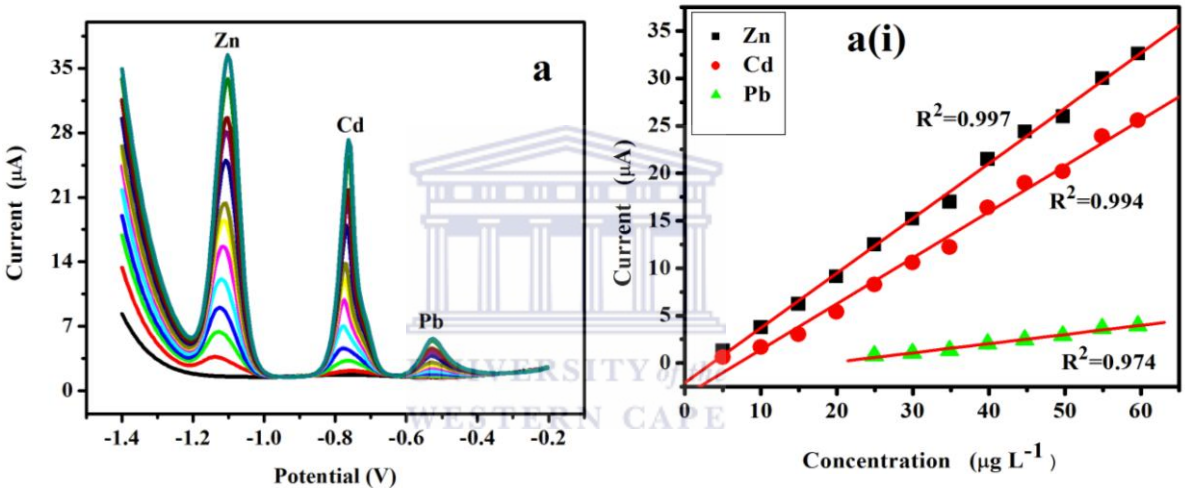

Figure 4.35: The effect of amplitude on the peak current of 30 µg L^{-1} of Zn^{2+}, Cd^{2+} and Pb^{2+} at the Gr-GC-SbE. Supporting electrolyte (0.1 M acetate buffer pH 4.6), deposition time (120 s at -1.3 V), rotation speed (1000), frequency (50 Hz), at varying amplitudes and sweep rate (0.2975 Vs^{-1}).

From the above calibration plots in Figure 4.35, the detection limits of the metal ions were determined using $3\sigma_{blank}$ divided by the slope of the calibration curve. The standard deviation of the blank, σ_{blank} was calculated from ten replications in the presence of Sb^{3+} ions only in acetate buffer. The excellent correlation coefficients and the detection limits for each metal ion are presented in the Table 4.5.

Table 4.5: Correlation coefficient (r^2), and detection limits of Zn^{2+}, Cd^{2+} and Pb^{2+} determined simultaneously on Gr-GC-SbE.

	Range 5 - 60 µg L^{-1}		
	Zn^{2+}	**Cd^{2+}**	**Pb^{2+}**
Slope (µA/µg L^{-1})	**0.57±0.018**	**0.43±0.049**	**0.05±0.038**
Standard Deviation (SD) of the blank	**0.023**	**0.044**	**0.022**
Correlation coefficient (r^2)	**0.997**	**0.994**	**0.974**
Detection limit (µg L^{-1})	**0.1**	**0.3**	**1.2**

*n = 3, where n is the number of replications

4.4.4.2 Individual analysis of Zn^{2+}, Cd^{2+} and Pb^{2+}

Individual analysis for Zn^{2+}, Cd^{2+} and Pb^{2+} was done in 0.1 M buffer acetate containing 0.5 mg L^{-1} Sb^{3+} ions over two concentrations ranges namely, 2 - 10 µg L^{-1} and 5 - 60 µg L^{-1} for Zn^{2+} and Cd^{2+}. While the Pb^{2+} analysis was done in the 20 - 90 µg L^{-1} concentration range; no peaks were detected at low concentrations due to the limited sensitivity of Pb^{2+} with the antimony film at pH 4.6, of the acetate buffer solution. On the other hand, Zn^{2+} and Cd^{2+} peak currents increased as the concentration of the metal ions increases.

UNIVERSITY of the
WESTERN CAPE

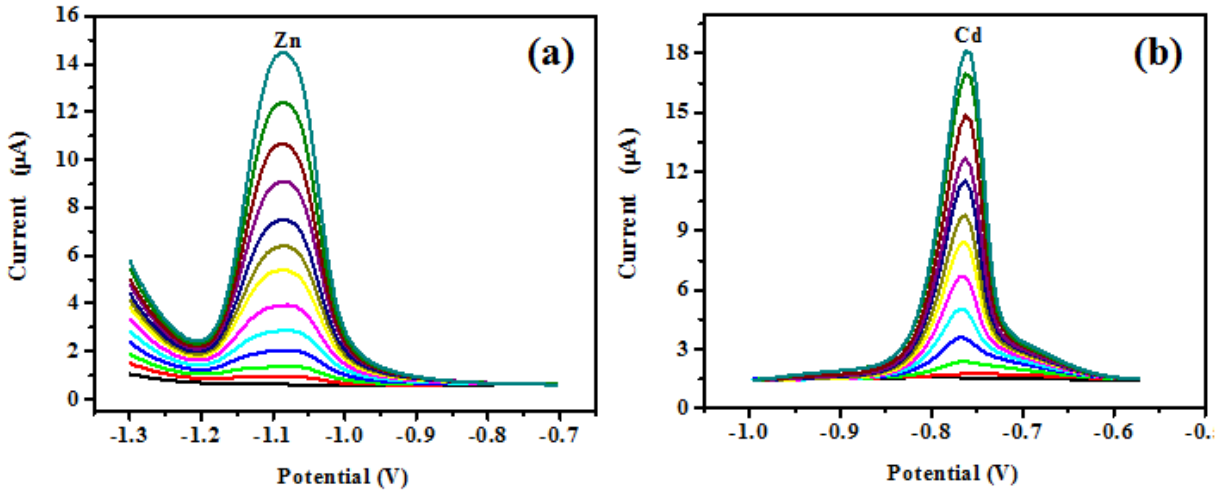

Figure 4.36: SWASV of (a) Zn^{2+} and (b) Cd^{2+} from 2 - 60 µg L^{-1} at the Gr-GC-SbE with an *in situ* deposited Sb film. Supporting electrolyte (0.1 M acetate buffer pH 4.6), deposition time (120 s at -1.3 V), rotation speed (1000 rpm), frequency (50 Hz), amplitude (0.04 V) and sweep rate (0.2975 Vs^{-1}).

The calibration plots for Zn^{2+} and Cd^{2+} extend over two concentration ranges, 2 - 10 µg L^{-1} and 5 -60 µg L^{-1} and these are presented in Figure 4.36. The detection limit for each metal was determined from the calibration plots for each metal ion based on three times the standard deviation ($3\sigma_{blank}$) of the blank divided by the slope of the calibration curve for each metal ion. Table 4.6 shows the correlation coefficients and the detection limits.

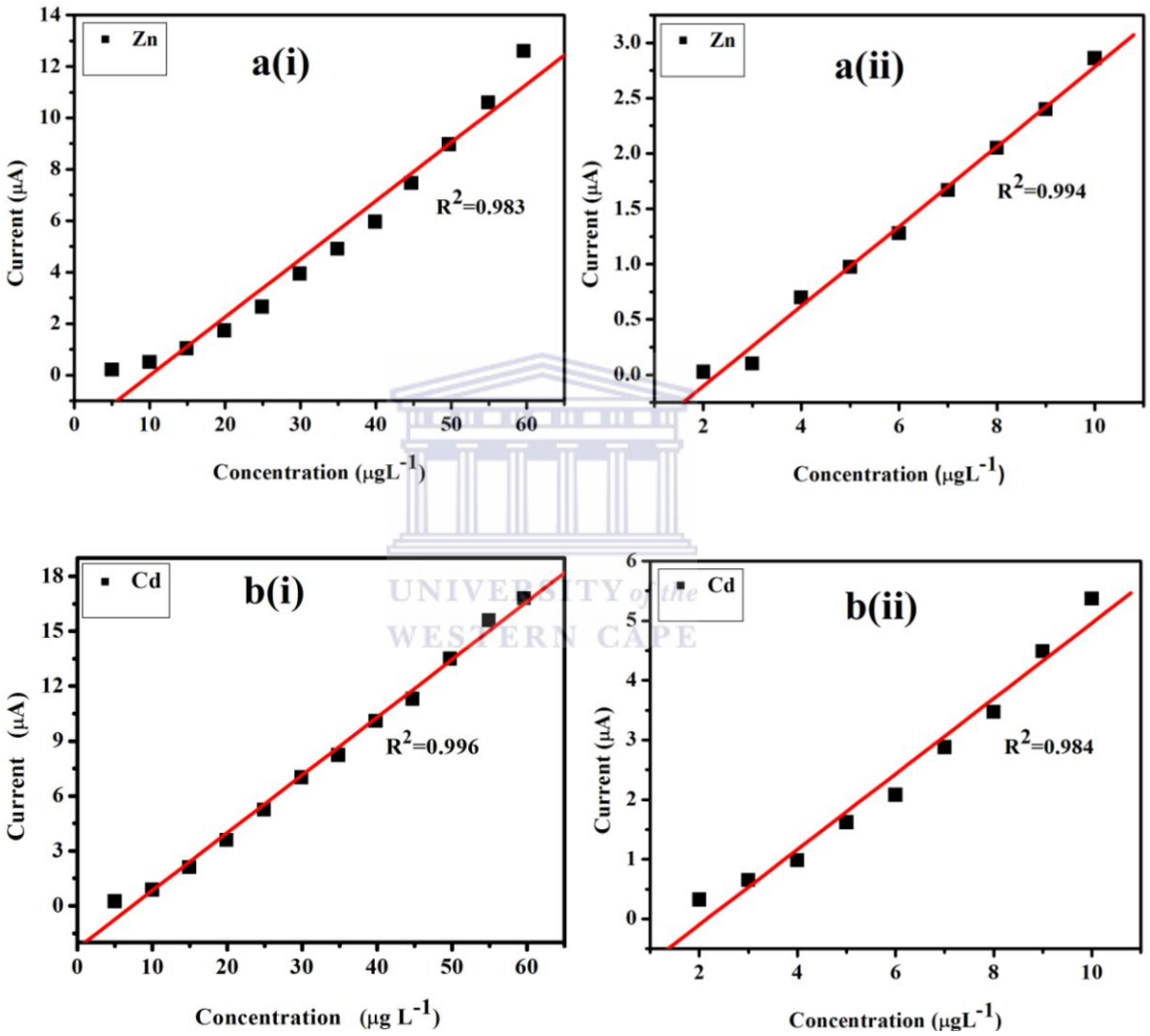

Figure 4.37: Calibration plots for (a) Zn^{2+} and (b) Cd^{2+} at the Gr-GC-SbE with an *in situ* deposited Sb film (i) 5 - 60 µg L^{-1} and (ii) 2 - 10 µg L^{-1}. Supporting electrolyte (0.1 M acetate buffer pH 4.6), deposition time (120 s at -1.3 V), rotation speed (1000 rpm), frequency (50 Hz), amplitude (0.04 V) and sweep rate (0.2975 Vs^{-1}).

UNIVERSITY of the WESTERN CAPE

Table 4.6: Correlation coefficient (r^2), and detection limits of Zn^{2+} and Cd^{2+} determined individually on Gr-GC-SbE.

	Range 2 -10 µg L^{-1}		Range 5 -60 µg L^{-1}	
	Zn^{2+}	Cd^{2+}	Zn^{2+}	Cd^{2+}
Slope (µA/µg L^{-1})	**0.32±0.05**	**0.65±0.02**	**0.22±0.01**	**0.36±0.04**
Standard Deviation (SD) of the blank	**0.02**	**0.059**	**0.02**	**0.0402**
Correlation coefficient (r^2)	**0.994**	**0.984**	**0.983**	**0.996**
Detection limits (µg L^{-1})	**0.2**	**0.3**	**0.3**	**0.3**

*n = 3, where n is the number of replications

As has been explained previously, the individual analysis of Pb^{2+} was done in 0.1 M buffer acetate (pH 4.6) in concentration range of 20 – 90 µg L^{-1}. Figure 4.37a shows the current response signals and the calibration plots in Figure 4.37a(i). The correlation coefficients and the detection limits are shown in the Table 4.7.

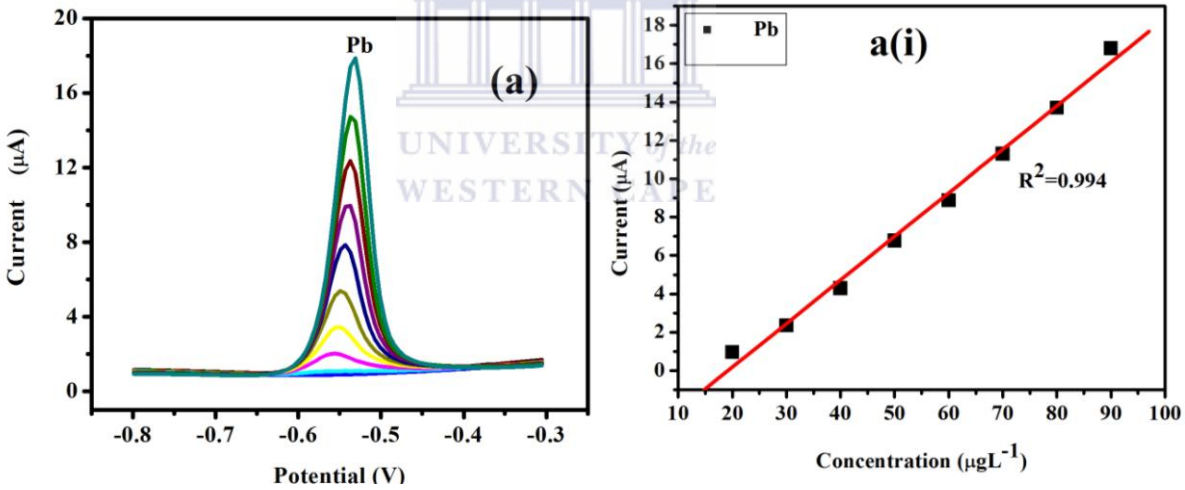

Figure 4.38: SWASV of Pb^{2+} at the Gr-GC-SbE with an *in situ* deposited Sb film. (a) signal responses, a(i) calibration plot in the range 20-90 µg L^{-1}. Supporting electrolyte (0.1 M acetate buffer pH 4.6), deposition time (120 s at -1.3 V), rotation speed (1000 rpm), frequency (50 Hz), amplitude (0.04 V) and sweep rate (0.2975 Vs^{-1}).

Table 4.7: Correlation coefficient (r^2), and detection limits of Pb^{2+} determined individually on Gr-GC-SbE.

Analytical parameter	Range 20 - 90 µg L^{-1}, Pb^{2+}
Slope (µA/µg L^{-1})	0.198±0.06
Standard Deviation (SD) of the blank	0.02
Correlation coefficient (r^2)	0.994
Detection limits (µg L^{-1})	0.3

*n = 3, where n is the number of replications

4.4.4.3 Comparison of individual and simultaneous determination

The detection limits of metals determined individually differed from those determined simultaneously. In general, lower detection limits were obtained for individual analysis, since only one of the metals binds to the limited number of active sites at the modified electrode surface and thus is involved in forming the alloy film during the deposition step. However, during simultaneous analysis all the different metal ions present in solution compete for the limited number of active sites and are all co-deposited during the formation of the alloy film.

UNIVERSITY of the
WESTERN CAPE

4.5 Part D: Graphene glassy carbon electrode (Gr-CGE)

In 2012, Colin Hong An Wong *et al.* [53], showed that chemically reduce graphene oxide (CR-GO) can be attached to a glassy carbon electrode without the use of any binding agents and, showed that the modified electrode to only detect cadmium ions.

In this section graphene (or chemically reduce graphene oxide, CR-GO) without any binding agents or metal film was used to modify bare glassy carbon electrode to give the graphene modified glassy carbon electrode, (Gr-GCE). The Gr-GCE was used to expand the work of Colin Hong An Wong *et al*. [53], to detect Zn^{2+}, Cd^{2+} and Pb^{2+}. Both simultaneous and individual analysis of the metal ions was performed in 0.1 M acetate buffer (pH 4.6) and, at the same experimental conditions as for the metal film electrodes in Sections A-C.

4.5.1 Simultaneous determination of Zn^{2+}, Cd^{2+} and Pb^{2+}

In simultaneous analysis all three metal ions were mixed together in the same solution and, the signal response (peak current) of each metal ion was obtained by measuring peak height in the voltammogram. The simultaneous analysis was conducted in 0.1 M acetate buffer using SWASV under the optimized conditions and is shown in Figure 4.38a. The corresponding calibration plots of peak current versus concentration over the concentration range 15-60 μgL^{-1} shown in Figure 4.38a(i).

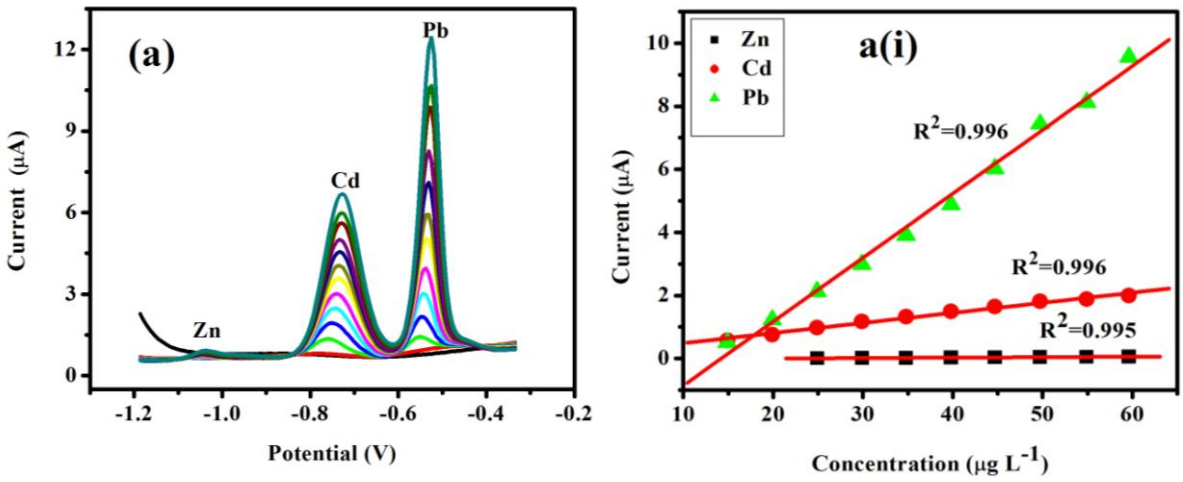

Figure 4.39: SWASV of Zn^{2+}, Cd^{2+} and Pb^{2+} at the Gr-GCE. (a) signal responses, a(i) calibration plot in the range 15 - 60 µg L^{-1}. Supporting electrolyte (0.1 M acetate buffer pH 4.6), deposition time (120 s at -1.3 V), rotation speed (1000 rpm), frequency (50 Hz), amplitude (0.04 V) and sweep rate (0.2975 Vs^{-1}).

As can be seen in Figure 4.38, the calibration plots for all the three metals were linear and the peak heights for Cd^{2+} and Pb^{2+} increased as the concentration increases while, for Zn^{2+}, the peak can be seen only at higher concentrations. The detection limits and correlation coefficients r^2 are given in Table 4.8.

UNIVERSITY of the
WESTERN CAPE

Table 4.8: Correlation coefficient (r^2), and detection limits of Zn^{2+}, Cd^{2+} and Pb^{2+} determined simultaneously on Gr-GCE

Analytical parameter	Range 15 - 60 µg L^{-1}		
	Zn^{2+}	Cd^{2+}	Pb^{2+}
Slope (µA/µg L^{-1})	0.01±0.01	0.1±0.06	0.3±0.17
Standard Deviation (SD) of the blank	0.03	0.04	0.05
Correlation coefficient (r^2)	0.995	0.996	0.996
Detection limits (µg L^{-1})	9	1.2	0.5

*n = 3, where n is the number of replications

4.5.2 Individual analysis of Zn^{2+}, Cd^{2+} and Pb^{2+}

The stripping voltammograms for the individual analysis of Zn^{2+}, Cd^{2+} and Pb^{2+} in the concentration range 5 - 60 µg L^{-1}, in 0.1 M acetate buffer (pH 4.6) and at a deposition time of

120 s are shown in Figure 4.39. For the Zn^{2+} analysis it is difficult to recognize a current peak at low concentrations because of the low sensitivity of Gr-GCE towards Zn^{2+} while, the peak currents for Cd^{2+} and Pb^{2+} were observed at lower concentrations and increased linearly with increasing concentration.

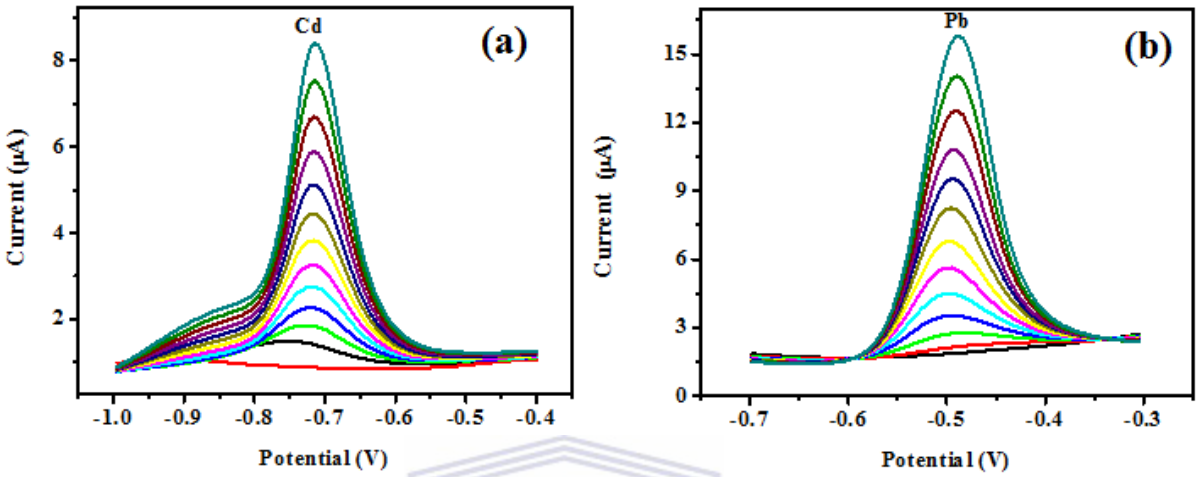

Figure 4.40: SWASV of (a) Cd^{2+} and (b) Pb^{2+} from 5 - 60 µg L^{-1} at the Gr-GCE. Supporting electrolyte (0.1 M acetate buffer pH 4.6), deposition time (120 s at -1.3 V), rotation speed (1000 rpm), frequency (50 Hz), amplitude (0.04 V) and sweep rate (0.2975 Vs^{-1}).

UNIVERSITY of the
WESTERN CAPE

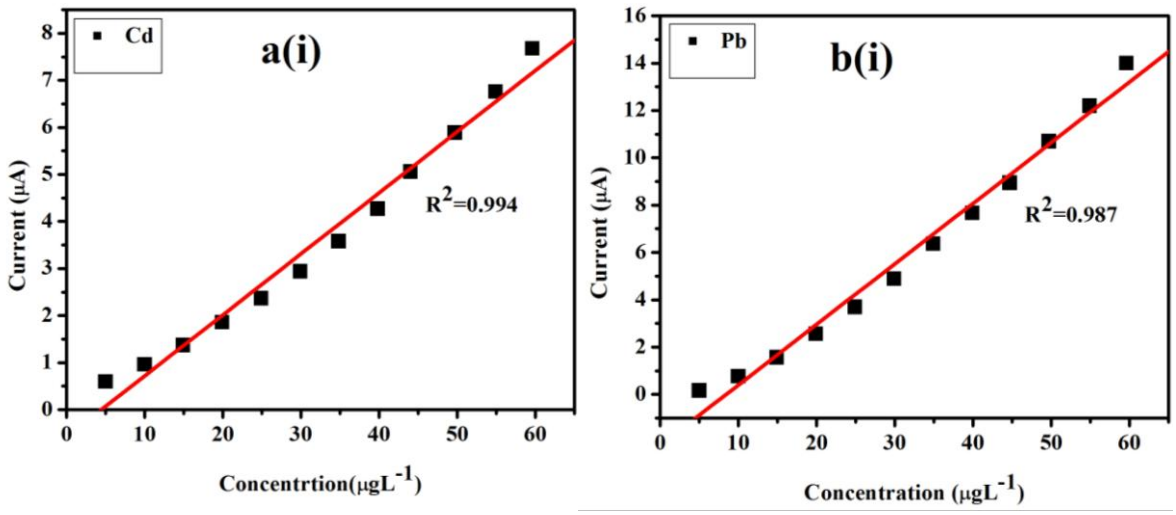

Figure 4.41: Calibration plots for (a) Cd^{2+} and (b) Pb^{2+} at the Gr-GCE. Supporting electrolyte (0.1 M acetate buffer pH 4.6), deposition time (120 s at -1.3 V), rotation speed (1000 rpm), frequency (50 Hz), amplitude (0.04 V) and sweep rate (0.2975 Vs^{-1}).

The calibration plots for cadmium and lead in the concentration range 5 - 60 µg L^{-1} are presented in Figure 4.40. The detection limit of each metal ion was determined from the calibration plots based on three times the standard deviation ($3\sigma_{blank}$) of the blank divided by the slope of the calibration curve. Table 4.9 shows the correlation coefficients and the detection limits for the metal ions.

Table 4.9: Correlation coefficient (r^2), and detection limits of Zn^{2+}, Cd^{2+} and Pb^{2+} determined individually on Gr-GCE.

Analytical parameter	**Range 5 – 60 µg L^{-1}**	
	Cd^{2+}	**Pb^{2+}**
Slope (µA/µg L^{-1})	**0.32±0.16**	**0.41±0.24**
Standard Deviation (SD) of the blank	**0.09**	**0.03**
Correlation coefficient (r^2)	**0.994**	**0.987**
Detection limits (µg L^{-1})	**0.8**	**0.2**

*n = 3, where n is the number of replications

UNIVERSITY of the
WESTERN CAPE

As has been mentioned previously it is difficult to identify the Zn^{2+} peak at low concentrations; this indicates that zinc is not sufficiently deposited onto the Gr-GCE hence, no stripping zinc peak is observed at that low concentration. However, the Zn^{2+} current peak is observed in the higher concentration range of 15 – 90 µg L^{-1}. Figure 4.41c shows the current responses and the corresponding calibration plot is shown in Figure 4.41c(i) from which the correlation coefficients and the detection limits were determined and then presented in Table 4.10.

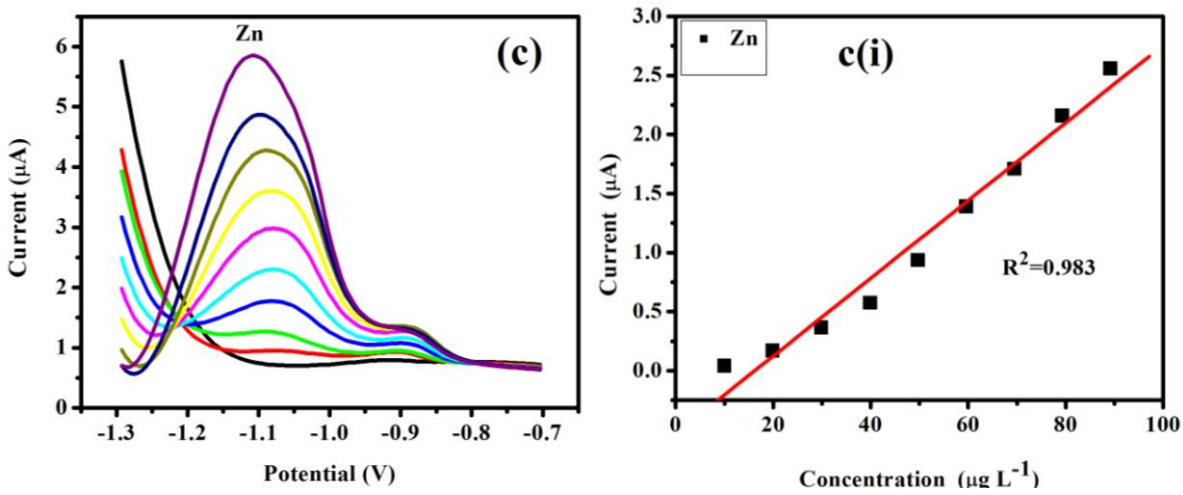

Figure 4.42: SWASV of Zn^{2+} at the Gr-GCE. (c) signal responses, c(i) calibration plot in the range 15 - 90 µg L^{-1}. Supporting electrolyte (0.1 M acetate buffer pH 4.6), deposition time (120 s at -1.3 V), rotation speed (1000 rpm), frequency (50 Hz), amplitude (0.04 V) and sweep rate (0.2975 Vs^{-1}).

Table 4.10: Correlation coefficient (r^2), and detection limits of Zn^{2+} determined individually on Gr-GCE.

Analytical parameter	Range 15 - 90 µg L^{-1}, Zn^{2+}
Slope (µA/µg L^{-1})	0.07±0.04
Standard Deviation (SD) of the blank	0.09
Correlation coefficient (r^2)	0.983
Detection limits (µg L^{-1})	3.9

*n = 3, where n is the number of replications

4.5.3 Comparison of individual and simultaneous determination

The detection limits were used to compare individual and simultaneous analysis. As can be seen from the tables the detection limits for individual analysis are higher than that in simultaneous analysis, this differences is due to the competition of the different metal ions for the limited number of active sites at the modified electrode surface in simultaneous analysis.

UNIVERSITY of the WESTERN CAPE

4.6 Comparison of metal platforms

The sensitivity for Zinc, Cadmium and Lead at different-metal platforms (Gr-GC-HgE, Gr-GC-BiE, Gr-GC-SbE and Gr-GCE) were compared in 0.1 M buffer acetate (pH 4.6) containing 60 µg L^{-1} of target metal ions and the required amounts of Hg^{2+}, Bi^{3+} and Sb^{3+} by SWASV. As can be seen from Figure 4.42 the highest and sharpest peaks for all the metals were observed at the Gr-GC-HgE. The peak height of Zn^{2+} and Cd^{2+} on Gr-G-HgE was around 2 times bigger than on Gr-GC-BiE and Gr-GC-SbE. While the peak height for Pb^{2+} on Gr-GC-HgE was eleven times greater than on Gr-GC-SbE. The peak height for Zn^{2+} at the Gr-GC-HgE was forty five times greater than that for Zn^{2+} at the Gr-GCE. For Cd^{2+} at the Gr-GC-BiE the peak heights was 5.8 times and, Pb^{2+} was two times bigger than at the Gr-GCE.

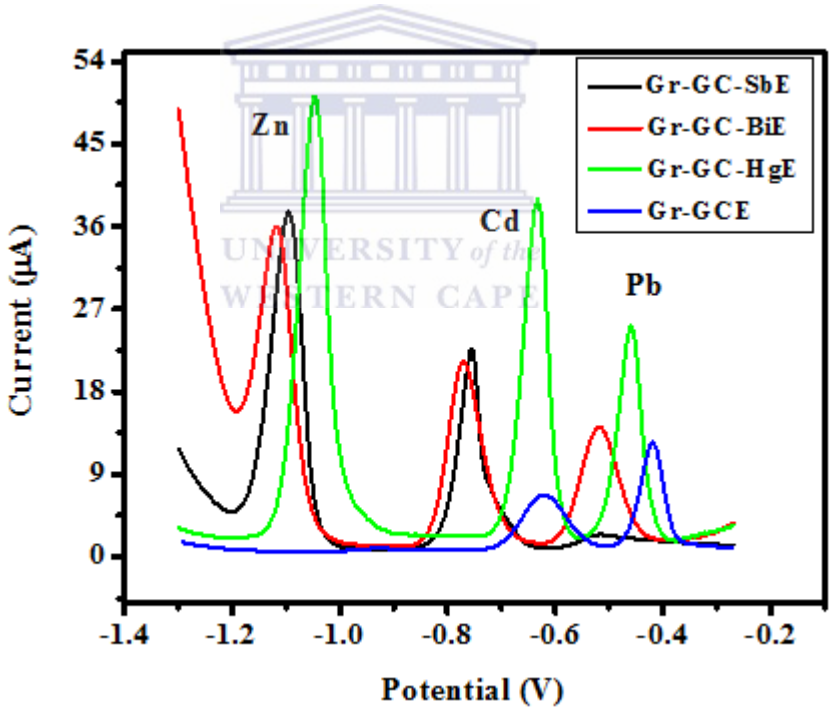

Figure 4.43: SWASV of 60 µg L^{-1} Zn^{2+}, Cd^{2+} and Pb^{2+} at a Gr-GC-HgE, Gr-GC-BiE, Gr-GC-SbE and Gr-GCE. Supporting electrolyte (0.1 M acetate buffer pH 4.6), deposition time (120 s at -1.3 V), rotation speed (1000 rpm), frequency (50 Hz), amplitude (0.04 V) and sweep rate (0.2975 Vs^{-1}).

4.7 Summary of detection limits for target metals ions at the different graphene- metal platforms

Table 4.11 shows that graphene-metal platforms offer a rational linear range and the detection limit was lower than most of previous reports. However, the detection limits for simultaneous analysis were higher than for individual analysis. This is due to the fact that during simultaneous analysis the metal ions have different affinities for the electrode surface and thus compete for the sites on the electrode surface.

Table 4.11: Correlation coefficient (r^2), slopes and detection limits for the simultaneous analysis of Zn^{2+}, Cd^{2+} and Pb^{2+} at the different graphene-metal platforms

Electrode type	Simultaneous	Slope (µA/µg L^{-1})	Standard Deviation (SD) of the blank	Correlation coefficient (r^2)	Detection limits (µg L^{-1})
Gr-GC-HgE	Zn^{2+}	2.65 ±0.42	0.07	0.996	0.08
	Cd^{2+}	1.99±0.43	0.035	0.998	0.05
	Pb^{2+}	0.96±0.01	0.046	0.996	0.14
Gr-GC-BiE	Zn^{2+}	0.56±0.03	0.022	0.996	0.12
	Cd^{2+}	0.37±0.01	0.027	0.992	0.22
	Pb^{2+}	0.22±0.01	0.021	0.990	0.28
Gr-GC-SbE	Zn^{2+}	0.57±0.018	0.023	0.997	0.1
	Cd^{2+}	0.43±0.049	0.044	0.994	0.3
	Pb^{2+}	0.05±0.038	0.022	0.974	1.2
Gr-GCE	Zn^{2+}	0.01±0.01	0.03	0.995	9
	Cd^{2+}	0.1±0.06	0.04	0.996	1.2
	Pb^{2+}	0.3±0.17	0.05	0.996	0.5

*n = 3, where n is the number of replications

Table 4.12: Correlation coefficient (r^2), slopes and detection limit values for the individual determination of Zn^{2+}, $Cd^{2+}$and Pb^{2+} at the different graphene-metal platforms.

Electrode type	Individual	Slope (µA/µg L^{-1})	Standard Deviation (SD) of the blank	Correlation coefficient (r^2)	Detection limits (µg L^{-1})
Gr-GC-HgE	Zn^{2+}	1.32±0.35	0.018	0.996	0.04
	Cd^{2+}	0.92±0.05	0.035	0.999	0.11
	Pb^{2+}	0.66±0.04	0.03	0.998	0.14
Gr-GC-BiE	Zn^{2+}	0.24±0.01	0.048	0.992	0.6
	Cd^{2+}	0.07±0.001	0.06	0.996	2.6
	Pb^{2+}	0.06±0.02	0.05	0.982	2.5
Gr-GC-SbE	Zn^{2+}	0.32±0.05	0.02	0.994	0.2
	Cd^{2+}	0.65±0.02	0.059	0.984	0.3
	Pb^{2+}	0.198±0.06	0.02	0.994	0.3
Gr-GCE	Zn^{2+}	0.07±0.04	0.09	0.983	3.9
	Cd^{2+}	0.32±0.16	0.09	0.994	0.8
	Pb^{2+}	0.41±0.24	0.03	0.987	0.2

*n = 3, where n is the number of replications

The detection limits of the Gr-GC-ME were compared with some of the electrodes found in literature and have found to have lower or comparable values for the detection limits as shown in Table 4.13.

UNIVERSITY of the WESTERN CAPE

Table 4.13: Detection limits found from previous studies of Zn^{2+}, Cd^{2+} and Pb^{2+} at various electrodes.

Metal detected	Electrode substrate	Measurement technique	Deposition time (s)	Detection limit metal ion (µg L^{-1})	Refs.
Cd^{2+}, Pb^{2+}, Zn^{2+}	Carbon based mercury thin film electrode	CV & (DPASV)	60	Cd^{2+}(0.25), Pb^{2+}(0.08), Zn^{2+}(5.5)	[206]
Pb^{2+}, Cd^{2+}	Thin-film Hg	SWASV	120	Pb^{2+}(1.8), Cd^{2+} (2.9)	[207]
Pb^{2+}, Cd^{2+}, Zn^{2+}	Bi–C- nanotubes	SWASV	300	Pb^{2+}(1.3), Cd^{2+}(0.7), Zn^{2+}(12)	[208]
Cd^{2+}, Pb^{2+}	Porous antimony films	ASV	100	Cd^{2+}(0.7), Pb^{2+}(0.5)	[209]
Cd^{2+}, Pb^{2+}	Non-porous antimony films	ASV	100	Cd^{2+}(2.8), Pb^{2+}(1.8)	[209]
Cd^{2+}, Pb^{2+}	BiF-ZDCPE	DPSV	120	Cd^{2+}(0.08), Pb^{2+}(0.1)	[210]
Zn^{2+}, Cd^{2+}, Pb^{2+}	In situ plated NCBFE	DPASV	180	Zn^{2+}(0.3), Cd^{2+}(0.17), Pb^{2+}(0.17)	[211]
Pb^{2+}	Sb/poly(p-ABSA)FE	SWASV	240	Pb^{2+} (0.1)	[202]
Cd^{2+}, Pb^{2+}	MFSPCE	SWASV	120	Cd^{2+}(2.0), Pb^{2+}(1.0)	[212]
Pb^{2+}, Cd^{2+}, Zn^{2+}	NC (Bpy)BiFE	SWASV	120	Pb^{2+}(0.08), Cd^{2+}(0.12), Zn^{2+}(0.56)	[50]
Pb^{2+}, Cd^{2+}	Bismuth film electrode	SWASV	90	Pb^{2+}(6.9), Cd^{2+}(1.4)	[213]
Zn^{2+}, Cd^{2+}, Pb^{2+}	Chemically synthesized Bi nanoparticles	SWASV	120	Zn^{2+}(0.52), Cd^{2+}(0.45), Pb^{2+}(0.41)	[214]
Zn^{2+}, Pb^{2+}, Cd^{2+}	Ex situ deposited bismuth	DPASV	60	Zn^{2+}(3.5), Pb^{2+}(0.5), Cd^{2+}(3.9)	[215]
Zn^{2+}, Pb^{2+}, Cd^{2+}	Gr-GC-HgE	SWASV	120	Zn^{2+}(0.08), Cd^{2+}(0.05), Pb^{2+}(0.14)	In this work
Zn^{2+}, Cd^{2+}, Pb^{2+}	Gr-GC-BiE	SWASV	120	Zn^{2+}(0.12), Cd^{2+}(0.22), Pb^{2+}(0.28)	In this work
Zn^{2+}, Cd^{2+}, Pb^{2+}	Gr-GC-SbE	SWASV	120	Zn^{2+}(0.1), Cd^{2+}(0.3), Pb^{2+}(1.2)	In this work
Zn^{2+}, Cd^{2+}, Pb^{2+}	Graphene-GCE	SWASV	120	Zn^{2+}(9), Cd^{2+} (1.2), Pb^{2+}(0.5)	In this work

UNIVERSITY of the WESTERN CAPE

4.8 Part E: Application of graphene – metal film electrodes

The graphene-metal film electrodes (Gr-GC-ME) was applied to the analysis of Zn^{2+}, Cd^{2+} and Pb^{2+} in tap water samples, which was collected in our laboratory. 19 ml of tap water was added to 1 ml of 2 M acetate buffer (pH 4.6) to give a 0.1 M acetate buffered tap water sample. The electrode was established in the buffered tap water sample after adding the appropriate metal ion for *in situ* metal film preparation. SWASV analyses were performed by *in situ* deposition of the metal film and target metals, using a deposition time of 240 s. A longer deposition time was used in order to obtain a signal since a deposition time of 120 s was not adequate for real samples [216].

The amount of metal ions present in the tap water sample was determined by the standard additions method and given in Tables 4.14 to 4.19 below. Only the Gr-GC-HgE was sensitive enough to detect metal ions the tap water sample whereas, the GC-BiE and GC-SbE could not. This result demonstrates the superiority of mercury since, only the Gr-GC-HgE was sensitive enough to detect metal ions the tap water sample without any additional sample pre-concentration techniques.

UNIVERSITY of the
WESTERN CAPE

In order to evaluate the accuracy of the method with the different electrodes, tap water samples were spiked with known amounts of target metal ions and then re-determined by applying the method of standards additions. In general, there is an improvement in the recoveries from the simultaneous to individual analysis and the results are presented in Tables 4.14 to 4.19.

Tables 4.14 and 4.15 show that tap water samples spiked with 3 μg L^{-1} of the target metal ions gave excellent recoveries with the Gr-GC-HgE namely, within 10% of the spiked amount. Much better recoveries were obtained for the individual analysis in comparison with simultaneous analysis. However, the recovery of Cd^{2+} was better for the simultaneous

analysis namely, 90 % compared to the 83% of the simultaneous analysis.

Table 4.14: Recoveries for the simultaneous determination of Zn^{2+}, Cd^{2+} and Pb^{2+} at the Gr-GC-HgE.

Sample	Simultaneous	Original ($\mu g\ L^{-1}$)	Added ($\mu g\ L^{-1}$)	Found ($\mu g\ L^{-1}$)	Recovery %
Tap water	**Zn^{2+}**	**1.84 ± 0.05**	**3**	**4.58 ± 0.2**	**91**
	Cd^{2+}	**0.014 ± 0.0025**	**3**	**2.71 ± 0.08**	**90**
	Pb^{2+}	**0.45 ± 0.09**	**3**	**3.29 ± 0.16**	**95**

*n = 3, where n is the number of replications

Table 4.15: Recoveries for the individual determination of Zn^{2+}, Cd^{2+} and Pb^{2+} at the Gr-GC-HgE.

Sample	Individual	Original ($\mu g\ L^{-1}$)	Added ($\mu g\ L^{-1}$)	Found ($\mu g\ L^{-1}$)	Recovery %
Tap water	**Zn^{2+}**	**0.93 ± 0.02**	**3**	**3.9 ± 0.005**	**99**
	Cd^{2+}	**0.013 ± 0.002**	**3**	**2.5 ± 0.02**	**83**
	Pb^{2+}	**0.3 ± 0.09**	**3**	**3.3 ± 0.04**	**100**

*n = 3, where n is the number of replications

Table 4.16: Recoveries for the simultaneous determination of Zn^{2+}, Cd^{2+} and Pb^{2+} at the Gr-GC-BiE.

Sample	Simultaneous	Original ($\mu g\ L^{-1}$)	Added ($\mu g\ L^{-1}$)	Found ($\mu g\ L^{-1}$)	Recovery %
Tap water	**Zn^{2+}**	**N.D**	**10**	**7.00 ± 0.10**	**70**
	Cd^{2+}	**N.D**	**10**	**7.08 ± 0.2**	**71**
	Pb^{2+}	**N.D**	**10**	**7.00 ± 0.15**	**70**

*n = 3, where n is the number of replications

Table 4.16 showed that tap water samples spiked with10 $\mu g\ L^{-1}$ of the target metal ions gave excellent recoveries within 30% of the spiked amount for all target metal ions when using the

UNIVERSITY of the WESTERN CAPE

Gr-GC-BiE. The recovery improved with individual analysis in comparison with simultaneous analysis for example, as in the case of Cd^{2+} the percentage recovery increased from 71% to 92%. However, further improvement in recoveries was obtained when the tap water sample was spiked with higher concentrations of the target metals, as shown in Table 4.17. The recovery percentages for Zn^{2+} and Pb^{2+} increased substantially (Table 4.17) and this result suggests that accuracy improves at higher metal ion concentrations.

Table 4.17: Recoveries for the individual determination of Zn^{2+}, Cd^{2+} and Pb^{2+} at the Gr-GC-BiE.

Sample	Individual	Original ($\mu g\ L^{-1}$)	Added ($\mu g\ L^{-1}$)	Found ($\mu g\ L^{-1}$)	Recovery %
Tap water	**Zn^{2+}**	**N.D**	**30**	**30.0 ± 1.6**	**100**
	Cd^{2+}	**N.D**	**10**	**9.2 ± 0.9**	**92**
	Pb2+	**N.D**	**20**	**20.0 ± 1.0**	**100**

*n = 3, where n is the number of replications

The percentage recovery in tap water samples spiked with 30 $\mu g\ L^{-1}$ of target metal ions and determined with the Gr-GC-SbE is shown in Tables 4.18 and 4.19. The percentage recovery for Zn^{2+} and Cd^{2+} are similar for simultaneous and individual analysis. However, the percentage recovery for Pb^{2+} is higher for the individual analysis namely, 95%.

Table 4.18: Recoveries for the simultaneous determination of Zn^{2+}, Cd^{2+} and Pb^{2+} at the Gr-GC-SbE.

Sample	Simultaneous	Original ($\mu g\ L^{-1}$)	Added ($\mu g\ L^{-1}$)	Found ($\mu g\ L^{-1}$)	Recovery %
Tap water	**Zn^{2+}**	**1.14 ± 0.03**	**30**	**30.0 ± 2**	**96**
	Cd^{2+}	**N.D**	**30**	**28.9 ± 1.5**	**96**
	Pb^{2+}	**N.D**	**30**	**21.8 ± 0.1**	**72**

*n = 3, where n is the number of replications

Table 4.19: Recoveries for the individual determination of Zn^{2+}, Cd^{2+} and Pb^{2+} at the Gr-GC-SbE.

Sample	Individual	Original ($\mu g\ L^{-1}$)	Added ($\mu g\ L^{-1}$)	Found ($\mu g\ L^{-1}$)	Recovery %
Tap water	**Zn^{2+}**	**1.17 ± 0.02**	**30**	**30.0 ± 1**	**96**
	Cd^{2+}	**N.D**	**30**	**27.9 ± 1.2**	**93**
	Pb^{2+}	**N.D**	**30**	**28.5 ± 1.5**	**95**

*n = 3, where n is the number of replications

The Gr-GC-BiE and Gr-GC-SbE platforms have lower sensitivity than the Gr-GC-HgE but they can be used to determine heavy metals at higher concentrations. In order to use these platforms for samples containing lower concentrations of heavy metals the deposition time can be increased or an additional sample pre-concentration technique such as, using a cation-exchange resin can be used to concentrate the metal ions.

UNIVERSITY of the
WESTERN CAPE

CHAPTER 5

Conclusions and Future work

5.1 Conclusions

Multilayer graphene nano-sheets has been successfully prepared by oxidizing graphite to graphene oxide using H_2SO_4 and $KMnO_4$ and reducing graphene oxide to graphene using $NaBH_4$. Graphene nano-sheets were characterized using FT-IR, TEM, SEM, XRD and Raman spectroscopy.

Gr-GC-MEs were prepared by immobilizing the multilayer graphene nano-sheets without binding agents onto a glassy carbon electrode using drop coating technique followed by the *in situ* deposition of mercury, bismuth or antimony thin films. These Gr-GC-MEs were employed to detect selected heavy metals namely Zn^{2+}, Cd^{2+} and Pb^{2+}. SWASV response of target ions using different graphene concentration showed that 0.25 mg L^{-1} responses is the optimized concentration that yields the highest response.

UNIVERSITY of the
WESTERN CAPE

The instrumental parameters (deposition potential, deposition time, rotation speed, frequency and amplitude) have been optimized. Hence, the deposition potential of -1.3 V, deposition time of 120 s, rotation speed of 1000 rpm, frequency of 50 Hz and amplitude of 0.04 V were identified to be most suitable for the determination of the target metal ions.

The detection limits using Gr-GC-HgE for simultaneous analysis were 0.08, 0.05 and 0.14 µg L^{-1} for Zn^{2+}, Cd^{2+} and Pb^{2+}, respectively and 0.04, 0.11 and 0.14 µg L^{-1} for Zn^{2+}, Cd^{2+} and Pb^{2+}, respectively, for by individual analysis.

When using Gr-GC-BiE, the simultaneous analysis the detection limits was; 0.12, 0.22 and 0.28 µg L^{-1} for Zn^{2+}, Cd^{2+} and Pb^{2+}, respectively, while detection limits for individual analysis

for Zn^{2+}, Cd^{2+} and Pb^{2+}, at the concentration range of 1 – 10 µg L^{-1} and 5 – 60 µg L^{-1} were; N.D, 0.36 and 1.7 µg L^{-1} and 0.6, 2.6 and 2.5 µg L^{-1}, respectively.

For Gr-GC-SbE the detection limits for simultaneous analysis were done in the concentration range 5 - 60 µg L^{-1}, the Pb^{2+} peak was not detected at low concentration with SbFE due to the pH effect and the Pb^{2+} for individual analysis determined in the range 20 - 90 µg L^{-1}. The detection limit for simultaneous analysis was; 0.1, 0.3 and 1.2 µg L^{-1} for Zn^{2+}, Cd^{2+} and Pb^{2+}, respectively and for individual analysis ; 0.2, 0.3 and 0.3 µg L^{-1} for Zn^{2+}, Cd^{2+} and Pb^{2+}, respectively.

A Gr-GCE without binding agents and no metal film was used to detect Zn^{2+}, Cd^{2+} and Pb^{2+} the detection limit values for simultaneous analysis was; 9, 1.2 and 0.5 µg L^{-1} for Zn^{2+}, Cd^{2+} and Pb^{2+}, respectively while, for individual analysis they were; 3.9, 0.8 and 0.2 µg L^{-1} for Zn^{2+}, Cd^{2+} and Pb^{2+}, respectively.

From the detection limits obtained at the Gr-GC-ME and Gr-GCE, it is clearly shown that by using a metal film (mercury, bismuth and antimony films) the sensitivity of the Zn^{2+} signal was tremendously enhanced.

The applicability of the modified electrodes used for the detection of Zn^{2+}, Cd^{2+} and Pb^{2+} in tap water. The amount of metal ions present in tap water was determined by the standard additions method. The results obtained show that only Gr-GC-HgE was sensitive enough to detect metal ions at extremely low concentrations of metal ions the tap water samples whereas, the GC-BiE and GC-SbE could not.

In general, there is an improvement in the recoveries from the simultaneous to individual analysis for the metal ions in this study except for Cd^{2+} at the Gr-GC-HgE which showed better detection for the simultaneous analysis namely, 90 % compared to the 83% of the individual analysis.

5.2 Future work

The future work in for this project will deal with:

The application of the Gr-GC-MEs on other real samples such as; mine water or other industrial waste water sample. Also, using the modified Gr-GC-MEs for detecting other heavy and hazardous metal ions such as; Arsenic.

Application Gr-GCE for detecting Sb^{2+}, Bi^{3+}, Hg^{2+}, Zn^{2+}, Cd^{2+} and Pb^{2+} ions in real samples such as water, soils, plant tissue.

Developing a portable device using screen-printed electrodes (SPE) modified with multilayer graphene for the on-site detection of heavy metals ions.

REFERENCES

1. Heavy Metals. Water Treatment Solutions. ***http://www.lennech.com/heavymetals.htm***. LENNTECH 17:10:**2012**.

2. Olga, K.; Libuse, T.; Vojtech, A.; Josef, Z.; Jaromir, H.; Petr, B.; Rene K. *Electrochemical Microsensors for the Detection of Cadmium(II) and Lead(II) Ions in Plants.* Sensors, **2010,** 10, 5308-5328.

3. Merian, E. *Metals and their compounds in the environment: occurrence, analysis and biological relevance*. VCH Publishers, Weinheim, **1991**, 1438.

4. *Trace element speciation for environment*, food and health; Ebdon, L; Pitts, L; Cornelis, R; Crews, H; Donard, O F X; Quevauviller, P., Eds; Royal Society of Chemistry: Cambridge, **2001**, 392.

5. Fernandez-Leborans, G. H.; Yolanda, O.; *Toxicity and bioaccumulation of lead and cadmium in marine protozoan communities.* Ecotoxicology and Environmental Safety **2000**, 47, 266-276.

6. Sayari, A.; Hamoudi, S.; Yang, Y. *Applications of pore-expanded malodorous silica, removal of heavy metal captions and organic pollutants from waste water.* Chemistry of Materials **2005**, 17, 212-216.

7. Heavy metals. ***http://www.psr.org/environment-and-health/conforming toxics/heavymetals***. 25:02:2013.

8. Environmental Protective Agency. ***http://www.epa.gov/safewater/contaminants/index.html*** 17:10:2012.

9. Cumings, J. N. *Heavy metals and the brain.* Blackwell Scientific Publications: Oxford, 1959.

UNIVERSITY of the WESTERN CAPE

10. Toxic substances portal-Cadmium. ***http://www.atsdr.cdc.gov/toxfaqs/tf.asp?id=47&tid=15*** 25:02:2013.

11. Hites, R.A. *Elements of environmental chemistry.* John Wiley & Sons, Inc.: Hoboken, New Jersey, 2007.

12. Wang, J. *Stripping Analysis: Principles, Instrumentation, and Application.* VCH Publishers, Inc.: Deerfield Beach, Florida, 1985.

13. Tercier, M.L.; Buffle, J. *In situ voltammetric measurements in natural waters: Future prospects and challenges.* Electroanalysis **1993**, 5, 187-200.

14. Brett, C.M.A.; Lima, J.L.F.C.; Garcia, M.B.Q. *Square-wave Anodic Stripping Voltammetry in Stationary and Flowing Solution: a Comparative Study.* Analyst **1994,** 119, 1229-1233.

15. Kachoosangi, R.T.; Banks C.; Ji X.; Compton, R. E*lectroanalytical determination of cadmium(II) and lead(II) using an in-situ bismuth film modified edge plane pyrolytic graphite electrode.* Analytical Science **2007,** 23, 283-289.

16. Sanna, G; Pilo, M; Piu, P. C; Tapparo, A; Seeber, R. *Determination of heavy metals in honey by anodic stripping voltammetry at microelectrodes.* Analytica. Chimica. Acta **2000,** 415, 165-173.

17. Wu, H.P. *Dynamics and perfirmance of fast linear scan anodic stripping voltammetry of cadmium, lead and copper using in situ-generated ultrathin mercury films*. Analytica Chemica Acta **1996**, 68, 1639-1645.

18. Demetriades, D.; Economou, A.; Voulgaropoulos, A. *A study of pencil-lead bismuth-film electrodes for the determination of trace metals by anodic stripping voltammetry*. Analytica Chimica Acta, **2004**, 519, 167–172.

UNIVERSITY of the
WESTERN CAPE

19. Kefala, G.; Economou, A.; Voulgaropoulos, A.; Sofoniou, M. *A study of bismuth-film electrodes for the detection of trace metals by anodic stripping voltammetry and their application to the determination of Pb and Zn in tap water and human hair.* Talanta **2003,** 61, 603–610.

20. Hwang, G.H.; Han, W.K.; Park, J.S.; Kang, S.G. *Determination of trace metals by anodic stripping voltammetry using a bismuth-modified carbon nanotube electrode*. Talanta **2008**, 76, 301–308.

21. Hwang, G.; Han W.; Hong, S.; Park, J.; Kang, S. *Determination of trace amounts of lead and cadmium using a bismuth/ glassy carbon composite electrode.* Talanta **2009**, 77, 1432–1436.

22. Zou, Z.; Jang, A.; Macknight, E.; Pei-Ming, W.; Jaephil, D.; Bishop, P.L.; Ahn C.H. *Environmentally friendly disposable sensors with microfabricated on-chip planar bismuth electrode for in situ heavy metal ions measurement.* Sensor and Actuator B **2008,** 134, 18–24.

UNIVERSITY of the
WESTERN CAPE

23. Zong, P.; Nagaosa, Y. *Determination of antimony(III) and (V) in natural water by cathodic stripping voltammetry with in-situ plated bismuth film electrode.* Microchimica Acta **2009**, 166, 139–144.

24. Valéria, G.; Hizuru, N.; Nobuaki, S.; Koji, N.; Toshihiko, I. *Antimony-film electrode for the determination of trace metals by sequential-injection analysis/anodic stripping voltammetry*. Analytica Chimica Acta **2010**, 658, 12–17.

25. Miao, F.; Wijeratne, S.; Coskun, U.; Zhang,Y.; Lau, C.N. *Phase Coherent Transport of Charges in Graphene Quantum Billiard*. **http://arxiv.org/ftp/cond-mat/papers/0703/0703052.pdf** 26:02:2013.

26. Xinran, W.; Scott, M.T.; Hongjie, D. *Atomic layer deposition of metal oxides on*

pristine and functionalized graphene. American Chemical Society **2008**, 130, 8152-8153.

27. Huafeng, Y.; Fenghua, L.; Changsheng, S.; Dongxue, H.; Qixian, Z.; Niu, L.; Ari, I. *Covalent functionalization of chemically converted graphene sheets via silane and its reinforcement.* Materials Chemistry **2009,** 19, 4632–4638.

28. Fowler, J.D.; Allen, M.J.; Tung, V.C.; Yang, Y.; Kaner, R.B.; Weiller, B.H. *Practical Chemical sensors from Chemically Dervied Graphene.* ACS Nano **2009**, 3, 301-306.

29. Yongchao, S.; Edward, T S. *Synthesis of Water Soluble Graphene.* Nano Letters **2008,** 8, 1679–1682.

30. Kimberly, A.; Worsly, P.R.; Swadhin, K.M.; Sandip, N.; Mikhail, E.I.; Robert, C.H.; *Soluble graphene derived from graphite fluoride.* Chemical Physical Letters **2007,** 445, 51-56.

31. Gilje, S.; Han, S.; Wang, M.; Wang, K.L.; Kaner, R.B. *A Chemical Route to Graphene for Device Applications.* Kaner Nano Letters **2007,** 7, 3394-3398.

32. Wang, G.; Yang, J.; Park, J.; Gou, X.; Wang, B; Liu, H.; Yao, J. *Facile Synthesis and Characterization of Graphene Nanosheets.* Journal of Physical. Chemistry C **2008,** 112, 8192-8195.

33. Subrahamanyam, K. S.; Vivekchand, S. R. C.; Govindaraj, A.; Rao, C. N. R. *A study of graphenes prepared by different methods: characterization, properties and solubilization.* Materials Chemistry **2008**, 18, 1517-1523.

34. Michael, J.M.; Je-Luen, L.; Douglas H.A.; Hannes C.S.; Ahmed A.A.; Jun L.; Herrera-Alonso, M.; David L.M.; Roberto, C.; Prud'homme, R.K.; Ilhan A.A. *Single Sheet Functionalized Graphene by Oxidation and ThermalExpansion of Graphite.* Chemistry of Materials **2007,** 19, 4396-4404.

UNIVERSITY of the
WESTERN CAPE

35. Schniepp, H.C.; Li, J-L.; Mcallister, M.J.; Sai, H.; Herrera-Alonso, M.; Adamson, D.H.; Prud'homme, R.K.; Car, R.; Saville D.A.; Aksay, I.A. *Functionalized single graphene sheets derived from splitting graphite oxide.* Journal of Physical Chemistry B **2006,** 110, 8535-8539.

36. Tian, G.; Shengshui, H. *Electrochemical sensors based on graphene materials.* Microchimica Acta **2011,** 175, 1–19.

37. Shen, J.; Yizhe, H.; Li, C.; Qin, C.; Shi, M.; Mingxin, Y. *Layer-by-Layer Self-Assembly of Graphene Nanoplatelets.* Langmiur **2009,** 25, 6122-6128.

38. Lia, Y.H.; Dib, Z.; Dingd, J.; Wub, D.; Luanc, Z.; Zhu, Y. *Adsorption thermodynamic, kinetic and desorption studies of Pb^{2+} on carbon nanotubes.* Water Research **2005,** 39, 605–609.

39. Friberg, L.; Nordberg, G.F.; Vouk, V.B. *Handbook on the Toxicology of Metals,* Elsevier/ North-Holland Biomedical Press, 1979.

40. Rashed, M.N. *Lead removal from contaminated water using mineral adsorbents*. Environmentalist **2001,** 21, 187–195.

41. Korolczuk, M.; Stepniowska, A.; Tyszczuk, K. *Determination of cadmium by stripping voltammetry at a lead film electrode.* Internatonal Journal of Environmental Analytical Chemistry **2009**, 89, 727–734.

42. Tesarova, E.; Baldrianova, L.; Hocevar, S. B.; Svancara, I.; Vytras, K.; Ogorevc, B. *Anodic stripping voltammetric measurement of trace heavy metals at antimony film carbon paste electrode.* Electrochimica Acta **2009**, 54, 1506-1510.

43. Novoselov, K.S.; Geim, A.K.; Morozov, S.V.; Jiang, D.; Katsnelson, M.I.; Grigorieva, I.V.; Dubonos, S.V.; Firsov, A.A. *Two-dimensional gas of massless dirac fermions in graphene*. Nature **2005,** 438, 197–200**.**

UNIVERSITY of the
WESTERN CAPE

44. Tombros, N.; Jozsa, C.; Popinciuc, M.; Jonkman, H.; Van, W.B. *Electronic spin transport and spin precession in single graphene layers at room temperature.* Nature **2007,** 448, 571–574.

45. Fang.; J.; Ya-Li, L.; Jian-Min, F.; Dong.; S.; Yang-Yang, W.; Feng, Y.; Hou, F. *Electrochemical performance of graphene nanosheets and ceramic composites as anodes for lithium batteries.* Materials Chemistry **2009**, 19, 9063–9067.

46. Balandin, A.A.; Ghosh, S.; Bao, W.; Calizo, I.; Teweldebrhan, D.; Miao, F.; Lau, C.N. *Superior thermal conductivity of single-layer graphene.* Nano Letters, **2008**, 8, 902–907.

47. Dikin, D.A.; Stankovich, S.; Zimney E.J.; Piner, R.D.; Dommett, G.H.B.; Evmenenko, G.; Nguyen, S.T.; Ruoff, R.S. *Preparation and characterization of graphene oxide paper*. Nature **2007**, 448, 457–460.

48. Stankovich, S.; Dikin, D.A.; Dommett, G.H.B.; Kohlhaas K.M.; Zimney E.J.; Stach E.A.; Piner, R.D.; Nguyen, S.T.; Ruoff, R.S. *Graphene-based composite materials.* Nature **2006**, 442, 282–286.

49. Li, J.; Guo, S.; Zhai, Y.; Wang, E. *High-sensitivity determination of lead and cadmium based on the Nafion-graphene composite film*. Analytica Chimica Acta **2009,** 649, 196–201.

50. Li, J.; Guo, S.; Zhai, Y.; Wang, E. *Nafion-graphene nanocomposite film as enhanced sensing platform for ultrasensitive determination of cadmium*. Electrochemistry Communications **2009**, 11, 1085–1088.

51. Khomyakov, P.A.; Giovannetti, G.; Rusu, P.C.; Brocks, G.; Van Den Brink, J.; Kelly, P.J. *First-principles study of the interaction and charge transfer between graphene and metals.* Physical Review **2009,** 79, 195425-195437.

UNIVERSITY of the
WESTERN CAPE

52. Willemse, C.M.; Tlhomelang, K.; Jahed, N.; Baker, P.G.; Iwuoha, E.I. *Metallo-Graphene Nanocomposite Electrocatalytic Platform for the Determination of Toxic Metal Ions.* Sensors **2011,** 11, 3970-3987.

53. Wong, C.H.A.; Pumera, M. *Stripping voltammetry at chemically modified graphenes.* Royal Society of Chemistry Advances **2012**, 2, 6068-6072.

54. Voltammetric Techniques. ***http://www.prenhall.com/settle/chapters/ch37.pdf*** 27:02:2013.

55. Voltammetric analysis methods. ***http://www.ecochemie.nl/export/Homepages/Autolab/download/NavaTutorials/VA-tut***. 28:02:2013.

56. Skoog, D.A.; West, D.M.; Holler, F.J.; Crouch, S.R. *Fundamentals of Analytical Chemistry,* 9th ed.; Cengage Learning: USA, 2004.

57. Bard, A.J.; Faulkner, L.R. *Electrochemical Methods: Fundamentals and Applications*, 2nd ed.; John Wiley & Sons: New York, 2000.

58. Cyclic voltammetry. ***http://www.csun.edu/jeloranta/CHEM351L/experiment3pdf***. 28:02:2013.

59. Voltammetry. ***http://www.kutztown.edu/acad/chem/instruments.html/electrochemistry.htm.*** 28:02:2013.

60. Reference electrode: Definition. ***http://www.events.nace.org/library/corrosion/references/introduction.asp***. 28:02:2013.

61. Counter electrode. Electrochemistry Dictionary. ***http://chemistry.science-dictionary.org/Electrochemistry-Dictionary/counter-electrode.*** 28:02:2013.

UNIVERSITY of the
WESTERN CAPE

62. Eric, P.A.; Charlotte, B. *Stripping voltammetry for the determination of trace metal speciation and in-situ measurements of trace metal distributions in marine waters*. Analytica Chimica Acta **1999**, 400, 381–397.

63. Stripping voltammetry. ***http://www.basinc.com/mans/EC-epsilon/Techniques/stripping/stripping.html.*** 28:02:2013.

64. Stripping voltammetry. ***http://faculty.uml.edu/david-ryan/84.514/Handouts/strippingvoltammetry.pdf.*** 28:02:2013.

65. Ozkan, S.A. *Principles and Techniques of Electroanalytical Stripping Methods for Pharmaceutically Active Compounds in Dosage Forms and Biological Samples*. Current Pharmaceutical Analysis **2009**, 5, 127-143.

66. Keawkim, K.; Chuanuwatanakul, S.; Chailapakul, O.; Motomizu, S. *Determination of Lead and Cadmium in Rice Samples by Sequential Injection/Anodic Stripping Voltammetry using a Bismuth Film/Crown Ether/Nafion Modified Screen-Printed Carbon Electrode*. Food Control **2012**, 12, 525-527.

67. Robery, K.; Miloslav K. *Adsorptive stripping voltammetry in trace analysis.* Pure and Applied Chemistry **1989**, 61, 97-112.

68. Protti, P. *Introduction to Modern Voltammetric and Polarographic Analisys Techniques*. AMEL Electrochemistry, 4th ed.; New York, 2001.

69. Stripping voltammetry. ***http://www.tau.ac.il/advanal/strippingvoltammetry.htm.*** 04:03:2013.

70. Linear sweep voltammetry. ***http://www.files.chem.vt.edu/chem-ed/echem/linsweep.html.*** 05:03:2013.

71. Linear sweep voltammetry: The principles.

UNIVERSITY of the
WESTERN CAPE

http://www.ceb.cam.ac.uk/pages/linearsweep-and-cyclic-voltammetry-the-principles.html. 05:03:2013.

72. 797 VA Computrace, Metrodata, 8.797.8003 Software Manual

73. Kissinger, P.T.; Heineman, W.R. *Laboratory Techniques in Electroanalytical Chemistry*. 2 ed. 1996: New York.

74. Zoski, C.G.; *Handbook of Electrochemistry.* First Edition, Publisher: Elsevier Science 2007.

75. Jovanovski, V.; Hocevar, S.B.; Ogorevc, B. *Ex Situ Prepared Antimony Film Electrode for Electrochemical Stripping Measurement of Heavy Metal Ions.* Electroanalysis **2009**, 21, 2321 – 2324.

76. Florence, T.M. *Anodic Stripping Voltammetry with a Glassy Carbon Electrode Mercury-Plated in situ.* Journal of Electroanalytical Chemistry **1970**, 27,273-281.

77. Dhaktode, S.S. *Simultaneous determination of lead, copper, cadmium and zinc in pure zirconium metal by differential-pulse anodic stripping voltammetry*. Analytica Chimica Acta **1987**, 199,181-183.

78. Oehme, M.; Lund, W.; Jonsen, J.J. *Determination of Copper, Lead, Cadmium and Zinc in Human Teeth by Anodic Stripping Voltammetry*. Analytica Chimica Acta **1978**, 100,389.

79. Ogorevc, B.; Krasna, A.; Hudnik, V. *A novel approach to decomposition of foodstuffs for stripping voltammetric determination of lead, cadmium and copper*. Analytica Chimica Acta **1987**, 196, 183-191.

80. Labuda, J.; Vanickova, M. *Anodic stripping voltammetry with mercury electrodes in extracts of Cd, Pb, TI and In diethyl-dithiocarbamate complexes and analysis of*

UNIVERSITY of the WESTERN CAPE

mixtures. Analytica Chimica Acta **1988**, 208, 219-230.

81. Newton, M.P.; Van Den Berg, C. M. G. *Determination of nickel, cobalt, copper and uranium in water by cathodic stripping chronopotentiometry with continuous flow*. Analytica Chimica Acta **1987**, 199, 59-76.

82. Zhang H.; Wollast, R.; Vire, J-C.; Patriarche, G.J. *Simultaneous determination of cobalt and nickel in sea-water by adsorptive cathodic stripping square-wave voltammetry*. Analyst **1989**, 114, 1597-1602.

83. Van Den Berg, C.M.G.; Nimmo, M. *Direct determination of uranium in water by cathodic stripping voltammetry.* Analytical Chemistry **1987**, 59, 924-928.

84. Wu T.G.; Xiang W.Z.; Zhang F.Z.; Deng J.Q. *Differential anodic stripping voltammetric determination of selenium in hair and flour at a gold-film electrode*. Analyst, **1988**, 113, 1431-1433.

85. Van Den Berg, C.M.G. *Adsorptive Cathodic Stripping Voltammetry of Trace Elements in Sea Water*. Analyst **1989**, 114, 1527.

86. Nürnberg, H.W. *The voltammetric approach in trace metal chemistry of natural waters and atmospheric precipitation*. Analytica Chimica Acta **1984**, 164, 1-21.

87. Cees, J.M K.; Guo-Hui, Y.; Jan C D. *Optimization and comparison of four mercury working electrodes in speciation studies by differential-pulse anodic stripping voltammetry*. Analytica Chimica Acta **1984**, 164, 163-170.

88. Pinchin, M.J.; Newham, J. *The determination of lead, copper and cadmium by anodic stripping voltammetry at a mercury film electrode*. Analytica Chimica Acta **1977** 90, 91-102.

89. Ertas, F.N.; Gokcel, H.I.; Tural, H. *The Effect of Acetone on Calomel Formation on a*

UNIVERSITY of the
WESTERN CAPE

Mercury Film Electrode Surface in Chloride Medium. Turkish Jornal of Chemistry **2000**, 24, 261- 267.

90. Yoshida, Z. *Preparation of an ideal thin mercury film electrode and its electrochemical property*. Bulletin of the Chemical Society of Japan **1981,** 54, 562–567.

91. Stojek, Z.; Kublik, Z.J. *Silver based mercury film electrode. III. Comparison of theoretical and experimental anodic stripping results for lead and copper*. Electroanalalytical Chemistry **1977**, 77, 205-224.

92. Stojek, Z.; Kublik, Z.J. *Silver based mercury film electrode. I. General characteristics and stability of the electrode*. Electroanalytical Chemistry **1975**, 60, 349-358.

93. Daniele, S.; Baldo, M.A.; Ugo, P.; Mazzocch, G.A. *Determination of heavy metals in real samples by anodic strypping voltammetry with mercury microelectrodes.Part 2. Application to rain and sea waters.* Analytica Chimica Acta **1989**, 219, 19-26.

94. Wang J.; Tuzhi P.; Zadeii J. *Evaluation of Differential-Pulse Anodic Stripping Voltammetry at Mercury-Coated Carbon Fiber Electrodes. Comparison to Analogous Measurements at Rotating Disk Electrodes*. Analytical Chemistry **1987,** 59, 2119

95. Economou, A.; *Bismuth film electrodes: Recent developments and potentialities for electroanalysis.* TrAC Trends in Analytical Chemistry **2005,** 24, 334–340.

96. Wang, J. *Stripping analysis at bismuth electrodes. A Review.* Electroanalysis **2005**, 17, 1341–1346.

97. Wang, J.; Lu, J.; Hocevar, S.B.; Farias, P.A.M.; Ogorevc, B. *Bismuth-coated carbon electrodes for anodic stripping voltammetry*. Analytical Chemistry **2000**, 72, 3218–3222.

UNIVERSITY of the
WESTERN CAPE

98. Krueger, J.; Winkler, P.; Luederitz, E.L., (5th ed.; In Wolfgang Gerhartz, Gail Schulz, et al., Ed). Lueck, M.,*Ullman's encyclopedia of industrial chemistry,* Wiley-VCH: Weinheim, Germany, **1985**, 4, 171–189.

99. Long, G.G.; Freeman, L.D.; Doak, G.O., In M. Grayson (Ed.). *Kirkothmer encyclopedia of chemical technology*; John Wiley and Sons: New York, **1978**, 3, 912–937.

100. Hocevar, S.B.; Ogorevc, B.; Wang, J.; Pihlar, B. *A study on operational parameters for advanced use of bismuth film electrode in anodic stripping voltammetry*. Electroanalysis **2002**, 14, 1707.

101. Krolicka, A.; Pauliukaite, R.; Svancara, I.; Metelka, R.; Bobrowski, A.; Norkus, E.; Kalcher, K.; Vytras, K. *Bismuth-film-plated carbon plated electrodes.* Electrochemistry Communications **2002**, 4, 193-196.

102. Uhl, A.; Kestranek, W. *The Electrometric Titration of Acids and Bases with the Antimony Indicator Electrode*. Monatsch **1923**, 44, 29-34.

103. Hočevar, S.B.; Švancara, I.; Ogorevc, B.; Vytřas, K. *Antimony Film Electrode for Electrochemical Stripping analysis.* Analytical Chemistry **2007**, 79, 8639-8643.

104. Toghill, K.E.; Xiao, L.; Wildgoose, G.G.; Compton, R.G. *Electroanalytical Determination of Cadmium(II) and Lead(II) Using an Antimony Nanoparticle Modified Boron-Doped Diamond Electrode*. Electroanalysis **2009**, 21, 1113-1118.

105. Gangolli, S. *The Dictionary of Substances and Their Effects*, 3rd ed.; Electronic, Royal Society of Chemistry/Knovel: Cambridge, 2005.

106. Svancara, I.; Hocevar, S.B.; Baldrianova, L.; Tesarova, E.; Vytras, K. *Antimony modified carbon paste electrodes.* Scientific papers of the University of Pardubic, Series **2007,** 13, 5-9.

UNIVERSITY of the
WESTERN CAPE

107. Wang, J. *Analytical Electrochemistry,* 3rd ed.; John Wiley & Sons, Inc.: New Jersey, Canada, 2006.

108. Goldberg, E.D. Edmlond, J.M. *The Nature of Seawater,* Dahlem Konferenzen, Berlin, 1975.

109. Branica, M. E*nvironmental Research in Aquatic Systems,* Forschungszentrum Jiilich. Scientific Series of International Bureau,1990, 3.

110. Bond, A.M. *Moderm Polarographic Methods in Analytical Chemistry,* Marcel Decker: New York, 1980.

111. Plavšić, M.; Kozar, S.; Krznarić, D.; Bilinski, H.; Branica, M. *The influence of organics on the adsorption of copper (II) on Y-AI203 in seawater, model studies with EDTA.* Marine Chemistry **1980**, 9, 175-182.

112. Plavšić, M.; Krznarić D.; Branica M. *Determination of the apparent copper complexing capacity of seawater by anodic stripping voltammetry*. Marine Chemistry **1982**, 11, 17-31.

113. Khandekar, R.N.,Dhaneshwar, R.G.; Palrecha, M.M.; Zarapkar, L.R. *Simultaneous determination of lead, cadmium and zinc in aerosols by anodic stripping voltammetry.* Analytical Chemistry **1981**, 307, 365-368.

114. Holak, W. *Differential pulse polarographic determination of iodine in thyroid tablets.* Analytical Chemistry **1982**, 65, 1059-1062.

115. Amankwa, L.; Chatten, L.G.; Pons, S. *Electrochemical studies on minoxidil and its determination in tablets by differential-pulse polarography.* Analyst London **1983**, 108, 1221-1226.

116. Chatten, L.G.; Pons, S.; Amankwa, L. *Voltammetric studies of zomepirac sodium and*

UNIVERSITY of the
WESTERN CAPE

its determination in tablets by differential-pulse polarography. Analyst London **1983**, 108, 997-1002.

117. Ivaska, A.; Nordstrom, F. *Determination of some cephalosporins by differential pulse polarography and linear scan voltammetry*. Analytical Chimca Acta **1983**, 146, 87-95.

118. Oelschlfiger, H. *Polarographic analysis of psychotropic drugs.* Bioelectrochem. Bioenerget **1983**, 10, 25-36.

119. Wang, J.; Dewald, H.D. *Determination of trace elements in pharmaceutical tablets using anodic stripping voltammetry.* Analyt Letters **1983**, 16, 925-939.

120. Novoselov, K.S.; Geim, A.K.; Morozov, S.V.; Jiang ,D.; Zhang, Y.; Dubonos, S.V.; Grigorieva, I.V.; Firsov, A.A. *Electric Field Effect in Atomically Thin Carbon Films.* Science **2004**, 306, 666-669.

121. Geim, A.K.; Novoselov, K.S. *The rise of graphene. Nature Materials.* Nature materials **2007**, 6, 183-191.

122. Shenderova, O.A.; Zhirnov V.V.; Brenner D.W. *Carbon nanostructures.* Critical Reviews Solid state materials sciences **2002**, 27, 227-356.

123. Lee, C.; Wei, X.; Kysar, J.W.; Hone, J. *Measurement of the elastic properties and intrinsic strength of monolayer graphene*. Science **2008**, 321, 385-388.

124. Wallace, P.R. *The band theory of graphite.* Physical Review **1947**, 71,622-634.

125. Novoselov, K.S.; Geim, A.K.; Morozov, S.V.; Jiang, D.; Katsnelson, M.I.; Grigorieva, I.V.; Dubonos, S.V.; Firso A.A. *Two-dimensional gas of massless direct fermions in graphene.* Nature **2005**, 438, 197-200.

126. Zhang, Y.; Tan, Y-W.; Stormer, H.L.; Kim, P. *Experimental observation of the*

UNIVERSITY of the
WESTERN CAPE

quantum hall effect and berry's phase in graphene. Nature **2005**, 438, 201-204.

127. Reich, S.; Maultzsch, J.; Thomsen, C.; Ordejon, P. *Tight-biding description of graphene.* Physical Review **2002**, 66, 035412.

128. Reich, S.; Thomsen, C.; Maultzsch, J. *Carbon Nanotubes*,1st ed.; Wiley-VCH Verlag GmbH & Co. KGaA: Weinheim, 2004.

129. Dubois, S.M.-M.; Zanolli, Z.; Declerck, X.; Charlier, J.-C. *Electronic properties and quantum transport in graphene-based nanostructures.* European physical **2009**, 72, 1-24.

130. Graphene makes movement easy for electrons. ***http://www.physorg.com/news119030362.html***. 08:03:2013.

131. Kharissova, O.V.; Kharisov,.B.I. Graphenes, *One of the Hottest Areas in the Nanotechnology: Attention of Chemists is Needed*. The Open Inorganic Chemistry Journal **2008**, 2, 39-49.

132. Introduction to the physical properties of graphene ***http://chercheurs.lps.u_psud.fr/GOERBIG/CoursGraphene2008.pdf***

133. Bunch J.S.; Van Der Zande, A.M.; Verbridge S.S.; Frank I.W.; Tanenbaum D.M.; Parpia J.M.; Craighead H.G.; Mceuen P.L. *Electromechanical resonators from graphene sheets.* Science **2007**, 315, 490-493.

134. Jamie H.W.; Franziska S.; Alicja, B.; Mark, H.R. *graphene fundamentals and emergent applications.* Elsevier Inc, 2013.

135. Bae, S, Kim, H.; Lee, Y.; Xu, X.; Park, J-S.; Zheng,Y.; Balakrishnan, J.; Lei, T.; Song, Y.; Kim, Y.J.; Kim, K.S.; Ozyilmax, B.; Ahn, J-H.; Hong, B.H.; Iijima, S. *Roll-to-roll production of 30-inch graphene films for transparent electrodes.* Nat

UNIVERSITY of the WESTERN CAPE

Nanotechnol **2010**, 5, 574-578.

136. Nair, R.R.; Blake, P.; Grigorenko A.N.; Novoselov K.S.; Booth T.J.; Stauber T.; Peres, N.M.R.; Geim, A.K. *Fine structure constant defines visual transparency of graphene.* Science **2008**, 320, 1308.

137. Li, Z.Q.; Henriksen, E.A.; Jiang, Z.; Hao, Z.; Martin, M.C.; Kim, P.; Stormer, H.; Basov, D. *Bend structure asymetric of bilayer graphene revealed by infrared spectroscopy.* physical Review Letter **2009**, 102, 037403.

138. Zhang, H.; Bao, Q.; Tang, D.; Zhao, L.; Loh, K. *Large energy solution erbium-doped fiber laser with graphene-polymer composite mode locker.* Applied Physics Letters **2009**, 95, 141103.

139. Bao, Q.; Zhang, H.; Wang, Y.; Ni, Z.; Yan, Y.; Shen, Z.X.; Loh, K.P.; Tang, D.Y. *Atomic-Layer graphene as a saturable absorber for ultrafast pulsed lasers.* Advanced Functional Material **2009**, 19, 3077-3083.

UNIVERSITY of the
WESTERN CAPE

140. Delhaes, P. *Graphite and Precursors,* CRC Press, 2001.

141. Kim, K.S.; Zhao,Y.; Jang, H.; Lee, S.Y.; Kim, J.M.; Kim, K.S.; Ahn, J-H.; Kim, P.; Choi, J-Y.; Hong, B.H. *Larg-scale pattren growth of graphene films for stretchable transparent electrodes.* Nature **2009**, 457, 706-710.

142. Li, X.; Cai, W.; An, J.; Kim, S.; Nah, J.; Yang, D.; Piner, R.; Velamakanni, A.; Jung, I.; Tutuc, E.; Banerjee, S.K.; Colombo, L.; Raoff, R.S. *Large-Area Synthesis of high-Quality and Uniform Graphene Film on Copper Foils.* Science **2009**, 324, 1312-1314.

143. Hummers, W.S.; Offeman, R.E. *Preparation of graphitic oxide.* Journal of the American Chemical Society **1958**, 80, 1339.

144. Graphene. ***http://cnx.org/content/m29187/latest*** 13:03:2013.

145. Forbeaux, I.; Themlin J.-M; Debever J.-M. *Heteroepitaxial graphite on 6H–SiC(0001): interface formation through conductionband electronic structure*. Physical Review **1998**, 58, 16396-16406.

146. Hass J.; Heer, W.A.; Conrad, E.H. *The growth and morphology of epitaxial multilayer graphene.* Journal of physics: Condensed Matter **2008**, 20, 323202.

147. Varchon F.; Feng R.; Hass J.; Li X.; Nguyen B.N.; Naud C.; Mallet P.; Veuillen J.Y.; Berger C.; Conrad E.H.; Magaud L. *Electronic structure of epitaxial graphene layers on SiC: effect of the substrate.* physical Review letter **2007**, 99, 126805-126809.

148. Heer, W.A.; Berger, C.; Wu, X.; First, P.N.; Conrad, E.H.; Li, X.; Tianbo, L.; Sprinkle, M.; Hass, J.; Sadowski, M.L.; Potemski, M. *Epitaxial graphene.* Solid State Communications **2007**, 143, 92.

149. Park, Yoon-Soo, *SiC materials and devices.* San Diego, Calif: Academic Press, 1998.

150. Penuelas, J.; Ouerghi, A.; Lucot, D.; David, C.; Gierak, J.; Estrade-Szwarckopt, H.; Andreazza-Vignolle, C. *Surface morphology and characterization of thin graphene films on SiC vicinal substrate.* Physical Review **2009**, 79, 033408-033411.

151. Vakkasoglu, A.S. *FT-IR Difference Spectroscopy Studies on Membrane Proteins.* ProQuest LLC, 2009.

152. Infra-Red Absorption Spectroscopy- Theoretical Principles. ***http://teaching.shu.ac.uk/hwb/chemistry/tutorials/molspec/irspec1.htm***. Sheffield Hallam University Biosciences Online Learning 2010.

153. Kittel, C.; *Introduction to Solid State Physics.* Eighth Edition, John Wiley & Sons Ltd.: Chichester, 2005.

154. Brennan, J.F.; Romwr T.J.; Lees, R.S.; Tercyak, A.M.; Kramer, J.R.; Feld M. S.

UNIVERSITY of the
WESTERN CAPE

Determination of human coronary artery composition by Raman spectroscopy. Circulation **1997**, 96, 99-105.

155. Instruments, P. Raman spectroscopy basics. ***www.piacton.com***. 16:03:2013.

156. Fischer, E.; Van.Den.Berg, C.M.G. *Anodic stripping voltammetry of lead and cadmium using a mercury film electrode and thiocyanate*. Analytica Chimica Acta **1999**, 385, 273-280.

157. Calizo, I.; Miao, F.; Bao, W.; Lau, C.N.; Balandin, A.A. *The effect of substrates on the Raman spectrum of graphene: Graphene-on-sapphire and graphene-on-glass.* Applied Physics Letters **2007**, 91, 201904.

158. Weisstein, E. W, *Math World: Fraunhofer Diffraction.* **http://scienceworld.wolfram.com/physics/FraunhoferDiffraction.html** URL, 2005.

159. Guinier, A. *X-Ray Diffraction: In Crystals, Imperfect Crystals, and Amorphous Bodies.* Ltd: Canada, 1994.

160. Williams, D.B.; Carter, C.B. *Transmission Electron Microscopy: A Textbook for Materials Science.* Plenum Press: New York, 1996.

161. Liu, X.; Tong, J.; Sun, Y. *A millimeter-sized nanomanipulator with subnanometer positioning resolution and large force output.* Smart Material Structures **2007**, 16, 1742-1750.

162. Lyman, C.E.; Newbury, D.E.; Goldstein, J.I.; Williams, D.B.; Romig, A.D.J.; Armstrong, J.T.; Echlin P.; Fiori C.E.; Joy D.C.; Lifshin, E.; Peters K. *Scanning Electron Microscopy, X-Ray Microanalysis and Analytical Electron Microscopy.* A Laboratory Workbook, Plenum Press: New York, 1990.

UNIVERSITY of the
WESTERN CAPE

163. Pumera, M. *The Electrochemistry of Carbon Nanotubes: Fundamentals and Applications.* Chemistry - A European Journal **2009**, 15,4970-4978.

164. Wongong, C.; Jo-Won L. *Graphene: Synthesis and Applications.* Taylor & Francis Group, LLC 2012.

165. McCreery, R.L. *Advanced electrode materials for molecular electrochemistry.* Chemical Reviews **2008**, 108, 2646-2687.

166. Yao, Y.-L.; Shin, K.-K. *Direct electrochemistry of glucose oxidase at carbon nanotube-gold colloid modified electrode with poly(diallyldimethylammonium chloride) coating.* Electroanalysis **2008**, 20, 1542-1548.

167. Leger, C.; Bertrand, P. *Direct electrochemistry of redox enzymes as a tool for mechanistic studies*. Chemical Reviews **2008**, 108, 2379-2438.

168. Shan, C; Yang, H.; Song, J.; Han, D.; Ivaska, A.; Niu, L. *Direct Electrochemistry of Glucose Oxidase and Biosensing for Glucose Based on Graphene.* Analytical Chemistry **2009**, 81, 2378–2382.

169. Ghindilis, A.L.; Atanasov, P.; Wilkins, E. *Enzyme-catalyzed direct electron transfer: Fundamentals and analytical applications.* Electroanalysis **1997**, 9, 661-674.

170. Wang, J. *Carbon-Nanotube Based Electrochemical Biosensors*: *A Review*. Electroanalysis **2005**, 17,7-14.

171. Willner, I.; Katz, E. *Integrated Nanoparticle–Biomolecule Hybrid Systems: Synthesis, Properties, and Applications.* Angewandte Chemie INternational Edition **2004**, 43, 6042 – 6108.

172. Sarma, A.K.; Vatsyayan, P.; Goswami, P.; Minteer, S.D. *Recent advances in material science for developing enzyme electrodes.* Biosensors Bioelectronics **2009**, 24, 2313-

UNIVERSITY of the
WESTERN CAPE

2322.

173. Kang, X.; Wang, J.; Wu, H.; Aksay, I.; Liu, J.; Lin, Y. *Glucose oxidase-graphene-chitosan modified electrode for direct electrochemistry and glucose sensing.* Biosensors Bioelectronics **2009**, 25, 901–905.

174. Wu P.; Shao Q.; Hu, Y.; Jin, J.; Yin, Y.; Zhang, H.; Cai, C. *Direct electrochemistry of glucose oxidase assembled on graphene and application to glucose detection.* Electrochimica Acta **2010**, 55, 8606–8614.

175. Becerril, H.A.; Mao, J.; Liu, Z.; Stoltenberg, R.M.; Bao, Z.; Chen, Y. *Evaluation of solution-processed reduced graphene oxide films as transparent conductors.* ACS Nano **2008**, 2, 463-470.

176. Schmidt-Mende, L.; Fechtenkotter, A.; Mullen, K.; Moons, E.; Friend, R.H.; Mackenzie, J.D. *Self-organized discotic liquid crystals for high-efficiency organic photovoltaics.* Science **2001**, 293, 1119-1122.

UNIVERSITY of the
WESTERN CAPE

177. Schlatmann, A.R.; Floet, D.W.; Hilberer, A.; Garten, F.; Smulders, P.J.M.; Klapwijk, T.M.; Hadziioannou, G. *Indium contamination for the Indium-Tin-Oxide electrode in polymer light-emitting-diodes.* Applied Physics Letters **1996**, 69, 1764-1766

178. Li, J.; Guo, S.; Zhai, Y.; Wang, E. *High-sensitivity determination of lead and cadmium based on the Nafion-graphene composite film*. Analytica Chimica Acta **2009**, 649, 196–201.

179. Li, J.; Guo, S.; Zhai, Y.; Wang, E. N*afion-graphene nanocomposite film as enhanced sensing platform for ultrasensitive determination of cadmium*. Electrochemistry Communications **2009**, 11, 1085–1088.

180. Khomyakov, P.A.; Giovannetti, G.; Rusu, P.C.; Brocks, G.; Van Den Brink, J.; Kelly, P.J. *First-principles study of the interaction and charge transfer between graphene*

and metals. Physical Review **2009**, 79, 195425-195437.

181. Kan, E.-J.; Li, Z.; Yang, J.; Hou, J.G. *Will zigzag graphene nanoribbon turn half metal under electric field?* Applied physics Letters **2007**, 91, 243116.

182. Kinder, J.M.; Dorando, J.J.; Wang, H.; Chan, G.K.-L. *Perfect reflection of chiral fermions in gated graphene nanoribbon.* Nano Letters **2009**, 9, 1980-1983.

183. Kefala, G.; Economou, A.; Voulgaropoulos, A.; Sofoniou, M. *A study of bismuth-film electrodes for the detection of trace metals by anodic stripping voltammetry and their application to the determination of Pb and Zn in tap water and human hair*. Talanta **2003**, 61, 603–610.

184. Hummers W.S.; Offeman R.E. *Preparation of graphitic oxide.* Journal of the American Chemical Society **1958**, 80, 1339-1339.

185. Shen, J.; Hu, Y.; Shi, M.; Lu, X.; Qin, C.; Li, C.; Ye, M. *Fast and Facile Preparation of Graphene Oxide and Reduced Graphene Oxide Nanoplatelets.* Chemistry of Materials **2009**, 21, 3514–3520.

186. Shen, J.; Yan, B.; Li, T.; Long, Y.; Li, N.; Ye, M. *Mechanical, thermal and swelling properties of poly(acrylic acid)/graphene oxide composite hydrogels.* Soft Matter **2012**, 8, 1831-1836.

187. Stankovich, S.; Dikin, D.A.; Piner, R.D.; Kohlhaas, K.A.; Kleinhammes, A.; Jia, Y.; Wu, Y.; Nguyen, S.T.; Ruoff, R.S. *Synthesis of graphene-based nanosheets via chemical reduction of exfoliated graphite oxide.* Carbon **2007**, 45, 1558–1565.

188. Shen, J.; Yan, B.; Li, T, Long ,Y.; Li, N.; Mingxin, Y. *Mechanical, thermal and swelling properties of poly(acrylic acid)/graphene oxide composite hydrogels.* Soft Matter **2012**, 8, 1831-1836.

UNIVERSITY of the
WESTERN CAPE

189. Zhang, D.; Zhang, X.; Chen, Y.; Wang, C.; Ma, Y. *An environment-friendly route to synthesize reduced graphene oxide as a supercapacitor electrode material*. Electrochimica Acta **2012**, 69, 364-370.

190. Marcano, D.C.; Kosynkin, D.V.; Berlin, J.M.; Sinitskii, A.; Sun, Z.; Slesarev, A.; Alemany, L.B.; Lu, W.; Tour, J.M. *Improved Synthesis of Graphene Oxide.* ACS NANO **2010**, 4, 4806–4814.

191. Li, Z.; Zhang, W.; Luo, Y.; Yang, J.; Hou J.G. *How Graphene Is Cut upon Oxidation?* Journal of American Chemical Society **2009**, 131, 6320–6321.

192. Zhou, X.; Shi, T.; Zhou, H. *Hydrothermal preparation of ZnO-reduced graphene oxide hybrid with high performance in photocatalytic degradation*. Applide surface science **2012**, 258, 6204–6211.

193. Kassaee, M.Z.; Motamedi, E.; Majdi, M. *Magnetic Fe3O4-graphene oxide/polystyrene: Fabrication and characterization of a promising nanocomposite*. Chemical Engineering Journal **2011**, 172, 540-549.

194. Wu, J.; Tang, Q.; Sun, H.; Lin, J.; Ao, H.; Huang, M.; Huang, Y. *Conducting Film from graphite oxide Nanoplatelets and poly(acrylic acid) by layer-by-layer self-Assembly.* Langmuir **2008**, 24, 4800-4805.

195. Pham, T.A.; Kumar, N.A.; Jeong, Y.T. *Covalent functionalization of graphene oxide with polyglycerol and their use as templates for anchoring magnetic nanoparticles*. Synthetic Metals **2010**, 160, 2028-2036.

196. Zhu,Y.; Stoller, M.D.; Cai, W.; Velamakanni, A.; Piner, R.D.; Chen, D.; Ruoff R.S. *Exfoliation of Graphite Oxide in Propylene Carbonate and Thermal Reduction of the Resulting Graphene Oxide Platelets.* American Chemical Society **2010**, 2, 1227-1233.

197. Zhu, Y.; Murali, S.; Cai, W.; Li, X.; Suk, J.W.; Potts, J.R.; Ruoff, R.S. *Graphene and*

UNIVERSITY of the
WESTERN CAPE

Graphene Oxide: Synthesis, Properties, and Applications. Advanced Materials **2010**, 22, 3906–3924.

198. Singh, V.; Joung, D.; Zhai, L.; Das, S.; Khondaker, S.I.; Seal, S. *Graphene based materials: Past, present and future.* Science **2011**, 56, 1178–1271.

199. Shen, J.; Hu, Y.; Shi, M.; Lu, X.; Qin, C.; Li, C.; Ye, M. *Fast and Facile Preparation of Graphene Oxide and Reduced Graphene Oxide Nanoplatelets.* Chem. Mater **2009**, 21, 3514–3520.

200. Silva, N.A.F.; Leitoa, R.A.E.; Matos, M.J. *Bismuth an electrode material in the simultaneous determination of Cd and Pb in Poplar leaves by SWASV*. Portugaliae Electrochima Acta **2006**, 24, 283-293.

201. Baldrianova, L.; Svancara, I.; Vlcek, M.; Economouc, A.; Sotiropoulos, S. *Effect of Bi(III) concentration on the stripping voltammetric response of in situ bismuth-coated carbon paste and gold electrodes*. Electrochimica Acta **2006**, 52, 481–490.

202. Yi, W.J.; Li, Y.; Ran, G.; Luo, H.Q.; Li, N.B. *A glassy carbon electrode modified with antimony and poly (p-aminobenzene sulfonic acid) for sensing lead(II) by square wave anodic stripping voltammetry*. Microchimica Acta **2012**, 179, 171-177.

203. Rehacek, V.; Hotovy, I.; Vojs, M.; Kups, T.; Spiess, L. *An effect of bismuth film electroplating variables on electrode performance in electroanalysis* 54th Internationales Wissenschaftliches Kolloquium, 2009.

204. Al-Ghamdi, A.F. *Stripping Voltammetric Determination of Timolol Drug in Pharmaceuticals and Biological Fluids*. American Journal of Analytical Chemistry **2011**, 2, 174-181.

205. Svobodová, E , Baldrianová, L , Hočevar, S.B.; Švancara, I. *Electrochemical Stripping Analysis of Selected Heavy Metals at Antimony Trioxide-Modified Carbon*

UNIVERSITY of the
WESTERN CAPE

Paste Electrode. Intrnational Jornal of Electrochemical Science **2012**, 7, 197 - 210.

206. Ensafi, A.A.; Nazari, Z.; Fritsch, I. *Highly Sensitive Differential Pulse Voltammetric Determination of Cd, Zn and Pb Ions in Water Samples Using Stable Carbon-Based Mercury Thin-Film Electrode*. Electroanalysis **2010**, 22, 2551 – 2557.

207. Raquel, G.G.A.; Clàudia, F.; Enriqueta, A.; Arben, M. *Sensitive and stable monitoring of lead and cadmium in seawater using screen-printed electrode and electrochemical stripping analysis*. Analytica Chimica Acta **2008**, 627, 219–224.

208. Hwang, G.H.; Han, W.K.; Park, J.S.; Kang, S.G. *Determination of trace metals by anodic stripping voltammetry using a bismuth-modified carbon nanotube electrode.* Talanta **2008**, 76, 301-308.

209. Urbanová, V.; Vytřas K.; Kuhn, A. *Macroporous antimony film electrodes for stripping analysis of trace heavy metals.* Electrochemistry Communications **2010**, 12, 114–117.

UNIVERSITY of the
WESTERN CAPE

210. Cao, L.; Jia, J.; Wang, Z. *Sensitive determination of Cd and Pb by differential pulse stripping voltammetry with in situ bismuth-modified zeolite doped carbon paste electrodes*. Electrochimica Acta **2008**, 53, 2177–2182.

211. Xu, H.; Zeng, L.; Huang, D.; Xian, Y.; Jin, L. *A Nafion-coated bismuth film electrode for the determination of heavy metals in vegetable using differential pulse anodic stripping voltammetry: An alternative to mercury-based electrodes.* Food Chemistry **2008**, 109, 834-839.

212. Noh, M.F.M.; Tothill, I.E. *Determination of Lead(II), Cadmium(II) and Copper(II) in Waste-Water and Soil Extracts on Mercury Film Screen-Printed Carbon Electrodes Sensor*. Sains Malaysiana **2011**, 40, 1153–1163.

213. Siriangkhawut, W.; Pencharee, S.; Grudpan, K.; Jakmunee, J. *Sequential injection*

monosegmented flow voltammetric determination of cadmium and lead using a bismuth film working electrode. Talanta **2009**, 79, 1118-1124.

214. Rico, M.A, Olivares-Marin, M.; Gil, E.P. *Modification of carbon screen-printed electrodes by adsorption of chemically synthesized Bi nanoparticles for the voltammetric stripping detection of Zn(II), Cd(II) and Pb(II)*. Talanta **2009**, 80, 631–635.

215. Serrano, N.; Diaz-Cruz, J.M.; Ariño, C.; Esteban, M. *Stripping analysis of heavy metals in tap water using the bismuth film electrode.* Analytical and Bioanalytical Chemistry **2010**, 396, 1365–1369.

216. Sosnin, E.A.; Batalova, V.M.; Buyanova, E.Y.; Tarasenko, V.F. *Comparative study of interference elimination in heavy metals control by anodic stripping voltammetry.* Proceedings of the Physics and Control **2003**, 1, 349-351.

UNIVERSITY of the
WESTERN CAPE